Dynamical Properties of Specific Black Holes

By

Muhammad Umair Shahzad

CIIT/FA13-PMATH-005/LHR

PhD Thesis

In

Mathematics

COMSATS University Islamabad
Lahore Campus - Pakistan

Fall, 2017

COMSATS University Islamabad

Dynamical Properties of Specific Black Holes

A Thesis Presented to

COMSATS University Islamabad

In partial fulfillment

of the requirement for the degree of

PhD (Mathematics)

By

Muhammad Umair Shahzad

CIIT/FA13-PMATH-005/LHR

Fall, 2017

Dynamical Properties of Specific Black Holes

A Post Graduate Thesis submitted to the department of Mathematics as partial fulfillment of the requirement for the award of Degree of Ph.D in Mathematics.

Name	Registration Number
Muhammad Umair Shahzad	CIIT/FA13-PMATH-005/LHR

Supervisor

Dr. Abdul Jawad

Assistant Professor Department of Mathematics

COMSATS University Islamabad, Lahore Campus

Certificate of Approval

This is to certify that the research work presented in this thesis entitled "Dynamical Properties of Specific Black Holes" was conducted by Mr. Muhammad Umair Shahzad, CIIT/FA13-PMATH-005/LHR, under the supervision of Dr. Abdul Jawad. No part of this thesis has been submitted anywhere else for any other degree. This thesis is submitted to the Department of Mathematics, COMSATS University Islamabad, in the partial fulfillment of the requirements for the degree of Doctor of Philosophy in the field of Mathematics.

Student Name: Muhammad Umair Shahzad Signature: ____________

External Committee:

External Examiner 1:
Prof. Dr. Muhammad Sajid
Department of Mathematics and Statistics,
Faculty of Basic and Applied Sciences,
International Islamic University,
Islamabad.

External Examiner 2:
Dr. Imran Javaid
Center for Advanced Studies in
Pure & Applied Mathematics,
Bahauddin Zakariya University,
Multan.

Dr. Abdul Jawad
Supervisor
Department of Mathematics,
CUI, Lahore Campus

Dr. Sarfraz Ahmad
HoD, Department of Mathematics,
CUI, Lahore Campus

Prof. Dr. Moiz ud Din Khan
Chairperson, Department of Mathematics,
COMSATS University Islamabad

Author's Declaration

I Muhammad Umair Shahzad, CIIT/FA13-PMATH-005/LHR, hereby state that my PhD thesis titled "Dynamical Properties of Specific Black Holes" is my own work and has not been submitted previously by me for taking any degree from this University i.e. COMSATS University Islamabad or anywhere else in the country/world.

At any time if my statement is found to be incorrect even after my Graduate the university has the right to withdraw my PhD degree.

Date: 27/9/2018

Muhammad Umair Shahzad

CIIT/FA13-PMATH-005/LHR

Plagiarism Undertaking

I solemnly declare that research work presented in the thesis titled "Dynamical Properties of Specific Black Holes" is solely my research work with no significant contribution from any other person. Small contribution/help wherever taken has been duly acknowledge and that complete thesis has been written by me.

I understand the zero tolerance policy of HEC and COMSATS University Islamabad towards plagiarism. Therefore, I as an author of the above titled thesis declare that no portion of my thesis has been plagiarized and any material used as reference is properly referred/cited.

I undertake that if I am found guilty of any formal plagiarism in the above titled thesis even after award of PhD degree, the University reserves the right to withdraw/revoke my PhD degree and that HEC and the University has the right to publish my name on the HEC/University website on which names of students are placed who submitted plagiarized thesis.

Date: 27/9/2018.

Muhammad Umair Shahzad

CIIT/FA13-PMATH-005/LHR

Certificate

It is certified that Muhammad Umair Shahzad with CIIT/FA13-PMATH-005/LHR has carried out all the work related to this thesis under my supervision at the Department of Mathematics, COMSATS University Islamabad, Lahore Campus and the work fulfills the requirement for award of PhD degree.

Date: 27/9/2018.

Supervisor:

Dr. Abdul Jawad
Assistant Professor

Head of Department:

Dr. Sarfraz Ahmad
Associate Professor
Department of Mathematics.

DEDICATION

To my Parents and Wife

ACKNOWLEDGMENTS

All praises to ALLAH Almighty who created the universe and knows whatever is in it hidden or evident, who bestowed upon me the intellectual ability and wisdom to search for it's secret and whose blessings flourished my thoughts and thrived my ambitions and enabled me to contribute sincerely to the sacred wealth of knowledge. Special praise and regards to his last messenger Muhammad (PBUH) who is a tower of guidance and knowledge for humanity.

I feel much pleasure in expressing my hearties gratitude to my ever-affectionate supervisor Dr. Abdul Jawad for his dynamic and friendly supervision. Whose indispensable guidance, deep consideration, constructive comments and active cooperation enable me to complete my work successfully. All the words I know are insufficient to pay my tribute to him.

I would like to thank to Head of Department Dr. Sarfraz Ahmed, Associate Head of Department Dr. Kashif Ali, PhD Coordinator Dr. Muhammad Hussain and all my teachers for their suggestions, guidance and constant support.

I would like to thank all my friends, class fellows and colleagues for their suggestions, sympathetic attitude and work discussion during my studies.

Of course, at this stage I cannot forget my whole family especially my respectable parents, my wife and my brothers for their prayers, continuing support and love. Their prayers have lightened up my spirit to finish this thesis.

COMSATS University Islamabad, Lahore Campus.

Muhammad Umair Shahzad

CIIT/FA13-PMATH-005/LHR

ABSTRACT

Dynamical Properties of Specific Black Holes

The present thesis comprises the study of three dynamical phenomenon such as thermal fluctuations, accretion and tidal forces of black holes/regular black holes.

We consider the logarithmic corrected entropy in order to analyze the thermal fluctuations. We examine the effects of thermal fluctuations on a regular black hole of the non-minimal Einstein-Yang-Mill theory with gauge field of magnetic Wu-Yang type and a cosmological constant. We investigate the first law of thermodynamics in the presence of logarithmic corrected entropy and non-minimal regular black hole. Furthermore, we discuss the thermal fluctuation problem by utilizing the higher order corrected entropy. We examine the thermodynamical behavior of two well-known black holes such as Reissner-Nordström Anti de Sitter black hole with global monopole and *f(R)* black hole in the presence of higher order corrected entropy.

We also discuss the accretion problem in two phases. In first phase, we analyze the accretion onto static spherically symmetric regular black holes for specific choices of the equation of state parameter. The underlying regular black holes are charged regular black holes using the Fermi-Dirac distribution, logistic distribution, non-linear electrodynamics, respectively, and Kehagias-Sftesos asymptotically flat regular black holes. In second phase, we develop the Hamiltonian dynamical system to tackle the accretion problem. We investigate the accretion of test fluids onto regular black holes such as Kehagias-Sftesos black hole and regular black holes with Dagum distribution function. We analyze the accretion process when different test fluids are falling onto these regular black holes. The behavior of fluid flow and the existence of sonic points is being checked for these regular black holes.

Finally, we investigate the tidal forces occurring in a Kiselev black hole surrounded by radiation and dust fluids. We also solve the geodesic deviation equation for radially free-falling bodies toward Kiselev black hole. We explain the geodesic deviation vector graphically and point out the location of the event and Cauchy horizons for specific values of the radiation and dust parameters.

TABLE OF CONTENT

1. Introduction **1**

2. Basic Concepts **10**

2.1 Black Hole 11

2.1.1 Schwarzschild Black Hole 12

2.1.2 Reissner-Nordström Black Hole 13

2.2 Regular Black Holes 14

2.3 Black Hole Thermodynamics 15

2.3.1 Laws of Black Hole Mechanics 15

2.3.2 Laws of Black Hole Thermodynamics 16

2.4 Thermal Fluctuations 17

2.5 Heat Capacities 21

2.6 Accretion 22

2.6.1 Role of Dark Energy in Accretion 22

2.6.2 General Formalism for Accretion 23

2.7 Tidal Forces in a Black Hole 26

2.7.1 Equation of Geodesic Deviation 27

3. Effects of Thermal Fluctuations on Non-minimal Regular Magnetic Black Hole **29**

3.1 Non-minimal Regular Black Hole 30

3.1.1 Logarithmic correction and thermodynamical relations 33

3.2 Stability of non-minimal Regular Black Hole 36

3.2.1 Phase Transition 38

3.2.2 Grand Canonical Ensemble 39

3.2.3 Canonical Ensemble 41

4. Thermodynamics of Higher Order Corrected Entropy on some well known Black holes **43**

4.1 Thermodynamical Analysis of RN-AdS Black Hole with Global Monopole .. 44

4.1.1 Stability of RN-AdS Black Hole with Global Monopole 47

4.1.2 Phase transition 49

4.1.3 Grand Canonical Ensemble 50

4.1.4 Canonical Ensemble 51

4.2 Thermodynamical Analysis of $f(R)$ Black Hole 52

4.2.1 Stability of $f(R)$ Black Hole 55
4.2.2 Phase transition 56
4.2.3 Grand Canonical Ensemble 57
4.2.4 Canonical Ensemble 58
5. Accretion onto Some Well-Known Regular Black Holes 60
5.1 Charged Regular Black Hole Using Fermi-Dirac Distribution 61
5.2 Charged Regular Black Hole Using Logistic Distribution 65
5.3 Charged Regular Black Hole from Nonlinear Electrodynamics 70
5.3 Kehagias - Sftesos asymptotically flat Regular Black Hole 73
6. Accreting Fluids onto Regular Black Holes Via Hamiltonian Approach 78
6.1 General Description 79
6.2 Hamiltonian system 82
6.3 Sonic points 83
6.3 Regular Black Holes 85
6.3.1 Regular Black hole using Dagum Distribution Function 85
6.4 Isothermal test fluids 87
6.4.1 Solution for ultra-stiff fluid ($\omega = 1$) 89
6.4.2 Solution for ultra-relativistic fluid ($\omega = 1/2$) 89
6.4.3 Solutions for ($\omega = 1/3$) and ($\omega = 1/4$): Separatrix heteroclinic flows 92
6.5 Polytropic test fluids 95
7. Tidal Forces in Kiselev Black Hole 99
7.1 Kiselev black holes and its two special cases 100
7.1.1 Radial Geodesics 101
7.2 Tidal forces in Kiselev space-time on a neutral body in radial free fall 102
7.2.1 Radial tidal forces 104
7.2.2 Angular tidal forces 105
7.3 Solutions of the geodesic equations for Kiselev Black Hole 106
8. Conclusions and Open Problems 115
9. References 122
Appendix 138

LIST OF FIGURES

Figure 3.1: Plot of pressure verses horizon radius 34
Figure 3.2: γ verses horizon radius 37
Figure 3.3: Specific heat at constant volume verses horizon radius 38
Figure 3.4: Gibb's free energy in terms of horizon radius 40
Figure 3.5: Helmhotz free energy in terms of horizon radius 41
Figure 4.1: The plot of pressure for RN-AdS BH with GM 46
Figure 4.2: The plot of γ versus horizon radius for RN-AdS BH with GM 48
Figure 4.3: The plot of specific heat at constant volume for RN-AdS BH with GM 49
Figure 4.4: The plot of Gibb's free energy for RN-AdS BH with GM 51
Figure 4.5: The plot of Helmhotz free energy versus horizon radius for RN-AdS BH 52
Figure 4.6: The plot of pressure for $f(R)$ BH 54
Figure 4.7: The plot of γ for $f(R)$ BH for 55
Figure 4.8: The plot of specific heat at constant volume for $f(R)$ BH 57
Figure 4.9: The plot of Gibb's free energy for $f(R)$ BH 58
Figure 4.10: The plot of Helmhotz free energy for $f(R)$ BH 59
Figure 5.1: Velocity profile against x of charged FDD RBH 62
Figure 5.2: Energy density against x of charged FDD RBH 63
Figure 5.3: Rate of change of mass against x of charged FDD RBH 64
Figure 5.4: Velocity profile against x of charged RBH using logistic distribution 67
Figure 5.5: Energy density against x of charged RBH using logistic distribution 68
Figure 5.6: Rate of change of mass against x of charged RBH using logistic distribution 69
Figure 5.7: Velocity profile against x of charged RBH from nonlinear electrodynamics 71
Figure 5.8: Energy density against x of charged RBH from nonlinear electrodynamics 72
Figure 5.9: Rate of change of mass against x of charged RBH from nonlinear electrodynamics 73
Figure 5.10: Velocity profile against x of KS RBH 74
Figure 5.11: Energy density against x of KS RBH 75
Figure 5.12: Rate of change of mass against x of KS RBH 76
Figure 6.1: Case $\omega = 1/2$ 91
Figure 6.2: Left panel: Case $\omega = 1/3$ and Right panel: Case $\omega \leq 1/4$ 92
Figure 6.3: Case $\omega \leq 1/3$ 94
Figure 6.4: Contour plot of (6.5.7) for KS RBH and DDF RBH 96
Figure 6.5: Contour plot of (6.5.7) for KS RBH and DDF RBH for different parameter 97
Figure 7.1: Radial tidal force for Kiselev BH surrounded by radiation 105
Figure 7.2: Radial tidal force for Kiselev BH surrounded by dust 106
Figure 7.3: Angular tidal force for Kiselev BH surrounded by radiation 107
Figure 7.4: Angular tidal force for Kiselev BH surrounded by dust 107
Figure 7.5: Radial components of geodesic deviation for Kiselev BH surrounded by radiation with IC1 110
Figure 7.6: Radial components of geodesic deviation for Kiselev BH surrounded by dust with IC1 110
Figure 7.7: Radial components of geodesic deviation for Kiselev BH surrounded by radiation with IC2 112

Figure 7.8: Radial components of geodesic deviation for Kiselev BH surrounded by dust with IC2 112
Figure 7.9: Angular components of geodesic deviation for Kiselev BH Kiselev BH surrounded by radiation with IC2 113
Figure 7.10: Angular components of geodesic deviation for Kiselev BH Kiselev BH surrounded by dust with IC2 113

LIST OF TABLES

Table 3.1: Location of horizons where first law of thermodynamics is satisfied 35
Table 4.1: Range of local stability and CPs of horizon radius for RN-AdS BH with GM 49
Table 4.2: Range of local stability and CPs of horizon for *f(R)* BH 56
Table 5.1: Charged FDD RBH.. 65
Table 5.2: Charged RBH using logistics distribution 68
Table 5.3: Charged RBH from nonlinear electrodynamics.. 72
Table 5.4: KS RBH.. 76
Table 7.1: Location of event horizon for chosen values of dust parameter 112
Table 7.2: Location of Cauchy horizon for chosen values of dust parameter........................ 113
Table 7.3: Location of event horizon for chosen values of radiation parameter.................... 114
Table 7.4: Location of Cauchy horizon for chosen values of radiation parameter 114

LIST OF ABBREVIATIONS

AdS	Anti de Sitter
BH	Black Hole
BTZ	Banados-Teitelboim-Zanelli
CP	Critical Point
DDF	Dagum Distribution Function
DE	Dark Energy
dS	de Sitter
EFEs	Einstein field equations
EoS	Equation of State
FDD	Fermi-Dirac Distribution
GM	Global Monopole
GR	General Relativity
KS	Kehagias-Sftesos
NEC	Null Energy Condition
RBH	Regular Black Hole
RN	Reissner and Nordström
SEC	Strong Energy Condition
SH	Schwarzschild
WEC	Weak Energy Condition

LIST OF NOMENCLATURE WITH SI UNITS

Symbol	Name	Quantity
A	ampere	electric current
°C	Celsius	temperature
K	kelvin	temperature
kg	kilogram	mass
m	meter	length
N	Newton	force
s	second	time

Chapter 1

Introduction

When a massive star exhausts the nuclear fuel whose burning keeps it hot, the stars internal pressure plunges. In this way, gravity overwhelms the pressure and pulls the star inward upon itself. The star implodes, shrinking smaller and smaller, and the gravity on its shrinking surface becomes stronger and stronger (because of Newtons inverse square law). Ultimately, when the star has shrunk to a few tens of kilometers size, its gravity grows so enormous that nothing, not even light, can escape its grip which leads to the formation of black hole (BH) [1]. Many scientist believe that BHs are widespread in the Universe, many BHs formed in the early Universe and it might be the result of massive star evolution. Supermassive BHs are located in the center of many types of galaxies including active galactic nuclei, quasars and our own Milky Way Galaxy.

In 1915, Einstein succeeded in formulating a theory of gravity obeying the general principle of relativity, i.e., physical laws are the same in all reference frames. Einstein's basic concept was to drop Newton's idea of a force that is responsible for the attraction of masses. By using the mathematical instrument of differential geometry, in which gravitation and motion of both matter and light result from the geometric properties of space-time. In turn the geometry of space-time, the matter and light in particular, determine its varying curvature [2]. The simplest solution that describes a spherically symmetric, static, uncharged BH is the Schwarzschild (SH) metric which is developed by Schwarzschild in 1916 with radius of its event horizon is named as SH radius. In 1918, Reissner and Nordström proposed an electrically charged vacuum BH solution referred as the Reissner-Nordström (RN) BH. In 1963, Kerr derived the new type of uncharged rotating BH solution which is known as Kerr BH which leads to the discovery of many charged rotating BH solutions with mass, angular momentum and charge.

In addition, one of the major challenges in general relativity (GR) is the existence of essential singularities (which leads to various BHs) and it looks like the common property in most of the solutions of the Einstein field equations (EFEs). In order to resolve this problem, regular black holes (RBHs) have been constructed. Since its metric is regular everywhere, essential singularities can be avoided in the solution of EFEs. The weak energy condition (WEC) is satisfied by these RBHs while some of these violate the strong energy condition (SEC) somewhere in space-time [3, 4]. Since the Penrose cosmic censorship conjecture claims that singularities predicted by GR occur, they can only form behind an event horizon, from within which no information may reach observers outside that surface [5, 6]. Bardeen [7] made a pioneer work who obtained a solution of EFEs without any essential singularity at origin enclosed by an event horizon, known as Bardeen BH which satisfies WEC. Later on, Borde [8] proved that in a large class of space-times that satisfy the WEC the existence of a RBH requires topology change. The coupling of GR to non-linear electromagnetic theory has brought about new sets of charged BHs, which came into the range of RBHs solution. Ayon-Beato and Garcia [9] also found such a RBH solution. Hayward [10] found RBH solution whose static region is Bardeen-like and dynamic regions are Vadiya-like. Berej et al. [11] constructed the first-order correction of the perturbative solution of the coupled equations of the quadratic gravity and nonlinear electrodynamics with the zeroth-order solution coinciding with the ones given by Ayon-Beato and Garcia. Leonardo et al. [12] used many distribution functions (such as the logistic, Fermi-Dirac, Dagum functions etc.) in order to obtain charged RBHs. Kehagias-Sftesos (KS) found an asymptotically flat RBH which usually behaves like a SH-BH in Horava theory [13].

There is an interesting non-minimal coupling theory that couples the gravitational field to other fields using cross terms of the curvature tensor, having arisen a long time ago as alternative theories of gravity. Within these non-minimal theories, exact solutions of stars [14, 15], wormholes [16, 17], BHs [18, 19] and regular magnetic BHs [20] with the Wu-Yang ansatz [21, 22] have been constructed. A family of regular exact spherically symmetric solutions of a non-minimal Einstein-Yang-Mills theory with a gauge field of magnetic Wu-Yang and cosmological constant are presented by Balakin et al. [23, 24]. They have suggested that these solutions and corresponding curvature are invariant being regular everywhere.

In the Universe, BHs are considered like thermal entities which are characterized by macroscopic parameters, such as mass, charge and angular momentum. Thermal properties of BHs are based on the behavior of their macroscopic quantities. Since quantum theories have proved to be the foundation in describing all the fundamental interactions in particle physics, it is natural to expect a quantum theory of gravity. However, due to the smallness of Newton's gravitational constant, the effect of quantum gravity will be very difficult to detect. The discovery of BH thermodynamics opened up a test ground where quantum gravity effects could be important. Pioneer idea about BH temperature and entropy was presented by Bekenstein [25], in which he proposed that BH has an entropy equal to its horizon area with some finite multiple $\varpi \approx \frac{\ln 2}{8\pi}$ for Planck units equal to unity ($G = c = \hbar = k_B = 1$, where G, c, $\hbar$ and k_B are Newton's gravitational constant, speed of light, reduced Planck constant and Boltzmann constant, respectively). Thus, the first law of BH mechanics implies that $S = \varpi A$ and $T = \bar{e}\kappa$ with $8\pi\varpi\bar{e} = 1$ which leads to $\bar{e} = 1/(\ln 2)$ and hence $T = \kappa/(\ln 2)$. Moreover, Bekenstein proposed the "first law of mechanics and thermodynamics" which implies that the term TdS is analogous to $\frac{\kappa}{8\pi}dA$, i.e., BH area and temperature are analogous to entropy and surface gravity, respectively. But his theory was proved inconsistent with given ϖ [26].

In addition, Hawking had a completely independent approach which is known as Hawking Temperature [27]. He proposed that BH emits thermal radiation at temperature proportional to its surface gravity i.e.

$$T = \frac{\kappa\hbar}{2\pi c k_B},$$

which involves gravity, quantum mechanics and thermodynamics. Later on, he realized that the idea of Bekenstein is consistent with his idea and presented BH temperature

$$T = \frac{\kappa}{2\pi},$$

by finding $\bar{e} = 1/2$ and $\varpi = 1/4$. Using this value the Bekenstein entropy area relationship is given by

$$S = S_{BH} = \frac{A}{4}.$$

This surprising result was obtained by using the approximation that the matter field behaves quantum mechanically, while the gravitational field (metric) satisfies the EFEs which holds good for energies below the Planck scale [27].

The concept of entropy allows us to describe the combinatorial problems in powerful language of statistical mechanics. The example of computer algorithm to test a hypothesis in lattice combinatorics is illustrated by Dethridge and Guttmann [28]. A major application of entropy occurred in information theory, likewise, Grimm [29] applies entropy to coding theory using lattice combinatorics. Moreover, the concept of entropy is used to find the structures of magnetohydrodynamic flow fields, which is developed by Dewar [30]. The scope of entropy as a diagnostic tool in higher order partial differential equations is constructed by [31]. Furthermore, the important problem of max-entropy distributions over discrete set of object with observe margins are studied by [32], which leads to the broad application in areas such as economics, information theory, statistical physics, combinatorics, machine learning and very recently, approximation algorithms. They show that how algorithms for counting can be translated into efficient algorithms using max-entropy distributions.

Thermodynamics of BH enables us to study various important thermodynamical quantities of solutions. One of the most important thermodynamical quantities is the thermal stability of BH. They should be stable in dynamical and thermodynamical frameworks due to their physical nature. The instability of BHs means that we may ask whether it may have a phase transition or if it is completely unphysical. BHs have higher entropy than any other object of the same volume [27, 33]. The event horizon only allows us to explore the information about mass, charge and angular momentum (no hair theorem) [34]. So, various BHs have same charge, mass and angular momentum which is formed by different configuration of in-falling matter. These variables are similar to the thermodynamical variables of pressure and energy. There are many possible configurations of a system leading to the same overall behavior. This leads to the concept of maximum entropy of BHs [35] which needs corrections because of quantum fluctuations and paved the way of holographic principle [36, 37]. As BH reduces its size due to Hawking radiation, these fluctuations become very important and are expected to modify the standard relation between entropy and area [38].

There exists several approaches in order to evaluate such corrections. Using non-pertubative quantum gravity, one can calculate the density of microstates for asymptotically flat BHs, which leads to the construction of logarithmic corrections to standard Bekenstein entropy-area relation [37]. In this work, the author has obtained such logarithmic corrections for Banados-Teitelboim-Zanelli (BTZ) BH by calculating the exact partition function. Cardy formula can be applied to generate logarithmic correction terms for all BHs whose microscopic degrees of freedom are explained by conformal field theory [39, 40]. Matter fields analysis in the presence of BHs is used to generate logarithmic corrections for the Bekenstein entropy-area formula [41, 42]. In fact, the corrections to the entropy of dilaton BHs are obtained, which turns out to be logarithmic corrections [43]. The Rademacher expansion of the partition function can also generate such correction terms [44]. However, it is also possible to evaluate higher order correction to BH entropy for analyzing the thermal fluctuations around the equilibrium [35]. It is argued that the results of higher order corrections are applicable to all classical BHs at thermodynamics equilibrium. Moreover, these corrections has been utilized on Schwarzschild-Beltrami-de Sitter BH. It is noted that these corrections are valid and can be applied on small fluctuations near equilibrium [45]. The effects of thermal fluctuations have also been investigated on charged anti de sitter BHs and modified Hayward BHs [38, 46].

A very interesting physical phenomenon in astrophysics is the accretion of fluids onto a BH in the presence of repulsive force called dark energy (DE) which is responsible for current cosmic expansion [47, 48, 49, 50]. When massive condensed objects (e.g. black holes, neutron stars, stars etc.) try to capture a particle of the fluid from its surroundings, then the mass of condensed object has been effected. This process is known as accretion of fluid by condensed object. Due to accretion, the planets and star form inhomogeneous regions of dust and gas. Supermassive BHs exist at the center of giant galaxies, which suggests that they could have formed through an accretion process. It is not necessary that the mass of BH increases due to the accretion process, sometimes in-falling matter is thrown away like cosmic rays [51]. The problem of accretion onto a compact object was firstly investigated by Bondi using the Newtonian theory of gravity [52]. In this extension, Michel [53] proposed its general relativistic version by considering the steady state flow of a perfect fluid onto BH along the radial direction. The stability of Michel type accretion in the subsonic region has been analyzed by Moncrief [54].

Further, it was suggested by Babichev et al. [55] that BH loses mass during the accretion of phantom DE onto it. Furthermore, many authors have worked on radial flows such as accretion of dark matter onto BHs [56] and radial accretion onto cosmological BHs [57, 58], for self-gravitating [59] and perturbation theories [60]. The accretion onto an Einstein-Maxwell-Gauss-Bonnet BH has been presented in [61, 62]. The nonlinear study of a phantom scalar field accreted onto a BH was done by Gonzalez and Guzman [63] with the help of numerical methods. In this direction, some works have also been done by various authors [51, 64, 65] and showed that when phantom-like fluids accrete onto BHs, then mass of BHs decreases, respectively. Kim and Kang [66] and Jimenez Madrid and Gonzalez-Diaz [67] studied accretion of DE on a static BH and a Kerr-Newman BH. Sharif and Abbas [68, 69] discussed the accretion on SH de Sitter and stringy charged BHs due to phantom energy. Radiative models of thin accretion disks for both SH and Kerr BHs in $f(R)$ gravity are investigated by Perez [70]. Cyclic, semi cyclic and heteroclinic flows near $f(R)$, $f(T)$ and general static spherically symmetric BHs are discussed in detail by [71, 72, 73]. The framework of accretion on general static spherical symmetric BHs has been presented by Bahamonde and Jamil [51].

With the passage of time, BH phenomena have become most fascinating in illustrating the significant physical properties. For example, there exists a well-known phenomenon in which a body experiences compression in the angular direction and stretching in radial direction when it falls toward the event horizon of uncharged static BHs [74]-[76]. However, for a RN-BH, a body may experience stretching in the radial direction and compression in the angular direction, depending upon two phenomena: (1) the location of the body, and (2) the charge to mass ratio of BH. Tidal forces change sign in the radial or the angular direction at certain points of the RN-BH, unlike the SH-BH [77]. Geodesic deviations of SH and RN space-times were studied in detail by [74, 78, 79, 80, 81]. However, several BHs of GR in the non-vacuum case have also been presented [82, 83, 84, 85], which need more physical examination. One of them is the Kiselev BH, which shows a new set of phenomena unlike the SH-BH because of the important complex properties [85] and this BH has been surrounded by various types of matter depending on the equation of state (EoS) parameter ω. The Kiselev BH has been investigated through various phenomena, i.e., accretion [86], strong gravitational lensing [87], thermodynamics and phase transitions [88].

In this thesis, we discuss the thermal fluctuations, accretion and tidal forces for several BHs. We analyze the effects of thermal fluctuations on RBH of non-minimal Einstein-Yang-Mill theory with gauge field of magnetic Wu-Yang type and a cosmological constant. We use logarithmic correction terms to discuss various thermodynamical quantities such as pressure, entropy, specific heats, Gibb's free energy and Helmothz free energy of non-minimal RBH. We also utilize the higher order corrected entropy in order to evaluate various thermodynamical properties for RN Anti de Sitter (AdS) with GM and $f(R)$ BHs. Moreover, we extend the framework of accretion on general static spherical symmetric RBHs. We analyze the effect of mass of RBH by choosing different values of EoS parameter. Furthermore, we use the Hamiltonian approach in order to discuss the accretion onto well-known RBHs. We discuss the tidal forces in Kiselev space-time and consider its two cases which leads to Kiselev space-time surrounded by dust ($\omega = 0$) and radiation ($\omega = 1/3$). We solve the geodesic deviation equations to observe the variation of test body in-falling radially toward the Kiselev BH for specific choices of dust and radiation parameter. The thesis is organized as follows:

- In chapter **two**, we discuss RBH of non-minimal Einstein-Yang-Mill theory with gauge field of magnetic Wu-Yang type and a cosmological constant, furthermore, we find logarithmic correction terms which produces various thermodynamical quantities. We investigate the stability of non-minimal RBH using corrected value of specific heat to analyze the phase transition. We also demonstrate the grand canonical and canonical ensembles.

- Chapter **three** discuss the thermal fluctuations by utilizing the higher order correction terms. We analyze the thermodynamical quantities as well as stability globally and locally for two well-known BHs, respectively.

- Chapter **four**, we derive general formalism for spherically static accretion process. We discuss the critical radius, critical points (CPs), speed of sound, radial velocities profile, energy density and rate of change of mass for RBHs.

- Chapter **five** provides the accretion process using Hamiltonian dynamical system and study the system at sonic points. We discuss two RBHs: KS RBH and RBH using Dagum Distribution Function (DDF RBH). We find the solutions for isothermal test fluids of each RBH for different kind of fluids. We investigate the accretion phenomena for polytropic fluid.

- In Chapter **six**, we discuss Kiselev BHs and its two special cases. We find the solutions of the geodesic equations in Kiselev space-time. We derive the tidal forces in Kiselev space-time on a neutral body in radial free fall.

- Concluding remarks are given in chapter **seven**.

Chapter 2

Basic Concepts

In this chapter, we provide some basic background require to understand the present thesis.

2.1 Black Hole

A BH is a region in spacetime where the gravitational field are immensely strong that no matter or light rays leave this region and escape to infinity [89]. BHs are intrinsically relativistic objects presenting two basic properties of Einstein's theory: spacetime singularities and casual horizons. It is believed that it is a region where curvature blows up or other pathological behavior of metric takes place [90]. Singularities occur in Einstein's theory as discussed in the theorems of Penrose and Hawking [5]. The physical significance of classical GR depends upon the protection mechanism from singularities known as Penrose Cosmic Censorship [91]. It states that no naked (essential) singularities exist, i.e., singularities occurring from realistic matter can only form behind the surface known as event horizon, which is defined as the region of spacetime that cannot communicate with the observers outside the surface. A BH is the region contained inside the event horizon which acts like a one way membrane.

According to GR, the relationship between the geometry of space-time and matter contents can be modeled by EFEs. These tensorial equations are related to the curvature of four dimensional (one temporal and three spatial components) manifold and the matter content inside it. These equations can be defined as

$$R_{\alpha\beta} - \frac{1}{2}Rg_{\alpha\beta} = \frac{8\pi G}{c^4}T_{\alpha\beta}, \tag{2.1.1}$$

here, $g_{\alpha\beta}$, R, $R_{\alpha\beta}$ and $T_{\alpha\beta}$ represent the metric tensor, Ricci scalar, Ricci tensor and energy-momentum tensor. By using above mathematical expression of EFEs, various well-known solutions have been developed.

2.1.1 Schwarzschild Black Hole

In 1915, Karl Schwarzschild found the static solution by considering the vacuum in EFEs, i.e, ($T_{\alpha\beta} = 0$). He showed that there is a spherical symmetric BH solution describing empty space outside a concentration of mass located in a point [92]. The line element of spherically symmetric SH-BH solution is given by

$$ds^2 = X(r)dt^2 - (X(r))^{-1}dr^2 - r^2(d\theta^2 + \sin\theta d\phi^2), \tag{2.1.2}$$

where the metric function is defined by

$$X(r) = 1 - \frac{2M}{r}. \tag{2.1.3}$$

The horizon of SH-BH lies at the radius $r = r_+$, i.e.,

$$r_+ = 2M. \tag{2.1.4}$$

From SH metric, it can be seen that ds^2 (by setting $dr = d\theta = d\phi = 0$) behaves timelike, lightlike, or spacelike depending on whether the radius is greater than, equal to, or less than r_+:

$$ds^2 = (1 - \frac{r_+}{r}). \tag{2.1.5}$$

Since the world-line of a massive observer must be timelike which follows that a massive observer can remain on rest only outside the horizon, $r > r_+$. An object at rest at the horizon, $r = r_+$, follows a null geodesic, which is to say it is a possible world-line of a massless particle, a photon. Inside the horizon, $r < r_+$, neither massive nor massless objects can remain at rest. To remain at rest, a particle inside the horizon would have to go faster than speed of light [93].

2.1.2 Reissner-Nordström Black Hole

This is the first charged BH which was developed by Hans Reissner (1916), Hermann Weyl (1917) and Gunnar Nordström (1918). The metric function of RN-BH is

$$X(r) = 1 - \frac{2M}{r} + \frac{q^2}{r^2}, \tag{2.1.6}$$

where q is the electric charge of the BH. However, this BH reduces to SH-BH by setting $q = 0$. It can be seen from above metric function that this BH possesses two horizons which can be obtained through the vanishing of $X(r)$, i.e., $X(r) = 0$ which leads to

$$r_{\pm} = M \pm \sqrt{M^2 - q^2}, \tag{2.1.7}$$

here r_+ and r_- are the outer and inner horizons, respectively. It is straightforward to check that RN time coordinate t is timelike outside the outer horizon, $r > r_+$, spacelike between the horizons $r_- < r < r_+$, and again timelike inside the inner horizon $r < r_-$. Conversely, the radial coordinate r is spacelike outside the outer horizon, $r > r_+$, timelike between the horizons $r_- < r < r_+$, and spacelike inside the inner horizon $r < r_-$ [93].

The physical meaning of this strange behavior is akin to that of SH-BH. As in SH-BH, outside the outer horizon, space is falling at less than the speed of light; at the outer horizon space hits the speed of light; and inside the outer horizon space is falling faster than speed of light. But a new ingredient appears such as charge (q) whose gravitational repulsion caused by the negative pressure of the electric field reduces the flow of space, which results the reduction of speed of light at the inner horizon. Inside the inner horizon, space is falling at less than the speed of light [93].

2.2 Regular Black holes

One of the major challenge in BH physics and GR is the existence of curvature singularities (which leads to many BHs) beyond the event horizon and it looks like the most natural physical conditions in BH solutions. Singularities are the regions where GR does not work since those regions do not belong to the Riemannian space-time. Many scientists have made numerous attempts in the hope that the singularities will be cured by the effects of quantum gravity [94]. In order to elaborate this issue, we consider the line element of asymptotically flat static, spherical symmetric metric as follows

$$ds^2 = X(\bar{\rho})dt^2 + \frac{dr^2}{X(\bar{\rho})} - r^2(\bar{\rho})(d\theta^2 + \sin\theta d\phi^2), \tag{2.2.1}$$

where $\bar{\rho}$ is the quasi global coordinate which is particularly convenient for dealing with Killing horizons. At $\bar{\rho} \to \infty$ (asymptotically flat), we have $X(\bar{\rho}) \to 1$ and $r \equiv \bar{\rho}$ [94].

Bardeen [7] was the first who put forward the very idea of singularity free RBH solution, as an example, a particular metric function

$$X(\bar{\rho}) = 1 - \frac{M\bar{\rho}^2}{\left(\bar{\rho}^2 + q^2\right)^{3/2}} \quad r \equiv \bar{\rho}, \tag{2.2.2}$$

where M is the mass, q is the electric charge. For $q^2 < \frac{16M}{27}$, there exist two horizons $r_\pm$ where r_- and r_+ are Cauchy (inner) and event (outer) horizons, respectively [95]. The range $r_- < r < r_+$ corresponds to the trapped surfaces such that the ingoing and outgoing light rays bounded by the surfaces $r = r_-$ and $r = r_+$ converge towards the singularity. In gravitational collapse such trapped surfaces produce the singularity. For $r \to 0$, Bardeen solution behaves like a de Sitter while for large r, it corresponds to SH-BH asymptotically [96].

However, one can set $r \equiv \bar{\rho}$ in RBH solutions [97, 98]. This exists by virtue of EFEs which implies that energy-momentum tensor of the matter configuration satisfies the condition,

$$T_0^0 = T_1^1,$$

which can also be written in the form of $p_r = -\varepsilon$ where p_r and ε are the radial pressure and energy density, respectively. The aforementioned condition is invariant under the radial boosts, making it possible to describe the vacuum matter [98]. One can construct RBHs by replacing BH interior by its core (which is regular) [99, 100]. The singularity of BH is connected with de Sitter core by a thin boundary [101]. A general class of BH solutions satisfying the WEC but violates the SEC which are regular at center and everywhere else.

2.3 Black hole Thermodynamics

The first hints of a fundamental relationship between gravitation, thermodynamics, and quantum theory came from studying BHs. It is shown that the laws of BH mechanics are equivalent to the ordinary laws of thermodynamics applied to a system containing a BH. The subject inextricably blends both classical thermodynamics and quantum physics, yielding deep insights into both the nature of quantum phenomena occurring in strong gravitational fields and some of the most baffling paradoxes in physics [102].

2.3.1 Laws of Black Hole Mechanics

The laws of BH mechanics are as follows [103]:

- Zeroth Law can be defined as the surface gravity κ of a stationary BH which does not change throughout its event horizon. The surface gravity is, by definition, the value of the free-fall acceleration, calculated at the event horizon in terms of the particle acceleration.

- The first Law of BH thermodynamics read to be

$$dM = \frac{\kappa}{8\pi} dA + \Omega dJ, \tag{2.3.1}$$

where A and Ω are horizon area and angular velocity, respectively. Also the last term of above equation is known as the work done over BH by adding the angular momentum dJ.

- Second Law can be defined as the horizon area of a BH could never be decreased by any physical process, i.e.,

$$\delta A \geq 0. \tag{2.3.2}$$

  The *second law* is also known as *area law*.

- Third Law is known as there is no procedure able to bring the surface gravity of a BH to zero through arbitrary finite sequence of operations.

2.3.2 Laws of Black Hole Thermodynamics

Four laws of BH thermodynamics are given as follows [104]:

- Zeroth Law can be defined by the temperature does not change throughout the system in thermal equilibrium.

- First Law describes the small variations between equilibrium configuration of a system [103]

$$dE = TdS + work\ \ terms, \tag{2.3.3}$$

  where E is the energy, T is the temperature and S is the entropy of BH.

- Second Law is the entropy S of a BH always increases in any physical process for a closed system, i.e.,

$$dS \geq 0. \tag{2.3.4}$$

- Third Law is defined by BH temperature could never be decreased to absolute zero by a finite sequence of operations.

2.4 Thermal Fluctuations

In statistical mechanics, thermal fluctuations are the random variations (deviations) of a system from its average state, which occur in a system at equilibrium. As the temperature rises, all thermal fluctuations become rapidly increase, otherwise it decreases as the temperature become absolute zero. All the degree of freedom of any system is affected by the thermal fluctuations. There may be a random rotations, random variations an so forth. Thermodynamical variables such as entropy, pressure and temperature undergo the thermal fluctuations [105]. In BH thermodynamics, the quantum fluctuations give rise to many important problems and thermal fluctuations in the geometry of BH is one of them. To solve this problem, it is necessary to contribute the correction terms of entropy when the size of BH is reduced due to the Hawking radiation and its temperature is increased. One can neglect the correction terms for large BHs, as the thermal fluctuations may not occur in it. Hence, the thermodynamics of BH is modified by the thermal fluctuations and becomes more important for smaller size BHs with sufficiently high temperature [106]. The effect of thermal fluctuations on the entropy of general spherical symmetric metric can be done by utilizing the Euclidean quantum gravity formalism whose partition function can be defined as [107, 108, 109, 110, 111]

$$\mathbb{Y} = \int DgDAe^{-I},$$

where the Euclidean action is represented by $I \to -iI$ for this system. The partition function can be related to statistical mechanical terms as follows [112, 113]

$$\mathbb{Y} = \int_0^\infty DE\xi(E)e^{(-\vartheta E)},$$

where $\vartheta = T^{-1}$.

Moreover, the density of states can be obtained with the help of partition functions together with Laplace inverse as

$$\xi(E) = \frac{1}{2\pi i}\int_{\vartheta_0 - i\infty}^{\vartheta_0 + i\infty} d\vartheta e^{S(\vartheta)},$$

where $S = \vartheta E + \ln \mathbb{Y}$. This entropy can be calculated by neglecting all thermal fluctuations around the equilibrium temperature ϑ_0. However, by utilizing the thermal fluctuations along with Taylor series expansion around ϑ_0, $S(\vartheta)$ can be written as [106, 114]

$$S = S_0 + \frac{1}{2!}\left(\vartheta - \vartheta_0\right)^2 \left(\frac{\partial^2 S(\vartheta)}{\partial \vartheta^2}\right)_{\vartheta=\vartheta_0} + \frac{1}{3!}\left(\vartheta - \vartheta_0\right)^3 \left(\frac{\partial^3 S(\vartheta)}{\partial \vartheta^3}\right)_{\vartheta=\vartheta_0} + \ldots.$$

As we know that the first derivative will vanish and hence, density of states turn out to be

$$\xi(E) = \frac{e^{S_0}}{2\pi i}\int_{\vartheta_0 - i\infty}^{\vartheta_0 + i\infty} d\vartheta e^{\frac{1}{2!}\left(\vartheta - \vartheta_0\right)^2 \left(\frac{\partial^2 S(\vartheta)}{\partial \vartheta^2}\right)_{\vartheta=\vartheta_0} + \frac{1}{3!}\left(\vartheta - \vartheta_0\right)^3 \left(\frac{\partial^3 S(\vartheta)}{\partial \vartheta^3}\right)_{\vartheta=\vartheta_0} + \ldots}. \tag{2.4.1}$$

For simplicity, we assume the first term in the exponential, so one can write it as

$$\xi(E) = \frac{e^{S_0}}{2\pi i}\int_{\vartheta_0 - i\infty}^{\vartheta_0 + i\infty} d\vartheta e^{\frac{1}{2}\left(\vartheta - \vartheta_0\right)^2 \left(\frac{\partial^2 S(\vartheta)}{\partial \vartheta^2}\right)_{\vartheta=\vartheta_0}},$$

here, we consider the second derivative is positive and defined as

$$\delta_1 = \left(\frac{\partial^2 S(\vartheta)}{\partial \vartheta^2}\right)_{\vartheta=\vartheta_0}.$$

By changing variable $(\vartheta - \vartheta_0)$ to $i\mathbb{Z}$, we get

$$\xi(E) = \frac{e^{S_0}}{2\pi i}\int_{-i\infty}^{i\infty} d\mathbb{Z} e^{-\frac{1}{2}\delta_1 \mathbb{Z}^2}.$$

Using standard integral and re-substituting, we can obtain

$$\xi(E) = \frac{e^{S_0}}{\sqrt{2\pi}\Big(\frac{\partial^2 S(\vartheta)}{\partial \vartheta^2}\Big)^{1/2}_{\vartheta=\vartheta_0}}.$$

Note that the density function $\xi(E)$ and $\Big(\frac{\partial^2 S(\vartheta)}{\partial \vartheta^2}\Big)_{\vartheta=\vartheta_0}$ have dimensions of inverse energy and energy squared, respectively. Henceforth, the logarithm of density of states $\xi(E)$ is then the microcanonical entropy,

$$S := \ln \xi(E) = S_0 - \frac{1}{2}\ln\Big(\frac{\partial^2 S(\vartheta)}{\partial \vartheta^2}\Big)^{\frac{1}{2}}_{\vartheta=\vartheta_0}.$$

It is possible to simplify this expression by using the relation between the conformal field theory and the microscopic degrees of freedom of a BH . Thus, we can consider the entropy of the form $S = m_1\vartheta^{n_1} + m_2\vartheta^{-n_2}$, where m_1, m_2, n_1, n_2 are all positive constants [35]. This has an extremum at $\vartheta_0 = \Big(\frac{m_2 n_2}{m_1 n_1}\Big)^{\frac{1}{n_1+n_2}} = T^{-1}$ and expanding entropy around this extremum is

$$\begin{aligned} S(\vartheta) &= \Big[\big(\frac{n_2}{n_1}\big)^{\frac{n_1}{n_1+n_2}} + \big(\frac{n_1}{n_2}\big)^{\frac{n_2}{n_1+n_2}}\Big]\Big(m_1^{n_2} m_2^{n_1}\Big)^{\frac{1}{n_1+n_2}} \\ &+ \frac{1}{2}\Big[(n_1+n_2) n_1^{\frac{n_2+2}{n_1+n_2}} n_2^{\frac{n_2-2}{n_1+n_2}}\Big]\Big(m_1^{n_2+2} m_2^{n_1-2}\Big)^{\frac{1}{n_1+n_2}}(\vartheta-\vartheta_0)^2. \end{aligned}$$

Here, we can write

$$\begin{aligned} S_0 &= \Big(\big(\frac{n_2}{n_1}\big)^{\frac{n_1}{n_1+n_2}} + \big(\frac{n_1}{n_2}\big)^{\frac{n_2}{n_1+n_2}}\Big)\Big(m_1^{n_2} m_2^{n_1}\Big)^{\frac{1}{n_1+n_2}} \\ \Big(\frac{\partial^2 S(\vartheta)}{\partial \vartheta^2}\Big)_{\vartheta=\vartheta_0} &= \frac{1}{2}\Big[(n_1+n_2) n_1^{\frac{n_2+2}{n_1+n_2}} n_2^{\frac{n_2-2}{n_1+n_2}}\Big]\Big(m_1^{n_2+2} m_2^{n_1-2}\Big)^{\frac{1}{n_1+n_2}} \end{aligned}$$

One can solve the above equation for m_1, m_2 and express the entropy as

$$\Big(\frac{\partial^2 S(\vartheta)}{\partial \vartheta^2}\Big)_{\vartheta=\vartheta_0} = \Im S_0 T^2$$

where

$$\Im = \frac{(n_1+n_2)n_1^{\frac{n_2+2}{n_1+n_2}} n_2^{\frac{n_2-2}{n_1+n_2}}}{\left(\frac{n_2}{n_1}\right)^{\frac{n_1}{n_1+n_2}} + \left(\frac{n_1}{n_2}\right)^{\frac{n_2}{n_1+n_2}}} \times \left(\frac{n_2}{n_1}\right)^{\frac{2}{n_1+n_2}},$$

which can be absorbed using a redefinition, as it does not depend upon BH parameter [46]. By using $T = \frac{1}{\vartheta_0}$, we can get

$$\left(\frac{\partial^2 S(\vartheta)}{\partial \vartheta^2}\right)_{\vartheta=\vartheta_0} = S_0 \vartheta_0^{-2}$$

Hence, the logarithmic corrected entropy can be written in generalized form as follows

$$S = S_0 - \frac{b_1}{2} \ln S_0 T^2. \tag{2.4.2}$$

Now consider the higher order terms in Eq.(2.4.1) and using the similar technique which is also discussed in [35], one can obtain the higher order corrected entropy as

$$S = S_0 - \frac{b_1}{2} \ln S_0 T^2 + \frac{b_2}{S_0}, \tag{2.4.3}$$

where b_1 and b_2 are introduced as constant parameters.

- The original results can be obtained by setting $b_1, b_2 \to 0$, i.e., the entropy without any correction terms. One can consider this case for large BHs where temperature is very small.

- The usual logarithmic corrections can be recovered by setting $b_1 \to 1$ and $b_2 \to 0$ which leads to Eq.(2.4.2).

- The second order correction term can be obtained by setting $b_1 \to 0$ and $b_2 \to 1$ which represents the inverse proportionality of original entropy.

- Finally, higher order corrections can be found by setting $b_1 \to 1$ and $b_2 \to 1$.

Hence, the first order correction term represent the logarithmic correction but the second order correction term represents the inverse proportionality of original entropy.

So, quantum correction can be considered by these correction terms. As mentioned above, one can avoid these correction terms for larger BHs. However, these correction terms can be considered for BHs whose size decreases due to Hawking radiation, while temperature increases and also thermal fluctuation in the geometry of BH increases [106].

2.5 Heat Capacities

The heat capacity (C) of a system is the amount of heat required to increase the temperature of system by $1c^{\circ}$ (= 1K), i.e.

$$C = \frac{dq}{dT},$$

where q is the heat.

- Constant Volume:

  $q_V = \Delta E$, and $\partial q_V = dE$

  $$C_V = \frac{\partial q_V}{\partial T} = \left(\frac{\partial E}{\partial T}\right)_V.$$

  Using the well known relation internal energy (E)

  $$E = \int T dS, \tag{2.5.1}$$

  we can obtain

  $$C_V = \left(T\frac{\partial S}{\partial T}\right)_V.$$

- Constant Pressure:

  $q_P = \Delta H$, and $\partial q_P = \partial H$

  $$C_P = \frac{\partial q_P}{\partial T} = \left(\frac{\partial H}{\partial T}\right)_P.$$

Using the relation of enthalpy H

$$\begin{aligned} H &= E + PV, \\ C_P &= \left(T\frac{\partial(E+PV)}{\partial T}\right)_V. \end{aligned}$$

2.6 Accretion

When massive condensed objects (e.g. BHs, neutron stars, stars etc.) try to capture a particle of the fluid from its surroundings, then the mass of condensed object has been effected. This process is known as accretion of fluid by condensed object. Due to accretion the planets and star form inhomogeneous regions of dust and gas. Supermassive BHs exist at the center of giant galaxies, which suggests that they could have formed through an accretion process. Accretion is the process that allows BH sources to emit electromagnetic radiation and other forms of energy, because BHs are so small in size compared to the spatial scale of their sources of fueling. Accretion is generally believed to be a process involving rotationally supported flows. Matter in such a flow must lose angular momentum in order to move inward and release gravitational binding energy.

2.6.1 Role of Dark Energy in Accretion

At present, the type 1a supernova [115], cosmic microwave background radiation [116], and the large scale structure [117] have shown that our universe is currently in an accelerating expansion period. This acceleration is caused by some unknown matter which the property that negative pressure and positive energy density satisfy $\rho + 3p < 0$; it is known as 'dark energy'. It is well-known observation that DE is responsible for current acceleration of Universe which violates the null energy condition (NEC) and WEC [118, 119], and produces strong repulsive gravitational effects. Recent observations suggest that approximately 74% of our universe is occupied by DE and the rest 22% and 4% is of dark matter and ordinary matter, respectively. Nowadays, DE is the most challenging problem in astrophysics. The mathematical description of DE can be acquired through the relationship between energy density and pressure by a perfect fluid with EoS $p = \omega\varepsilon$. One can characterize different accelerated eras of the universe through EoS parameter (ω) such as phantom-like era ($\omega < -1$), quintessence ($-1 < \omega < -1/3$) and the cosmological constant ($\omega = -1$) [120]. In order to explain DE phenomenon, various DE models have been proposed such as k-essence, DBI-essence, H-essence, dilaton, tachyon, Chaplygin gas, etc [121, 122, 123, 124, 125, 126, 127, 128]. The presence of an event horizon is a distinctive feature of a BH, which act as one way membrane through which accreting fluid or gas disappears and leads to several important issues. For instance, radiation emitted near BH undergoes the effect of strong gravitational lensing and appears as the image of BHs shadow surrounded by sharp light ring. However, no inner boundary conditions are necessary for the equation of motion in case of BH accretion [129].

2.6.2 General Formalism for Accretion

The generalized static spherical symmetry is characterized by the following line element

$$ds^2 = -X(r)dt^2 + \frac{1}{Y(r)}dr^2 + Z(r)(d\theta^2 + \sin\theta^2 d\phi^2), \tag{2.6.1}$$

where $X(r) > 0$, $Y(r) > 0$ and $Z(r) > 0$ are the functions of r only. The energy-momentum tensor is considered as perfect fluid which is isotropic and inhomogeneous and defined as follows

$$T_{\mu\nu} = (\varepsilon + p)u_\mu u_\nu + pg_{\mu\nu}, \tag{2.6.2}$$

where p is pressure, ε is energy density and u^μ is the four velocity which is given by

$$u^\mu = \frac{dx^\mu}{d\tau} = (u^t, u^r, 0, 0), \tag{2.6.3}$$

where τ is the proper time. We have u^θ and u^ϕ both equal to zero due to spherical symmetry restrictions. Here pressure, energy density and four velocity components are only the functions of r. The normalization condition of four velocity must satisfy $u^{\mu}u_{\mu} = -1$, we get

$$u^{t} := \frac{dt}{d\tau} = \sqrt{\frac{u^{2}+Y}{XY}}, \tag{2.6.4}$$

where $u = dr/d\tau = u^{r}$[51] while u^{t} can be negative or positive due to square root which represents the backward or forward in time conditions. However, $u < 0$ is required for accretion process otherwise for any outward flows $u > 0$. Both inward and outward flows are very important in astrophysics. One can assume that the fluid is DE or any kind of dark matter. In generalized Michel's theory, the formalism of accretion process onto a spherical symmetric BH have been developed in the presence of DE. In DE accretion, Babichev et al. [55] have introduced the above generalization on SH-BH. Similarly, some authors [51, 64] have extended this procedure for generalized static spherically symmetric BH. In these works, energy momentum conservation law plays an important role which turns out to be

$$(\varepsilon+p)u\frac{X(r)}{Y(r)}\sqrt{u^{2}+Y(r)}Z(r) = A_{0}, \tag{2.6.5}$$

where A_{0} is the constant of integration. Using $u_{\mu}T^{\mu\nu}_{\mu} = 0$, we obtain continuity (or relativistic energy flux) equation

$$u^{\mu}\varepsilon_{,\mu} + (\varepsilon+p)u^{\mu}_{;\mu} = 0, \tag{2.6.6}$$

here $p = p(\varepsilon)$ which may be a certain EoS. After some calculations, the above equation becomes

$$\frac{\varepsilon^{'}}{\varepsilon+p} + \frac{u^{'}}{u} + \frac{X^{'}}{2X} + \frac{Y^{'}}{2Y} + \frac{Z^{'}}{Z} = 0, \tag{2.6.7}$$

here prime represents the derivative with respect to r. By integrating the last equation, we obtain

$$uZ(r)\sqrt{\frac{X(r)}{Y(r)}}e^{\int\frac{d\varepsilon}{\varepsilon+p(\varepsilon)}} = -A_{1}, \tag{2.6.8}$$

where A_1 is a constant of integration. By equating Eqs.(2.6.5) and (2.6.8), we get

$$(\varepsilon+p)\sqrt{\frac{X(r)}{Y(r)}}\sqrt{u^2+Y}e^{-\int\frac{d\varepsilon}{\varepsilon+p(\varepsilon)}}=-\frac{A_0}{A_1}=A_3. \tag{2.6.9}$$

Moreover, the equation of mass flux yields

$$\varepsilon u\sqrt{\frac{X(r)}{Y(r)}}Z(r)=A_2, \tag{2.6.10}$$

where A_2 is the constant of integration. By using Eqs.(2.6.5) and (2.6.10), we obtain the following important relation

$$\frac{(\varepsilon+p)}{\varepsilon}\sqrt{\frac{X(r)}{Y(r)}}\sqrt{u^2+Y}=\frac{A_1}{A_2}\equiv A_4. \tag{2.6.11}$$

Differentiation of Eqs.(2.6.10) and (2.6.11) and some manipulation leads to

$$\left(\mathbb{V}^2-\frac{u^2}{u^2+Y}\right)\frac{du}{u}+\left((\mathbb{V}^2-1)\left(\frac{X'}{X}-\frac{Y'}{Y}\right)+\frac{Z'}{Z}\mathbb{V}^2-\frac{Y'}{2\,(u^2+Y)}\right)dr=0. \tag{2.6.12}$$

In addition, we have introduced the variable

$$\mathbb{V}^2\equiv\frac{d\ln\varepsilon+p}{d\ln\varepsilon}-1. \tag{2.6.13}$$

If the bracketed terms in Eq.(2.6.12) vanishes, we obtain the CP (where speed of sound equal to speed of flow) which is located at $r=r_c$. Hence at CP, we get

$$\mathbb{V}_c^2=\frac{u_c^2}{u_c^2+Y(r_c)}, \tag{2.6.14}$$

and Eq.(2.6.12) turns out to be

$$(\mathbb{V}_c^2-1)\left(\frac{X'(r_c)}{X(r_c)}-\frac{Y'(r_c)}{Y(r_c)}\right)+\frac{Z'(r_c)}{Z(r_c)}\mathbb{V}_c^2=\frac{Y'(r_c)}{2\,(u_c^2+Y(r_c))}. \tag{2.6.15}$$

Also, u_c is the critical speed of flow evaluated at critical value $r = r_c$. We can obtain the following relations by using the above two expressions

$$u_c^2 = \frac{Y(r_c)Z(r_c)X'(r_c)}{2X(r_c)Z'(r_c)}, \quad \mathbb{V}_c^2 = \frac{Z(r_c)X'(r_c)}{2X(r_c)Z'(r_c)+Z(r_c)X'(r_c)}. \tag{2.6.16}$$

The speed of sound is evaluated at $r = r_c$ as follows

$$c_s^2 = \frac{dp}{d\varepsilon}|_{r=r_c} = A_4\sqrt{\frac{Y(r_c)}{X(r_c)(u_c^2+Y(r_c))}} - 1, \tag{2.6.17}$$

Obviously, u_c^2 and $\mathbb{V}_c^2$ can never be negative which leads to

$$\frac{X'(r_c)}{Z'(r_c)} > 0, \tag{2.6.18}$$

Moreover, the rate of change of BH mass can be defined as follows [64]

$$\dot{M}_{acc} = 4\pi A_3 M^2(\varepsilon + p), \tag{2.6.19}$$

Here dot is derivative with respect to time. We can observe that the mass of BH will increase for the fluid $\varepsilon + p > 0$ and hence the accretion occurs outside the BH. Otherwise, for $\varepsilon + p < 0$ like fluid, the mass of BH will decrease. The mass of BH cannot remain fixed because it will decrease due to Hawking radiations while it will increase in accretion [51].

2.7 Tidal Forces in a Black Hole

Consider the spherical symmetric distribution of non-interacting particles falling freely towards the Earth in Newtonian theory. Each particle moves toward the center of Earth on a straight line, but due to the gravitational pull near the Earth is stronger so those particles closer to Earth fall faster. Hence, the spherical particles no longer remain in spherical shape but is distorted into ellipsoid with same volume. Thus, the gravitation produces a tidal force on the spherical particles. Now, the tidal force effected the particle in two ways, firstly, an elongation of the distribution in the direction of motion and secondly, a compression of distribution in transverse direction. The same results happen in particles falling freely towards the spherical object in GR, but if the object is a BH then the effect of tidal forces becomes infinite as the particles reached towards the singularity. We can gain some idea of this by considering the equation of geodesics deviation as discussed in the following subsection, in which the spacelike components of orthogonal connecting vector ζ^{α} connecting two neighboring particles in free fall [74].

2.7.1 Equation of Geodesic Deviation

For elaborating this phenomenon, we consider a free test particles move on time-like geodesics in GR. Therefore, we assume two-surface $\mathbb{S}$ ruled by congruence of timelike geodesics. It means that exactly one curve moves through every point of $\mathbb{S}$ in a family of geodesics. The parametric equation of $\mathbb{S}$ is defined by

$$x^{\alpha} = x^{\alpha}(\tau, \mathbf{v}), \tag{2.7.1}$$

where τ and $\mathbf{v}$ is the proper time along geodesics and distinct geodesics, respectively. Two vectors field of $\mathbb{S}$ are defined by

$$v^{\alpha} = \frac{dx^{\alpha}}{d\tau}, \qquad \zeta^{\alpha} = \frac{dx^{\alpha}}{dv}, \tag{2.7.2}$$

where v^{α} and ζ^{α} are the tangent vector and connecting vector, respectively. The commutator of v^{α} and ζ^{α} satisfy the following conditions[74]

$$[v, \zeta]^{\alpha} = 0. \tag{2.7.3}$$

Now we replace the partial derivative by covariant derivative in Lie derivative as follows

$$\begin{aligned} L_v\zeta^\alpha &= 0 \\ v^\beta\partial_\beta\zeta^\alpha - \zeta^\beta\partial_\beta v^\alpha &= 0 \\ v^\beta\nabla_\beta\zeta^\alpha - \zeta^\beta\nabla_\beta v^\alpha &= 0 \\ \nabla_v\zeta^\alpha - \nabla_\zeta v^\alpha &= 0. \end{aligned} \tag{2.7.4}$$

Applying covariant derivative on Eq.(2.7.4) w. r. t v^α, we have

$$\nabla_v\nabla_\zeta v^\alpha = \nabla_v\nabla_v\zeta^\alpha. \tag{2.7.5}$$

Using the following identity

$$\nabla_{\bar{X}}(\nabla_{\bar{Y}}\bar{Z}^\alpha) - \nabla_{\bar{Y}}(\nabla_{\bar{X}}\bar{Z}^\alpha) - \nabla_{[\bar{X},\bar{Y}]}\bar{Z}^\alpha = R^\alpha_{\beta\gamma\delta}\bar{Z}^\beta\bar{X}^\gamma\bar{Y}^\delta. \tag{2.7.6}$$

If we replace $v^\alpha = \bar{Z}^\alpha = \bar{X}^\alpha$ and $\bar{Y}^\alpha = \zeta^\alpha$, then second term on right side vanishes and third term vanishes by using Eq.(2.7.4) and finally, we get

$$R^\alpha_{\beta\gamma\delta}\bar{Z}^\beta\bar{X}^\gamma\bar{Y}^\delta = \nabla_v\nabla_\zeta v^\alpha. \tag{2.7.7}$$

Using (2.7.5) and the definition $\frac{D^2\zeta^\alpha}{D\tau^2} = \nabla_v\nabla_v\zeta^\alpha$, Eq.(2.7.7) becomes the equation of geodesics deviation [74]

$$\frac{D^2\zeta^\alpha}{D\tau^2} - R^\alpha_{\beta\gamma\delta}v^\beta v^\gamma\zeta^\delta = 0. \tag{2.7.8}$$

Chapter 3

Effects of Thermal Fluctuations on Non-minimal Regular Magnetic Black Hole

In this chapter, we analyze the effects of thermal fluctuations on a RBH of the non-minimal Einstein-Yang-Mill theory with gauge field of magnetic Wu-Yang type and a cosmological constant. We consider the logarithmic corrected entropy in order to analyze the thermal fluctuations corresponding to non-minimal RBH thermodynamics. In this scenario, we develop various important thermodynamical quantities, such as entropy, pressure, specific heats, Gibbs free energy and Helmholtz free energy. We investigate the first law of thermodynamics in the presence of logarithmic corrected entropy and non-minimal RBH. We also discuss the stability of this RBH using various frameworks such as the γ factor (the ratio of heat capacities), phase transition, grand canonical ensemble and canonical ensemble.

3.1 Non-minimal Regular Black Hole

New exact regular spherically symmetric solution of non-minimal Einstein-Yang-Mills theory with magnetic charge of Wu-Yang gauge field and the cosmological constant is presented by Balakin et al. [23]. The metric function corresponding to static spherically symmetric space-time in the line element (2.1.2) is

$$X(r) = 1 + \left(\frac{r^4}{r^4 + 2Q_m^2\mathfrak{q}}\right)\left(-\frac{2M}{r} + \frac{Q_m^2}{r^2} - \frac{\Lambda r^2}{3}\right). \tag{3.1.1}$$

This contains four important parameters such as Λ, $\mathfrak{q}$, Q_m and M which represent the cosmological constant, non-minimal parameter of the theory, magnetic charge of gauge field Wu-Yang type and mass of the object, respectively. It is assumed that $\mathfrak{q} > 0$, $\Lambda > 0$, $\Lambda \leq 0$, $Q_m^2 > 0$ and $M \geq 0$. The limiting case $\mathfrak{q} = 0$ gives the magnetic RN solution with cosmological constant,

$$X(r) = 1 + \frac{2M}{r} - \frac{Q_m^2}{r^2} - \frac{\Lambda r^2}{3}. \tag{3.1.2}$$

At $r = 0$, we find the curvature singularities. For $\mathfrak{q} < 0$ with finite positive r, we have space-time curvature singularities.

One can obtain no singularities for $\mathfrak{q} > 0$ i.e. $X(r)$ near the center behaves

$$X(r) = 1 + \frac{r^2}{2q^2} - \frac{Mr^3}{Q_m^2\mathfrak{q}} + \ldots. \tag{3.1.3}$$

One can see $X(0) = 1$, $X'(0) = 0$ and $X''(0) = \frac{1}{\mathfrak{q}^2}$. Hence $r = 0$ is the minimum of the regular function $X(r)$ which is independent of cosmological constant and the mass of BH. Since $X(0) = 1$ and $R(0) = \frac{6}{\mathfrak{q}}$ shows the curvature scalar is regular at center. For $q > 0$, other curvatures invariants and quadratic scalar $R_{\mu\nu}R^{\mu\nu} = \frac{9}{\mathfrak{q}^2}$ are also finite at center [23]. Thus, due to non-minimality of the model, space-time is truly regular in center.

The metric function (3.1.1) is described by four parameters with different units: Λ, M, Q_m and $\mathfrak{q}$. We can rewrite the metric function (3.1.1) in dimensionless form by introducing the following dimensionless quantities [24]

$$\begin{aligned} \chi_\Lambda &= \sqrt{\frac{3}{|\Lambda|}},\ \chi_g = 2M,\ \chi_\mathfrak{q} = \left(2Q_m^2\mathfrak{q}\right)^{\frac{1}{4}},\ \chi_{Q_m} = Q_m \\ \sigma_a &= \frac{\chi_g}{\chi_\Lambda},\ \eta_a = \left(\frac{\chi_{Q_m}}{\chi_\Lambda}\right)^2,\ \zeta_a = \left(\frac{\chi_\mathfrak{q}}{\chi_\Lambda}\right)^4,\ \rho_a = \left(\frac{r}{\chi_\Lambda}\right)^2. \end{aligned} \tag{3.1.4}$$

In terms of these variables, the metric function $X(r)$ in (3.1.1) can be rewritten in $X(\rho_a)$ as follows

$$X(\rho_a) = 1 + \left(\frac{\rho_a^2\left(-\rho_a^4 - \sigma_a\rho_a + \eta_a\right)}{\rho_a^4 + \zeta_a}\right). \tag{3.1.5}$$

The most important feature of metric function (3.1.1) is horizons radius which are depending upon different values of parameters. The horizon radius of non-minimal RBH could be obtained by considering real roots of the following equation

$$-\frac{\Lambda r_+^6}{3} + r_+^4 - 2Mr_+^3 + Q_m^2 r_+^2 + 2Q_m^2\mathfrak{q} = 0. \tag{3.1.6}$$

For $\Lambda > 0$, the non-minimal RBH solution can have three horizons depending upon different values of parameters, the cosmological horizon, Cauchy horizon and event horizon. On the other hand, for $\Lambda \leq 0$, it can have two horizons depending upon different values of parameters, i.e, Cauchy and event horizons. There is no cosmological horizon in this case [12]. We want to discuss the thermal quantities on the outer horizon and we refer to it by r_+.

One can obtain the mass of the non-minimal RBH in horizon radius and other parameters as follows

$$M = \frac{-\Lambda r_+^6 + 3Q_m^2 r_+^2 + 3r_+^4 + 6Q_m^2 \mathfrak{q}}{6r_+^3}, \tag{3.1.7}$$

which implies that $r_+ \neq 0$. The entropy of non-minimal RBH which is related to area of BH horizon is

$$S_0 = \pi r_+^2, \tag{3.1.8}$$

and volume is

$$V = \frac{4}{3}\pi r_+^3. \tag{3.1.9}$$

The temperature of non-minimal RBH can be written as

$$\begin{aligned} T &= \frac{X'(r)}{4\pi} \\ &= \frac{-\Lambda r_+^9 + 3Mr_+^6 + 6Q_m^4 \mathfrak{q} r_+^2 - 18MQ_m^2 \mathfrak{q} r_+^2 - (6\mathfrak{q}\Lambda + 3)Q_m^2 r^5}{6\pi\left(r_+^4 + 2Q^2\mathfrak{q}\right)^2}, \end{aligned} \tag{3.1.10}$$

where the mass M is given in Eq.(3.1.7). One can examine the thermodynamics of non-minimal RBH in terms of mass M, horizon radius r_+, non-minimal parameter $\mathfrak{q}$, cosmological constant Λ and magnetic charge Q_m. By utilizing Eq.(3.1.7) in above expression, the temperature reduces to

$$T = \frac{r_+^4 - \Lambda r_+^6 - Q_m^2 r_+^2 - 6Q_m^2 \mathfrak{q}}{4\pi r_+\left(r_+^4 + 2Q_m^2 \mathfrak{q}\right)}. \tag{3.1.11}$$

For modeling of metric function (3.1.1) and of the thermodynamic quantities, the dimensionless parameters (3.1.4) are used, but for visibility of the graph presentation, we use the following explicit values of the different parameters.

For real positive temperature, the following three conditions can be obtained

- **Case 1:** For $\Lambda = 0.01$ (positive), $Q_m = 1$, $\mathfrak{q} = 0.1$, we have $1.2 \leq r_+ \leq 9.95$.
- **Case 2:** For $\Lambda = 0$, $Q_m = 2$, $\mathfrak{q} = 0.1$, we have $r_+ \geq 2.1283$.
- **Case 3:** For $\Lambda = -0.01$ (negative), $Q_m = 3$, $\mathfrak{q} = 0.1$, we have $r_+ \geq 2.9713$.

If we variate the values of Λ then the range of horizon also change for real positive temperature. For simplicity, we discuss above three special cases.

The first law of thermodynamics can be defined as [107, 130],

$$dM = TdS + VdP + ... \tag{3.1.12}$$

One can easily check the above relation is violated. For obtaining the thermodynamic quantities which have to satisfy the above relation, we will use the logarithmic corrections in the following subsections.

3.1.1 Logarithmic Correction and Thermodynamical Relations

In this section, we examine the effect of thermal fluctuations on non-minimal RBH thermodynamics. Using general expression for entropy (2.4.2) by neglecting higher order correction terms

$$S = S_0 - \frac{b_1}{2} \ln S_0 T^2, \tag{3.1.13}$$

where b_1 is added as constant parameter to handle the logarithmic correction terms coming from thermal fluctuations. One can recover the entropy without any correction terms by setting $b_1 = 0$. As mention before, one can take $b_1 \to 0$, for large BHs which temperature is very small and one can consider $b_1 \to 1$, for small BHs which temperature is sufficiently large. By using Eqs.(3.1.11) and (2.4.2), we can obtain the

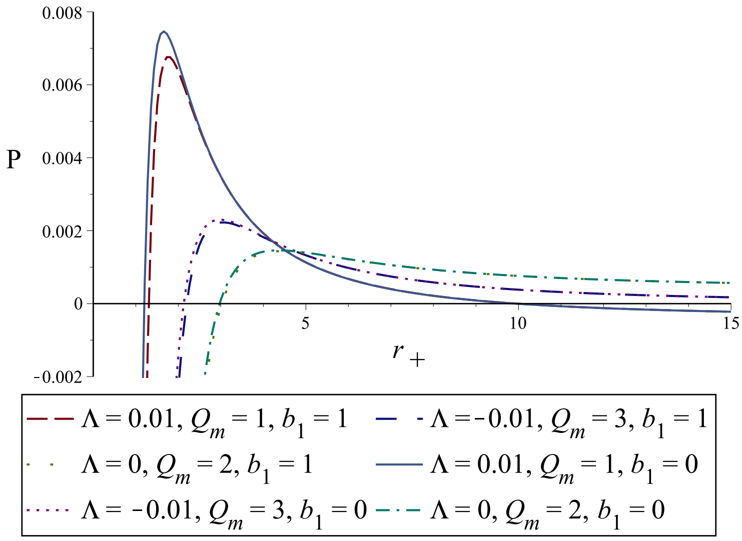

Figure 3.1: Plot of pressure verses horizon radius.

following corrected entropy:

$$S=\pi r_+^2-\frac{b_1}{2}\ln\left(\frac{\left(r_+^6\Lambda+Q_m^2r_+^2-r_+^4+6Q_m^2\mathfrak{q}\right)^2}{16\pi(r_+^4+2Q_m^2\mathfrak{q})^2}\right). \tag{3.1.14}$$

It is suggested that the presence of logarithmic correction causes the reduction of entropy of BH. We can calculate the pressure using Eqs.(3.1.9), (3.1.11), (3.1.14), and the following relation:

$$P=T\left(\frac{\partial S}{\partial V}\right)_V. \tag{3.1.15}$$

which turns out to be

$$\begin{aligned} P &= \frac{1}{8\pi^2r_+^2\left(r_+^4+2\mathfrak{q}Q_m^2\right)^2}\left(Q_m^2r_+^4(b_1\mathfrak{q}\Lambda-4\pi\mathfrak{q}-b_1)+2\mathfrak{q}Q_m^4(b_1-6\pi\mathfrak{q})-\pi r_+^{10}\Lambda\right.\\ &- \left.\pi Q_m^2r_+^6(2\mathfrak{q}\Lambda+1)+(b_1\Lambda+\pi)r_+^8-2r_+^2\mathfrak{q}Q_m^2(\pi Q_m^2+8b_1)\right). \end{aligned} \tag{3.1.16}$$

In Fig.**3.1**, we discuss the behavior of pressure for three cases of Λ. If we compare $b_1=0$ and $b_1=1$, we see that the pressure decreases due to logarithmic correction. Further, from Fig.**3.1**, we observe that pressure is maximum for positive cosmological constant but it becomes negative when $r\geq 9.945$, which is evident in case **1**. It means that when we increase the cosmological constant then the pressure also increases but the range of horizon for positive pressure decreases. Same behavior could be observed for temperature. We observe that the pressure is high for $\Lambda = 0$ as compare to negative cosmological constant. Hence we conclude that the pressure will decrease due to logarithmic correction and the lower values of cosmological constant.

Moreover, we can investigate the first law of thermodynamics by rewriting Eq.(3.1.12) as follows

$$dM - TdS - VdP = 0, \tag{3.1.17}$$

We construct the table for special three cases and find the horizon at which the first law of thermodynamics is satisfied. We also compare our results with respect to $b = 0$ and $b = 1$. From Table **3.1**, we observe that the location of horizon on which first law

Λ	Lograthmic correction term	r_+
0.01	$b_1 = 0$	$0.4034, 0.9053, 5.53679$
	$b_1 = 1$	$5.4261, 9.4958, 10.3665$
0	$b_1 = 0$	$0.527, 4.5474$
	$b_1 = 1$	$2.3 \times 10^{-5}, 2.4 \times 10^{-5}, 0.256, 0.329, 1.034, 1.581, 3.343, 4.018$
-0.01	$b_1 = 0$	$0.53269, 5.5951$
	$b_1 = 1$	$0.2279, 2.5257, 3.6834, 5.45336$

Table 3.1: Location of horizons where first law of thermodynamics is satisfied.

of thermodynamics satisfied is more for $b_1 = 1$ as compare to $b_1 = 0$. For positive cosmological constant, location of horizons are equal on $b_1 = 0$ and 1 but for negative cosmological constant the location of horizons increase for $b_1 = 1$ as compare to $b_1 = 0$. We obtain higher number of location of horizons on which first law of thermodynamics is satisfied in the absence of cosmological constant for $b_1 = 1$ as compare to $b_1 = 0$. Hence, we can conclude that logarithmic correction term increases the chance of first law of thermodynamics to satisfy.

3.2 Stability of non-minimal Regular Black Hole

In this section, we analyze the thermodynamical stability of non-minimal RBH due to the effect of thermal fluctuations. An important measurable physical quantity in BH thermodynamics is thermal capacity or heat capacity. It identifies the amount of heat required to change the temperature of a BH. The nature of heat capacity (positivity or negativity) represents the stability or instability of a BH. There are two different heat capacities associated with a system. C_P: measures the specific heat when the heat is added at constant pressure and C_V: measures the specific heat when the heat is added to the system by keeping the volume constant. We obtain the specific heat with constant volume by using the T and S as follows

$$C_V = T\left(\frac{\partial S}{\partial T}\right)_V. \tag{3.2.1}$$

Using Eqs.(3.1.9), (3.1.11) and (3.1.14), we have

$$\begin{aligned} C_V &= \Big(2\pi r_+^{12}\Lambda + 4\pi Q_m^2 \mathfrak{q} r_+^8\Lambda - 2b_1 r_+^{10}\Lambda + 2\pi Q_m^2 r_+^8 - 12Q_m^2 b_1 \mathfrak{q} r_+^6\Lambda - 2\pi r_+^{10} \\ &+ 4\pi Q_m^4 \mathfrak{q} r_+^4 + 8\pi Q_m^2 \mathfrak{q} r_+^6 + 24\pi Q_m^4 \mathfrak{q}^2 r_+^2 + 2Q_m^2 b_1 r_+^6 - 4Q_m^4 b_1 \mathfrak{q} r_+^2 \\ &+ 32Q_m^2 b_1 \mathfrak{q} r_+^4\Big)\Big(r_+^{10}\Lambda + 10Q_m^2 \mathfrak{q} r_+^6\Lambda - 3Q_m^2 r_+^6 + r_+^8 + 2Q_m^4 \mathfrak{q} r_+^2 \\ &- 36Q_m^2 \mathfrak{q} r_+^4 - 12Q_m^4 \mathfrak{q}^2\Big)^{-1}. \end{aligned} \tag{3.2.2}$$

Moreover, the specific heat at constant pressure can be obtained using the relation of E, P and V as follows

$$C_P = \left(\frac{\partial(E+PV)}{\partial T}\right)_P. \tag{3.2.3}$$

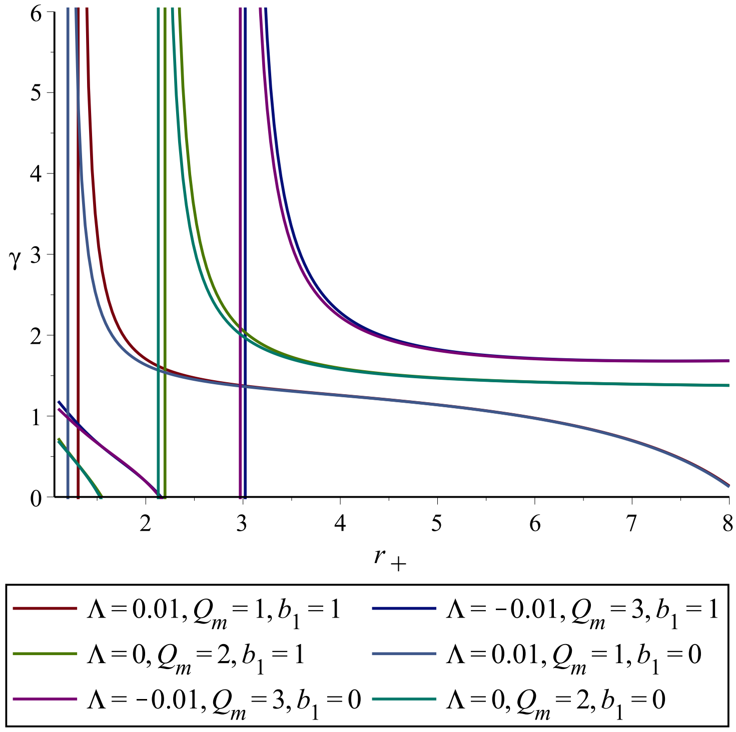

Figure 3.2: γ verses horizon radius.

Using Eqs.(3.1.9), (3.1.11), (3.1.16) and (2.5.1), we have

$$\begin{aligned} C_P &= \Big(64r_+^{12}\pi Q_m^2\mathfrak{q}\Lambda + 80r_+^8\pi Q_m^4\mathfrak{q}^2\Lambda + 4r_+^{12}\pi Q_m^2 - 48r_+^{10}Q_m^2 b_1\mathfrak{q}\Lambda + 32r_+^8\pi Q_m^4\mathfrak{q} \\ &- 48\pi Q_m^2\mathfrak{q}r_+^{10} - 192r_+^6 Q_m^4 b_1\mathfrak{q}^2\Lambda + 48r_+^4\pi Q_m^6\mathfrak{q}^2 + 32\pi Q_m^4\mathfrak{q}^2 r_+^6 + 48r_+^6 Q_m^4 b_1\mathfrak{q} \\ &+ 192r_+^2\pi Q_m^6\mathfrak{q}^3 - 64Q_m^2 b_1\mathfrak{q}r_+^8 - 32r_+^2 Q_m^6 b_1\mathfrak{q}^2 + 384Q_m^4 b_1\mathfrak{q}^2 r_+^4 - 8r_+^{14}b_1\Lambda \\ &+ 12r_+^{16}\pi\Lambda - 8\pi r_+^{14}\Big)\Big((r_+^{10}\Lambda + 10Q_m^2\mathfrak{q}r_+^6\Lambda - 3Q_m^2 r_+^6 - 36Q_m^2\mathfrak{q}r_+^4 + 2Q_m^4\mathfrak{q}r_+^2 \\ &+ r_+^8 - 12Q_m^4\mathfrak{q}^2)(r_+^4 + 2Q_m^2\mathfrak{q})\Big)^{-1}. \end{aligned} \tag{3.2.4}$$

The above two specific heat relations can be comprises into a ratio that is denoted by $\gamma = C_P/C_V$ and its plot is given in Fig.**3.2** for three special cases. We observe that due to logarithmic correction the value of γ increases. We obtain the maximum value of γ for negative cosmological constant and $\gamma \to 1.7$ for a large horizon. Further, we observe that $\gamma \to 1.4$ when $\Lambda = 0$ for a large horizon. It is interesting to note

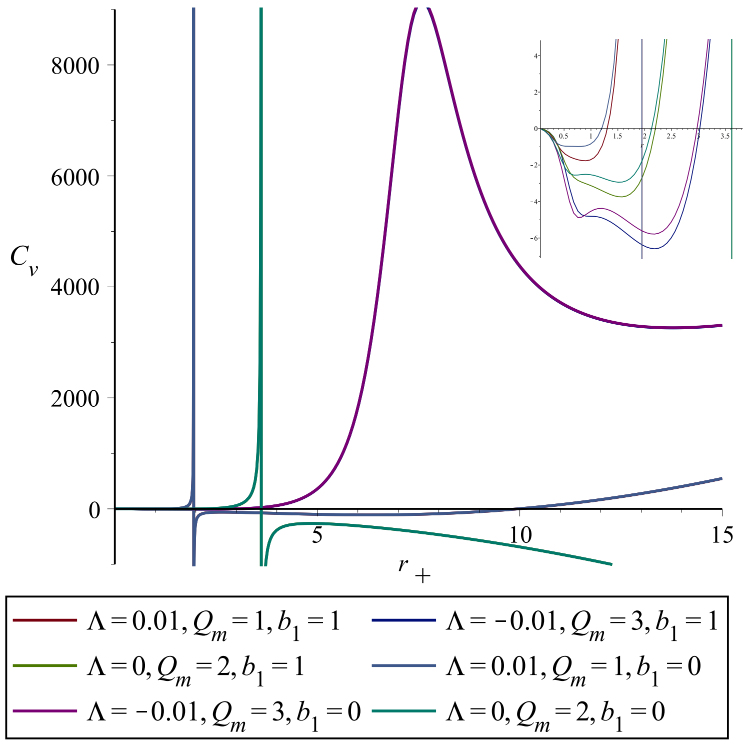

Figure 3.3: Specific heat at constant volume verses horizon radius.

that the value of γ decreases drastically and becomes zero at $r_+ = 9.92$ and the value of γ becomes negative for a large horizon. We can say that the value of γ shows stable behavior for negative and zero values of cosmological constant but represents unstable behavior for positive cosmological constant. Hence, we can conclude that if the value of cosmological constant decreases then the value of γ is higher and exhibits the more stable behavior but it experiences an unstable behavior for higher values of cosmological constant.

3.2.1 Phase Transition

Another way to find the thermodynamical stability of BH locally is to investigate the sign of specific heat given in Eq.(3.2.2). The BH is locally stable for $C_V > 0$, one can find the point of phase transition at $C_V = 0$ and BH is locally unstable for $C_V < 0$. We can find the range of horizon radius of BH stability for three specific cases in Fig.**3.3**.

We discuss the range of BH horizon of locally thermodynamical stability for each case. We observe that when $\Lambda = 0.01$ (positive) the horizon radius for local stability $1.3047 < r_+ < 1.9$ and $r_+ > 9.965$, when $\Lambda = 0$ the horizon radius for local stability is $2.1972 < r_+ < 3.6$ and the horizon radius is $r_+ > 3.0232$ for negative cosmological constant. Hence we can conclude that for negative cosmological constant the range of horizon radius for local stability of BH is higher than compare to positive and zero cosmological constant, respectively. Furthermore, we find the CP of horizon for phase transition in each case. We obtain two CPs of phase transition at $r_+ = 1.3047$ and 9.965 for positive cosmological constant, the CP for $\Lambda = 0$ is $r_+ = 2.1972$ and the CP is $r_+ = 3.0232$ for negative cosmological constant. We notice that the phase transition for positive cosmological constant is near to BH as compare to zero and negative cosmological constant. Hence we can conclude that if we increase the value of cosmological constant the phase transition shifted towards BH and vice versa. Furthermore, we also notice the singularity at $r_+ = 1.9$ and 3.6 for positive and zero value of cosmological constant, respectively, on the other hand, we find no singularity for negative value of cosmological constant.

3.2.2 Grand Canonical Ensemble

We may treat BH as a thermodynamical object by considering it as a grand canonical ensemble system where $\mu_1 = \frac{Q_m}{r_+}$ is a fix chemical potential. The corresponding temperature and entropy with logarithmic corrected term are

$$T_g = \frac{1}{4\pi r_+}\left(\frac{r_+^2 - r_+^4\Lambda - \mu_1^2 r_+^2 - 6\mu_1^2 \mathfrak{q}}{r_+^2 + 2\mu_1^2 \mathfrak{q}}\right), \tag{3.2.5}$$

$$S = \pi r_+^2 - \frac{b_1}{2}\ln\left(\frac{(r_+^6\Lambda + \mu_1^2 r_+^4 + 6\mu_1^2 \mathfrak{q} r_+^2 - r_+^4)^2}{16\pi(r_+^4 + 2\mu_1^2 \mathfrak{q} r_+^2)^2}\right). \tag{3.2.6}$$

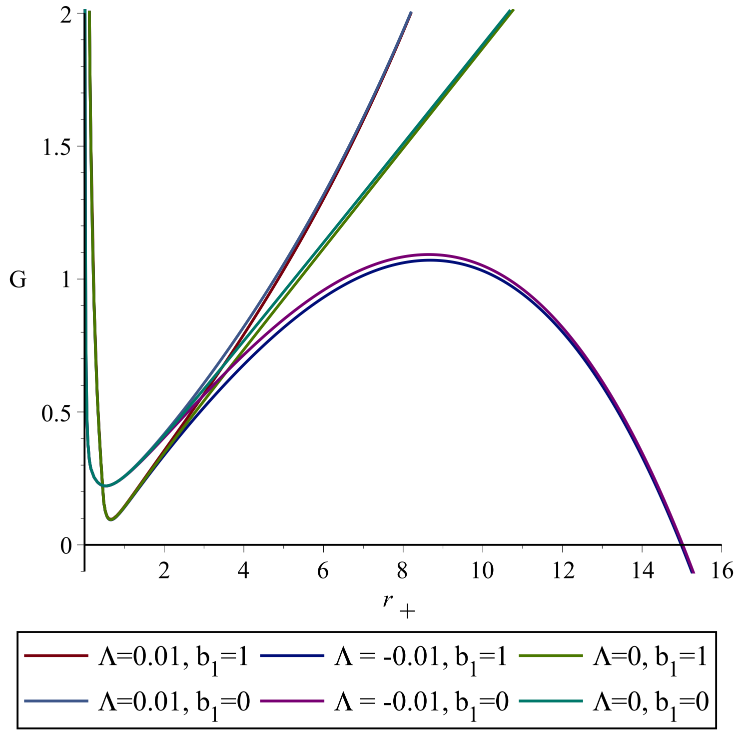

Figure 3.4: Gibb's free energy in terms of horizon radius with $\mu_1 = 0.5$.

The effect of chemical potential (μ_1) decreases the temperature. The free energy in the grand canonical ensemble, also called Gibbs free energy can be defined as

$$G = M - TS - \mu_1 Q_m, \tag{3.2.7}$$

which turns out to be

$$\begin{aligned} G &= \frac{-\Lambda r_+^6 + 3\mu_1^2 r_+^4 + 3r_+^4 + 6\mu_1^2 r_+^2 \mathfrak{q}}{6r_+^3} + \left(\frac{r_+^2 - r_+^4\Lambda - \mu_1^2 r_+^2 - 6\mu_1^2 \mathfrak{q}}{r_+^2 + 2\mu_1^2 \mathfrak{q}}\right) \\ &\times \left(\frac{r_+}{4} - \frac{b_1}{8\pi r_+} \ln\left(\frac{(r_+^6\Lambda + \mu_1^2 r_+^4 + 6\mu_1^2 \mathfrak{q} r_+^2 - r_+^4)^2}{16\pi(r_+^4 + 2\mu_1^2 \mathfrak{q} r_+^2)^2}\right)\right) - \mu_1^2 r_+. \end{aligned} \tag{3.2.8}$$

The effect of chemical potential reduces the free energy as we can see from the last term in Eq.(3.2.8). Fig.**3.4** represents the behavior of Gibbs free energy for special three cases. We observe that the Gibbs free energy is minimum at $r_+ \simeq 0.8$ due to

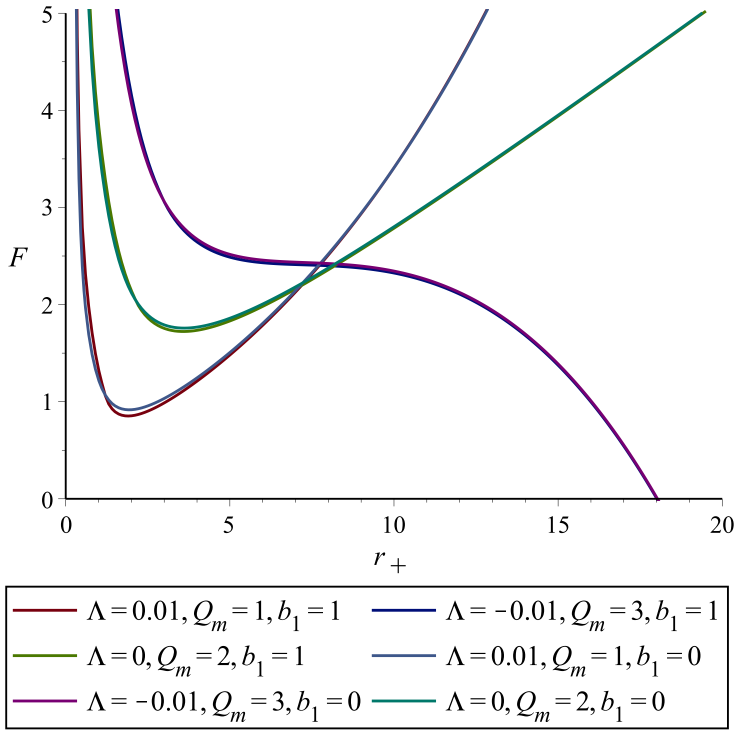

Figure 3.5: Helmhotz free energy in terms of horizon radius.

the contribution of logarithmic correction term. It means logarithmic correction term also reduces the Gibbs free energy. From the figure, we notice that free energy is higher for positive cosmological constant as compare zero and negative cosmological constant, respectively. It is interesting that free energy becomes negative at $r_+ \simeq 15$ for negative cosmological constant. It means free energy is globally thermodynamically unstable for negative cosmological constant. Hence, we can conclude that if the value of cosmological constant is higher, then free energy becomes globally more stable. Moreover, thermodynamical stability does not only depend on Λ and q but also on chemical potential μ_1.

3.2.3 Canonical ensemble

On the other hand, BH could be considered as a closed system (canonical ensemble) if charge transfer is prohibited. The mass and temperature is given by Eqs.(3.1.7) and

(3.1.11), respectively, and the corresponding entropy with logarithmic corrected term is given in Eq.(3.1.14). The free energy in canonical ensemble is known as Helmhotz free energy if the charge is fixed, which is

$$F = M - TS, \tag{3.2.9}$$

which turns out to be

$$\begin{aligned} F &= \frac{-\Lambda r_+^6 + 3Q_m^2 r_+^2 + 3r_+^4 + 6Q_m^2\mathfrak{q}}{6r_+^3} - \frac{r_+^4 - \Lambda r_+^6 - 6Q_m^2\mathfrak{q} - 6Q_m^2\mathfrak{q}}{4\pi r_+\left(r_+^4 + 2Q^2\mathfrak{q}\right)} \\ &\times \left(\pi r_+^2 - \frac{b_1}{2}\ln\left(\frac{\left(r_+^6\Lambda + Q_m^2 r_+^2 - r_+^4 + 6Q_m^2\mathfrak{q}\right)^2}{16\pi(r_+^4 + 2Q_m^2\mathfrak{q})^2}\right)\right). \end{aligned} \tag{3.2.10}$$

Fig.**3.5** represents the behavior of Helmhotz free energy for specific values of parameters. We observe that the logarithmic corrected term reduces the free energy in every case, which is evident. Initially, the free energy for negative cosmological constant is high till $r_+ = 7$ as compare to zero and positive cosmological constant, but for a large horizon, free energy is decreasing further, at $r_+ = 18$ it becomes negative. The free energy is highest for positive cosmological constant as compare to $\Lambda = 0$ and -0.01 for a large horizon. Hence, we can conclude that BH is more thermodynamically stable if the value of cosmological constant increases in large horizon and it becomes thermodynamically unstable for lower values of cosmological constant. Moreover, thermodynamical stability do not depend only on Λ and $\mathfrak{q}$ but also on magnetic charge Q_m rather than chemical potential.

Chapter 4

Thermodynamics of Higher Order Corrected Entropy on some well known Black holes

In this chapter, we investigate the thermodynamical behavior of two well-known BHs such as RN-AdS BH with global monopole (GM) and $f(R)$ BH by considering the higher order corrected entropy. We develop various thermodynamical properties such as, entropy, specific heats, pressure, Gibb's and Helmhotz free energies for both BHs in the presence of higher order corrected entropy. The versatile study on the stability of BHs is being made by using various frameworks such as the ratio of heat capacities (γ), grand canonical and canonical ensembles, and phase transition in view of higher order corrected entropy.

4.1 Thermodynamical Analysis of RN-AdS Black Hole with Global Monopole

During the phase transitions, many topological defects are produced such as domain walls, cosmic strings, monopoles, etc. Monopoles are the three-dimensional topological defects that are formed when the spherical symmetry is broken during the phase transition [131]. Barriola and Vilenkin [132] found the approximate solution of the EFEs for the static spherically symmetric BH with a GM. Many authors have also investigated different physical phenomena of BHs with GMs [133, 134].

We consider the spherical symmetric space-time with line element (2.1.2), in which the metric function of RN-AdS BH with GM is given by

$$X(r) = 1 + 2\big(\tilde{\alpha} - \frac{M}{r}\big) + \frac{q^2}{r^2} - \frac{\Lambda r^2}{3}. \tag{4.1.1}$$

Here, $\tilde{\alpha} = \frac{\lambda^2}{2}$ is the GM charge, λ is the scale of gauge symmetric breaking $\lambda \sim 10^6$ GeV [131] and M is the mass of BH. The metric function (4.1.1) reduces to RN-AdS BH for $\tilde{\alpha} = 0$ while it becomes RN-BH for $\tilde{\alpha} = \Lambda = 0$. By setting $X(r) = 0$, which leads to

$$r_+^4 - \frac{3(1+2\tilde{\alpha})}{\Lambda} r_+^2 + \frac{6Mr_+}{\Lambda} - \frac{3q^2}{\Lambda} = 0, \quad \Lambda \neq 0, \tag{4.1.2}$$

and four roots are given by [131]

$$r_1 = \frac{1}{2}\Big(\sqrt{\Omega}+\sqrt{-\Omega}-\frac{12M}{\Lambda\sqrt{\Omega}}\Big), \tag{4.1.3}$$
$$r_2 = \frac{1}{2}\Big(\sqrt{\Omega}-\sqrt{-\Omega}-\frac{12M}{\Lambda\sqrt{\Omega}}\Big), \tag{4.1.4}$$
$$r_3 = \frac{1}{2}\Big(\sqrt{\Omega}+\sqrt{-\Omega}+\frac{12M}{\Lambda\sqrt{\Omega}}\Big), \tag{4.1.5}$$
$$r_4 = \frac{1}{2}\Big(\sqrt{\Omega}-\sqrt{-\Omega}+\frac{12M}{\Lambda\sqrt{\Omega}}\Big). \tag{4.1.6}$$

where $\Omega = x_1 + \frac{3(1+2\tilde{\alpha})}{\Lambda}$ and $x_1 > -\frac{3(1+2\tilde{\alpha})}{\Lambda}$. The polynomial (4.1.2) has at most three real roots, which are Cauchy, cosmological and event horizons.

The mass, entropy, volume and temperature of RN-AdS BH with GM in horizon radius form can be written as

$$M = \frac{-r_+^4+6\tilde{\alpha}r_+^2+3q^2+3r_+^2}{6r_+}, \tag{4.1.7}$$
$$S_0 = \pi r_+^2, \tag{4.1.8}$$
$$V = \frac{4}{3}\pi r_+^2, \tag{4.1.9}$$
$$T = \frac{f'(r)}{4\pi} = \frac{-r_+^4+3Mr_+-3q^2}{6\pi r_+^3}, \tag{4.1.10}$$

where $r_+ \neq 0$. We can analyze the thermodynamics of RN-AdS BH with GM in terms of mass M, horizon radius r_+, cosmological constant Λ and charge q. Inserting the mass M in above equation, the temperature reduces to

$$T = \frac{-r_+^4\Lambda+2\tilde{\alpha}r_+^2-q^2+r_+^2}{4\pi r_+^3}. \tag{4.1.11}$$

For real positive temperature, we have the following condition

$$r_+^2 \geq \frac{(2\tilde{\alpha}+1)\pm\sqrt{(2\tilde{\alpha}+1)^2-4\Lambda q^2}}{2\Lambda} \quad \text{with} \quad (2\tilde{\alpha}+1)^2 \geq 4\Lambda q^2. \tag{4.1.12}$$

The corrected entropy of RN-AdS BH with GM can be obtained by using Eqs.(2.4.3),

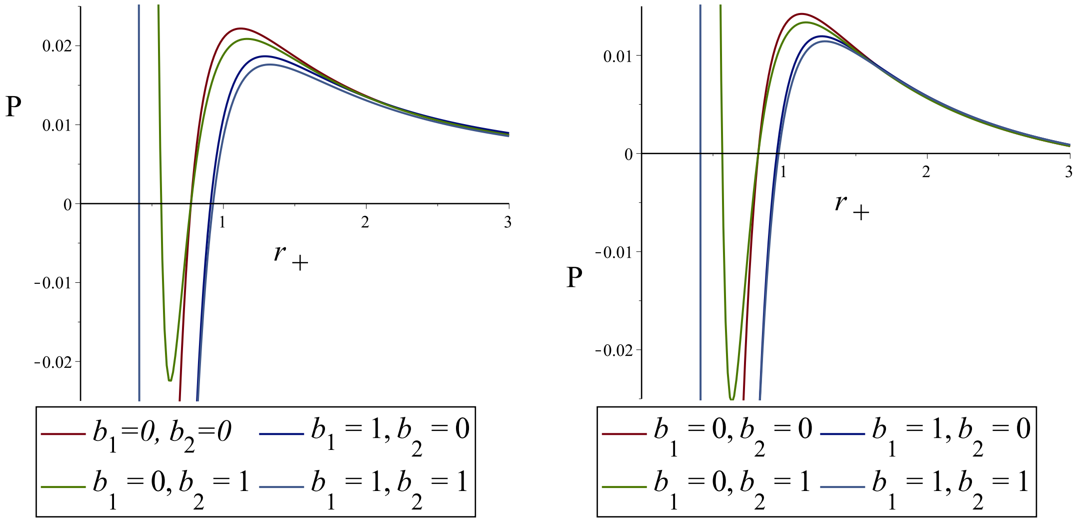

Figure 4.1: The plot of pressure for RN-AdS BH with GM for $\tilde{\alpha} = 0.075$, $q = 0.85$ and $\Lambda = -0.1$ (left panel), $\Lambda = 0.1$ (right panel).

(4.1.8) and (4.1.11), which turns out to be

$$S = \pi r_+^2 - \frac{b_1}{2} \ln\Big(\frac{(-r_+^4\Lambda + 2\tilde{\alpha} r_+^2 - q^2 + r_+^2)^2}{16\pi r_+^4}\Big) + \frac{b_2}{\pi r_+^2}. \tag{4.1.13}$$

The pressure can also be calculated in view of Eqs. (4.1.9), (4.1.11), (4.1.13) as

$$\begin{aligned} P &= T\Big(\frac{\partial S}{\partial V}\Big)_V = \frac{1}{8\pi^3 r_+^8}\Big(-\pi^2 r_+^8\Lambda + \pi(2\pi\tilde{\alpha} + b_1\Lambda + \pi)r_+^6 + (b_2\Lambda - \pi^2 q^2)r_+^4 \\ &- (\pi b_1 q^2 + 2\tilde{\alpha} b_2 + b_2)r_+^2 + b_2 q^2\Big). \end{aligned} \tag{4.1.14}$$

In Fig.**4.1**, we discuss the behavior of pressure for negative and positive values of cosmological constant. In both panels, we observe that the pressure decreases due to correction terms. For $b_1 = 1, b_2 = 1$, we observe the lowest trajectory of pressure then above it we have the trajectory of pressure at $b_1 = 1, b_2 = 0$ which becomes the logarithmic correction term. Furthermore, we see that the pressure increases for $b_1 = 0, b_2 = 1$ which is the second order correction term. The pressure is maximum if we avoid these correction terms. Also, we observe in both panels that the pressure increases for negative cosmological constant. However, the pressure becomes zero at $r_+ = 3.3$ for positive value of Λ and becomes negative for large horizon while remains positive for negative value of Λ. Hence, we can conclude that the pressure decreases due to higher order correction terms and positive values of Λ.

4.1.1 Stability of RN-AdS Black Hole with Global monopole

Here, we shall discuss the thermodynamical stability of RN-AdS BH with GM for which we can define

$$E = \int T dS. \tag{4.1.15}$$

In BH thermodynamics, an important measurable physical quantity is the heat capacity or thermal capacity. The heat capacity of BH may be stable or unstable by observing its sign (positive or negative), respectively. There are two types of heat capacities corresponding to a system such as C_V and C_P which determine the specific heat with constant volume and pressure, respectively. C_V can be defined as

$$C_V = T\left(\frac{\partial S}{\partial T}\right)_V. \tag{4.1.16}$$

Equations (4.1.11) and (4.1.13) lead to

$$\begin{aligned} C_V &= -\frac{2}{\pi r_+^2(r_+^4\Lambda + 2\tilde{\alpha}r_+^2 - 3q^2 + r_+^2)}\Big(-\pi^2 r_+^8\Lambda + 2\pi^2\tilde{\alpha}r_+^6 + \pi b_1 r_+^6\Lambda \\ &- \pi^2 q^2 r_+^4 + \pi^2 r^6 - \pi b_1 q^2 r_+^2 + b_2 r_+^4\Lambda - 2\tilde{\alpha} b_2 r_+^2 + b_2 q^2 - b_2 r_+^2\Big). \end{aligned} \tag{4.1.17}$$

Moreover, the C_P can be evaluated as

$$C_P = \left(\frac{\partial(E+PV)}{\partial T}\right)_P, \tag{4.1.18}$$

and its expression can be obtained with the help of Eqs.(4.1.9), (4.1.11), (4.1.14) and

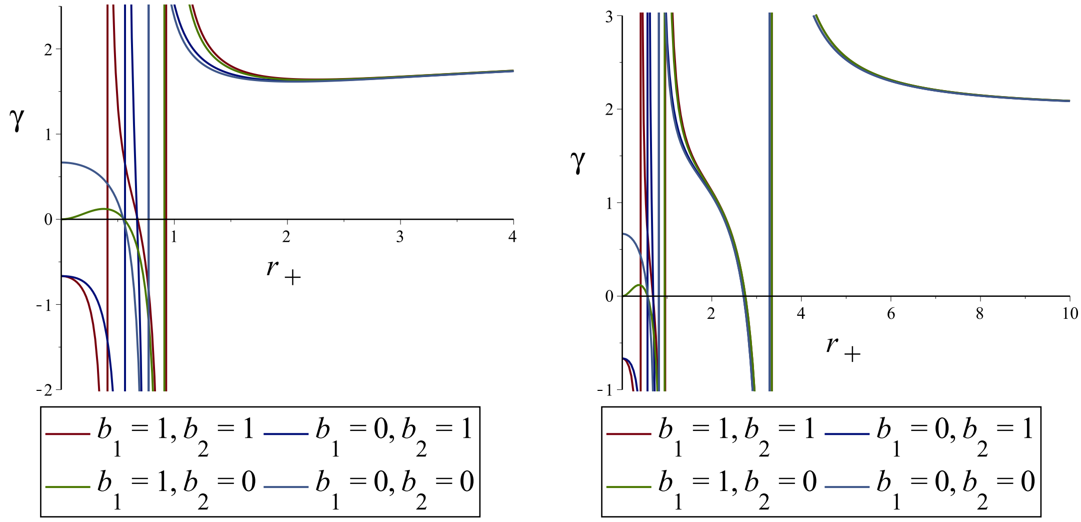

Figure 4.2: The plot of γ versus horizon radius for RN-AdS BH with GM for $\tilde{\alpha} = 0.075$, $q = 0.85$ and $\Lambda = -0.1$ (left panel), $\Lambda = 0.1$ (right panel).

(4.1.15) as

$$\begin{aligned} C_P &= -\frac{4}{\pi r_+^2(r_+^4\Lambda + 2\tilde{\alpha}r_+^2 - 3q^2 + r_+^2)}\Big(-3\pi^2 r_+^8\Lambda + 4\pi^2\tilde{\alpha}r_+^6 \\ &+ 2\pi b_1 r_+^6\Lambda - \pi^2 q^2 r_+^4 + 2\pi^2 r_+^6 - b_2 r_+^4\Lambda - b_2 q^2\Big). \end{aligned} \tag{4.1.19}$$

The above two specific heat relations can be comprises into a ratio that is denoted by $\gamma = C_P/C_V$ and its plot is given in Fig.**4.2**. It can be noted that the value of γ increases due to the correction terms. We find maximum value of γ as $\gamma \to 2.1$ for positive value of Λ and larger horizon, while for negative value of cosmological constant $\gamma \to 1.8$. Thus, one can observe that γ exhibits more stable behavior for lower value of Λ as compare to positive value of Λ. Hence, it is pointed out that the value of γ becomes higher due to correction terms and exhibits more stable behavior for lower values of Λ.

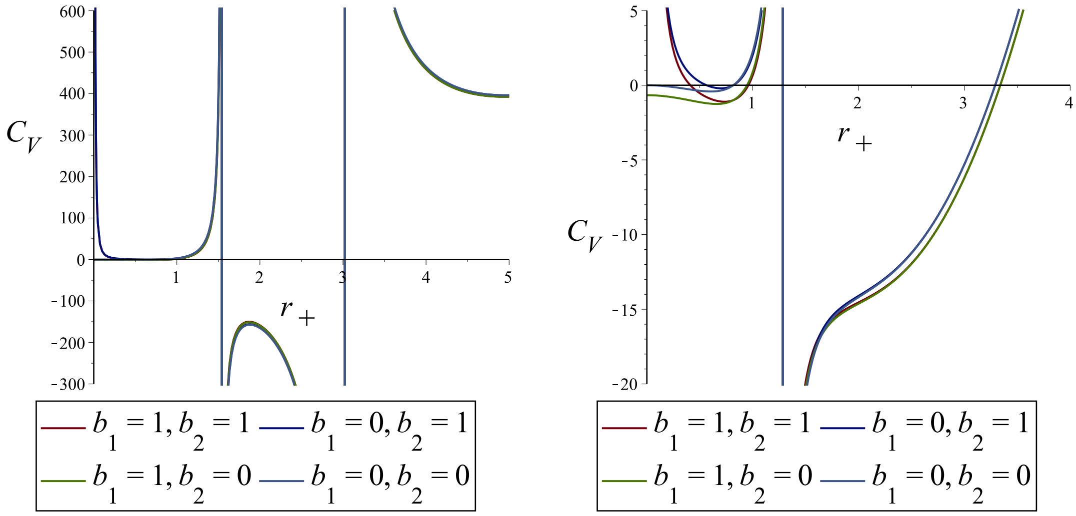

Figure 4.3: The plot of specific heat at constant volume for RN-AdS BH with GM for $\tilde{\alpha} = 0.075$, $q = 0.85$ and $\Lambda = -0.1$ (left panel), $\Lambda = 0.1$ (right panel)

4.1.2 Phase Transition

The stability of BH can be analyzed through C_V (Eq.(4.1.17)) because $C_V \lesseqgtr 0$ corresponds to local stability of BH, phase transition and local instability of the BH.

Λ	correction terms	range of local stability	phase transition
-0.1	$b_1 = 1, b_2 = 1$	$0 < r_+ < 0.4, 0.92 < r_+ < 1.53, r_+ > 3$	$0.41,\ 0.93$
	$b_1 = 0, b_2 = 1$	$0 < r_+ < 0.55, 0.76 < r_+ < 1.53,\ r_+ > 3$	$0.56,\ 0.77$
	$b_1 = 1, b_2 = 0$	$0.91 < r_+ < 1.53,\ r_+ > 3$	0.91
	$b_1 = 0, b_2 = 0$	$0.77 < r_+ < 1.53,\ r_+ > 3$	0.77
0.1	$b_1 = 1, b_2 = 1$	$0 < r_+ < 0.41,\ 0.95 < r_+ < 1.27,\ r_+ > 3.34$	$0.41,\ 0.96,\ 3.34$
	$b_1 = 0, b_2 = 1$	$0 < r_+ < 0.56,\ 0.81 < r_+ < 1.27,\ r_+ > 3.29$	$0.56,\ 0.82,\ 3.29$
	$b_1 = 1, b_2 = 0$	$0.95 < r_+ < 1.27,\ r_+ > 3.34$	$0.95,\ 3.34$
	$b_1 = 0, b_2 = 0$	$0.81 < r_+ < 1.27,\ r_+ > 3.33$	$0.82,\ 3.29$

Table 4.1: Range of local stability and CPs of horizon radius of phase transition for RN-AdS BH with GM due to the effect of higher order correction entropy.

We find the range of BH horizon of locally thermodynamical stability due to thermal fluctuations for negative and positive values of cosmological constant in left and right panels of Fig.**4.3**, respectively and in Table **4.1.2**. We can observe from Table that the range of local stability is maximum for second order correction terms ($b_1 = 0, b_2 = 1$) as well as for both correction terms ($b_1 = 1, b_2 = 1$) as compare to the others in both cases of Λ. Moreover, we obtain the CPs of horizon of phase transition for both case in Table **4.1.2**. We observe that one can obtain more CPs of phase transition for $b_1 = 0, b_2 = 1$ and $b_1 = 1, b_2 = 1$ as compare to others in both cases. Also we find more CPs for positive value of cosmological constant as compare to negative value. Hence it can be concluded that if we increases the value of Λ and consider the second order or both correction terms then we can find more CPs of phase transition and the range of local stability is also increased.

4.1.3 Grand Canonical Ensemble

The BH can be considered as a thermodynamical object by treating it as grand canonical ensemble system where fix chemical charge is represented by $\mu_1 = \frac{Q_m}{r_+}$. The temperature increases due to effect of chemical potential. The grand canonical ensemble is also known as Gibbs free energy, which can be defined as

$$G = M - TS - \mu_1 Q_m, \tag{4.1.20}$$

and it turns out to be

$$\begin{aligned} G &= -\frac{-r_+^4\Lambda + (2\tilde{\alpha}+1)r_+^2 - q^2}{8\pi^2 r_+^5}\Big(-2\pi^2 r_+^4 - 2b_2 \\ &+ b_1 \ln\big(\frac{(-r_+^4\Lambda + 2\tilde{\alpha}r_+^2 - q^2 + r_+^2)^2}{16\pi r_+^4}\big)\Big) - \mu_1 r_+. \end{aligned} \tag{4.1.21}$$

Fig.**4.4** indicates the view of Gibbs free energy for negative and positive cosmological constant. It can be noted from both panels of this figure that the correction terms reduce the Gibb's free energy. For negative cosmological constant, Gibb's free energy is positive only for second order correction term ($b_1 = 0, b_2 = 1$) while it becomes negative for large horizon in the case of other correction terms. Hence, it exhibits stable behavior for second order correction term and unstable behavior for other cor-

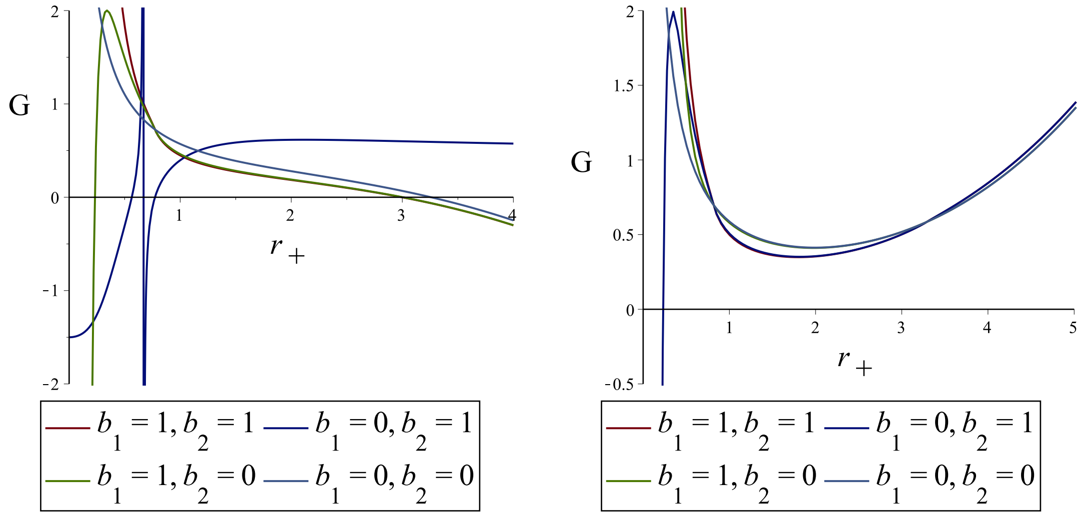

Figure 4.4: The plot of Gibb's free energy for RN-AdS BH with GM for $\tilde{\alpha} = 0.075$, $q = 0.85, \mu_1 = 0.5$ and $\Lambda = -0.1$ (left panel), $\Lambda = 0.1$ (right panel)

rection terms. For positive cosmological constant case, the Gibb's free energy remains positive. It means that RN-AdS BH with GM is thermodynamically stable for positive cosmological constant while it is conditionally stable ($b_1 = 0, b_2 = 1$) for negative value of Λ.

4.1.4 Canonical Ensemble

Here, we consider BH as a canonical ensemble (closed system) where transformation of charge is prohibited. For fixed charge, the free energy in canonical ensemble form termed as Helmhotz free energy and can be defined as

$$F = M - TS, \tag{4.1.22}$$

which becomes

$$\begin{aligned} F &= -\Big(-2\pi^2 r_+^4 - 2b_2 + b_1 \ln\big(\frac{(-r_+^4\Lambda + 2\tilde{\alpha} r_+^2 - q^2 + r_+^2)^2}{16\pi r_+^4}\big)\Big) \\ &\times \frac{-r_+^4\Lambda + (2\tilde{\alpha}+1) r_+^2 - q^2}{8\pi^2 r_+^5}. \end{aligned} \tag{4.1.23}$$

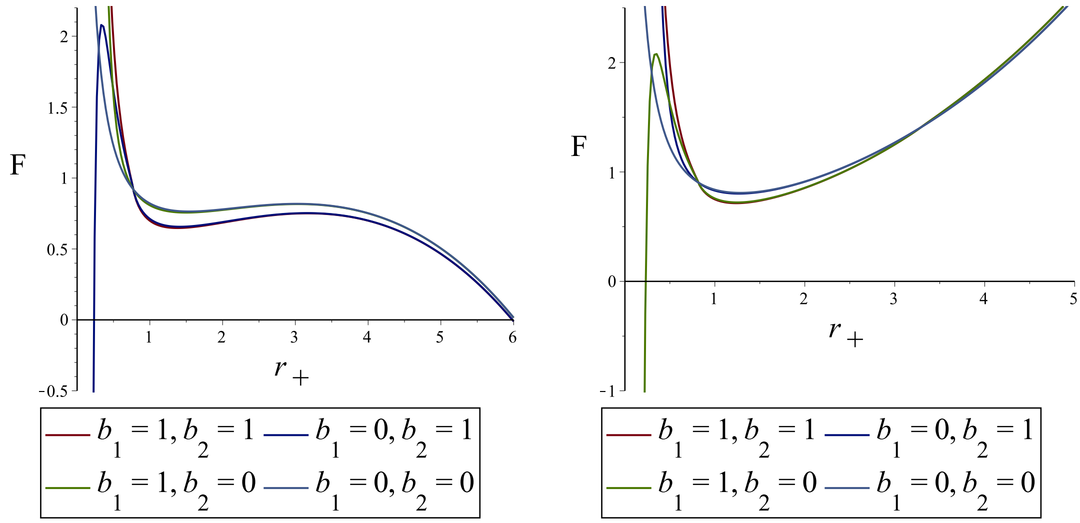

Figure 4.5: The plot of Helmhotz free energy versus horizon radius for RN-AdS BH with GM for $\tilde{\alpha} = 0.075$, $q = 0.85$ and $\Lambda = -0.1$ (left panel), $\Lambda = 0.1$ (right panel.

The behavior of Helmhotz free energy for negative and positive cosmological constant is plotted in Fig.**4.5**. In both panels, we observe that Helmhotz free energy decreases due to correction terms. In left panel, it can be observed that free energy is positive till $r_+ = 6$ then it becomes negative for large horizon in the case of negative cosmological constant. So it shows stable (positive) behavior till $r_+ = 6$ and unstable (negative) behavior for large horizon. On the other hand, for positive value of Λ, the free energy remains positive which shows stable behavior. Hence, it is pointed here that RN-AdS BH with GM exhibits stable behavior for positive values of Λ and indicated unstable behavior for large horizon for negative cosmological constant case.

4.2 Thermodynamical Analysis of $f(R)$ Black Hole

One of the modified theories is $f(R)$ theory of gravity [135, 136, 137, 138], which explains the accelerated expansion of the universe. There are a lot of valid reasons because of which $f(R)$ gravity has become one of the most interesting theories of this era. It is important and interesting to study the astrophysical phenomenon in $f(R)$ gravity [139].

We consider the spherical symmetric line element (2.1.2), in which the metric function of $f(R)$ BH is given by [140]

$$X(r) = 1 + \frac{2M}{r} + \tilde{\beta} r - \frac{\Lambda r^2}{3}. \tag{4.2.1}$$

Here, M is the mass of BH, $\tilde{\beta} = a_4/d_1 \geq 0$ is a constant with d_1 is the scale factor and a_4 is the dimensionless parameter [140]. The horizon radius can be obtained through metric function (4.2.1) as

$$r_+^3 \Lambda - 3r_+^2 \tilde{\beta} + 6M - 3r_+ = 0. \tag{4.2.2}$$

One can obtain the mass and temperature of $f(R)$ BH at horizon radius as

$$M = \frac{-r_+^3 \Lambda + 3\tilde{\beta} r_+^2 + 3r_+}{6}, T \quad = \quad \frac{f'(r)}{4\pi} = \frac{-2r_+^3 \Lambda + 3\tilde{\beta} r_+^2 + 6M}{12\pi r_+^2}. \tag{4.2.3}$$

By utilizing the mass M in above equation, the temperature reduces to

$$T = \frac{-r_+^2 \Lambda + 2r_+ \tilde{\beta} + 1}{4\pi r_+}. \tag{4.2.4}$$

For real and positivity of temperature, we have

$$r_+ \geq \frac{\tilde{\beta} + \sqrt{\tilde{\beta}^2 + \Lambda}}{\Lambda}. \tag{4.2.5}$$

The condition satisfied

$$\tilde{\beta}^2 + \Lambda \geq 0. \tag{4.2.6}$$

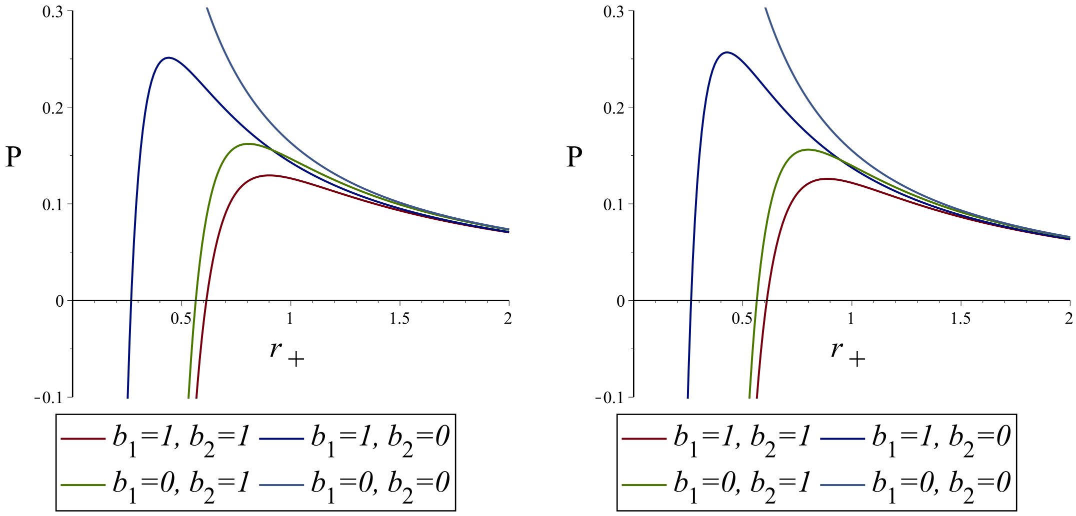

Figure 4.6: The plot of pressure for $f(R)$ BH for $\tilde{\beta} = 1.5$ and $\Lambda = -0.1$ (left panel), $\Lambda = 0.1$ (right panel)

The higher order corrected entropy and pressure for this BH take the form

$$S = \pi r_+^2 - \frac{b_1}{2}\ln\left(\frac{(r_+^2\Lambda - 2\tilde{\beta}r_+ - 1)^2}{16\pi}\right) + \frac{b_2}{\pi r_+^2}, \tag{4.2.7}$$

$$P = \frac{1}{8\pi^3 r_+^6}\big(-\pi^2 r_+^6\Lambda + 2\pi^2 r_+^5\tilde{\beta} + b_1\pi r_+^4\Lambda - b_1\pi r_+^3\tilde{\beta} + \pi^2 r_+^4 + b_2 r_+^2\Lambda - 2b_2 r_+\tilde{\beta} - b_2\big). \tag{4.2.8}$$

In Fig.**4.6**, we analyze the trajectories of pressure for negative and positive values of Λ. We can see pressure decreases due to correction terms. We obtain highest pressure in the absence of correction terms and the lowest pressure in the presence of both correction terms $(b_1 = 1, b_2 = 1)$. Also, we observe that the pressure is lower for second order correction term $(b_1 = 0, b_2 = 1)$ as compare to logarithmic correction term $(b_1 = 1, b_2 = 0)$. Interestingly, we find no change in pressure with respect to cosmological constant. Hence, it can be concluded that the pressure decreases due to higher order correction terms only.

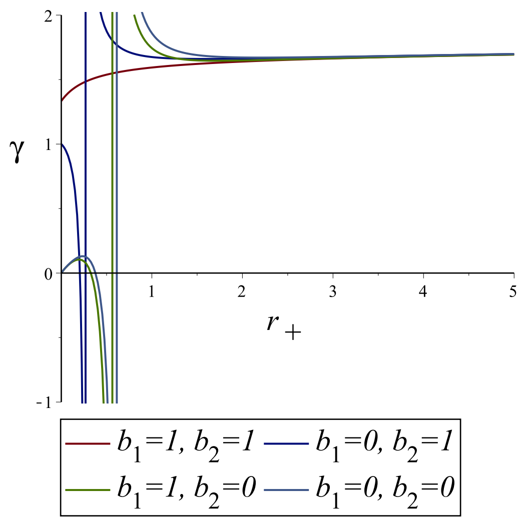

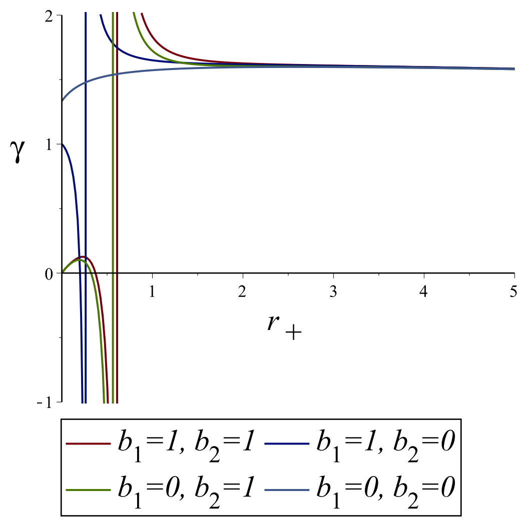

Figure 4.7: The plot of γ for $f(R)$ BH for $\tilde{\beta} = 1.5$ and $\Lambda = -0.1$ (left panel), $\Lambda = 0.1$ (right panel)

4.2.1 Stability of $f(R)$ Black Hole

For stability of $f(R)$ BH, we can obtain C_V by using Eqs.(4.2.4) and (4.2.7) as follows

$$\begin{aligned} C_V &= -\frac{2}{\pi r_+^2(r_+^2\Lambda+1)}\Big(-\pi^2 r_+^6\Lambda + 2\pi^2\tilde{\beta} r_+^5 + \pi b_1 r_+^4\Lambda \\ &- \pi r_+^3\tilde{\beta} + \pi^2 r_+^4 + b_1 r_+^2\Lambda - 2\tilde{\beta} b_2 r_+ - b_2\Big). \end{aligned} \tag{4.2.9}$$

Moreover, C_p can be obtained by using Eqs.(4.2.4) and (4.2.8), we have

$$\begin{aligned} C_P &= -\frac{2}{3\pi r_+(r_+^2\Lambda+1)}\Big(-6\pi^2 r_+^5\Lambda + 10\pi^2\tilde{\beta} r_+^4 \\ &+ 4\pi b_1 r_+^3\Lambda - 3\pi b_1\tilde{\beta} r_+^2 + 4\pi^2 r_+^3 + 2b_2 r_+\Lambda - 2b_2\tilde{\beta}\Big). \end{aligned} \tag{4.2.10}$$

For this BH, the plot of $\gamma = C_P/C_V$ is shown in Fig.**4.7**. We observe that the value of γ increases for larger horizon due to correction terms. Also, we find that the value of γ is same for both cases (positive and negative values of Λ), i.e., $\gamma \to 0.6$ for larger horizon. Thus, we can say that γ shows similar stable behavior for both cases of cosmological constant. It is realized that the value of γ becomes higher due to correction terms and exhibits similar stable behavior for both cases of Λ.

4.2.2 Phase Transition

Λ	correction terms	range of local stability	phase transition
-0.1	$b_1 = 1, b_2 = 1$	$0 < r_+ < 0.61,\ r_+ > 3.2$	0.61
	$b_1 = 0, b_2 = 1$	$0 < r_+ < 0.27,\ r_+ > 3.2$	0.27
	$b_1 = 1, b_2 = 0$	$r_+ < 0.56,\ r_+ > 3.2$	0.56
	$b_1 = 0, b_2 = 0$	$r_+ > 3.2$	ϕ
0.1	$b_1 = 1, b_2 = 1$	$0 < r_+ < 0.61,\ r_+ > 30.33$	$0.61,\ 30.33$
	$b_1 = 0, b_2 = 1$	$0 < r_+ < 0.26,\ r_+ > 30.33$	$0.26,\ 30.33$
	$b_1 = 1, b_2 = 0$	$r_+ < 0.56,\ r_+ > 30.33$	$0.56,\ 30.33$
	$b_1 = 0, b_2 = 0$	$r_+ > 30.33$	30.33

Table 4.2: Range of local stability and CPs of horizon radius of phase transition for $f(R)$ BH due to the effect of higher order correction entropy
.

We discuss the phase transition and range of local stability of BH horizon due to thermal fluctuation for negative and positive values of Λ. In both panels of Fig.**4.8**, it is observed that the range of local stability is maximum for both correction terms and then the range of local stability is higher for second order correction term as compare to first order logarithmic correction term. Furthermore, we also find the CPs of horizon of phase transition for both cases in Table **4.2**. We obtain more CPs of phase transition in the presence of correction term as compare to its absence. Moreover, we have more CPs for positive cosmological constant as compare to negative. Hence, we can conclude that if we utilize the correction terms and increases the value of cosmological constant then the range of local stability increases and we can obtain more CPs of phase transition.

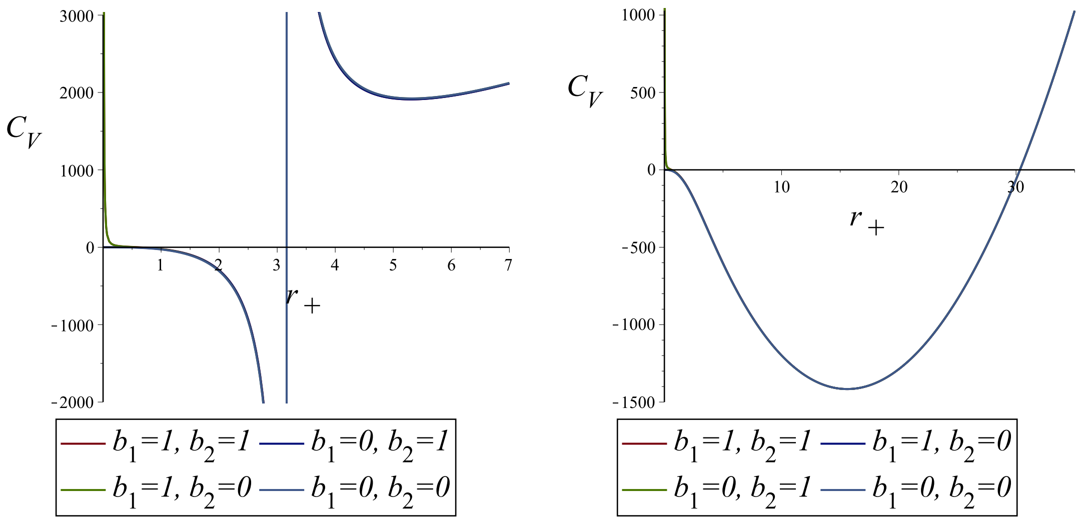

Figure 4.8: The plot of specific heat at constant volume for $f(R)$ BH for $\tilde{\beta} = 1.5$ and $\Lambda = -0.1$ (left panel), $\Lambda = 0.1$ (right panel)

4.2.3 Grand Canonical Ensemble

The free energy in grand canonical ensemble (Gibbs free energy) is given by

$$\begin{aligned} G &= -\frac{1}{24\pi^2 r_+^3}\Big(2r_+^6\pi^2\Lambda + 6r_+^4\pi^2 + 6b_2 r_+^2\Lambda - 12b_2 r_+\tilde{\beta} - 6b_2 \\ &- 3b_1 r_+^2\pi(r_+^2\Lambda - 2r_+\tilde{\beta} - 1)\ln\big(\frac{(-r_+^2\Lambda + 2\tilde{\beta}r_+ - 1)^2}{16\pi}\big)\Big) - \mu_1 r_+. \quad (4.2.11) \end{aligned}$$

Fig.**4.9** represents the behavior of Gibbs free energy for negative and positive cosmological constant. In both panels, it is observed that the correction terms reduce the Gibb's free energy. For lower value of the cosmological constant, Gibb's free energy is negative for all correction terms. So it shows unstable behavior for all correction terms in the case of negative value of Λ. In the case of positive cosmological constant, the Gibb's free energy remains positive. From right panel, we can see that Gibb's free energy is higher for both correction terms and logarithmic correction term as compare to others. Hence, we can conclude that $f(R)$ BH is thermodynamically stable for positive cosmological constant while it is unstable for negative cosmological constant.

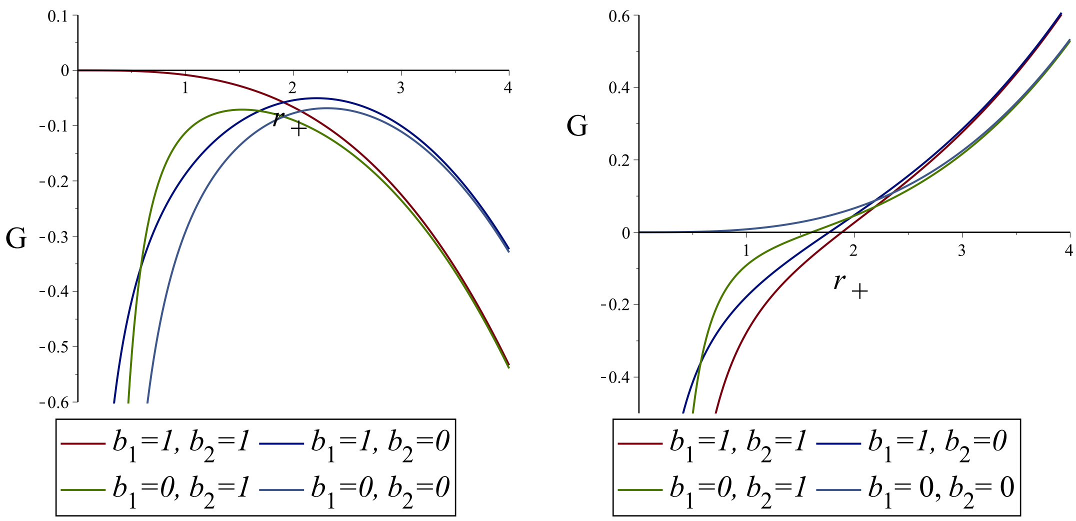

Figure 4.9: The plot of Gibb's free energy for $f(R)$ BH for $\tilde{\beta} = 1.5$, $\mu_1 = 0.5$ and $\Lambda = -0.1$ (left panel), $\Lambda = 0.1$ (right panel)

4.2.4 Canonical Ensemble

The free energy in canonical ensemble is known as Helmhotz free energy if the charge is fixed, which is

$$\begin{aligned} F &= -\frac{1}{24\pi^2 r_+^3}\Big(2r_+^6\pi^2\Lambda + 6r_+^4\pi^2 + 6b_2 r_+^2\Lambda - 12b_2 r_+\tilde{\beta} - 6b_2 \\ &- 3b_1 r_+^2\pi(r_+^2\Lambda - 2r_+\tilde{\beta} - 1)\ln\big(\frac{(-r_+^2\Lambda + 2\tilde{\beta}r_+ - 1)^2}{16\pi}\big)\Big) \end{aligned} \tag{4.2.12}$$

The behavior of Helmhotz free energy for negative and positive cosmological constant is plotted in Fig.**4.10**. In both panels, we observe that free energy decreases due to correction terms. In left panel, one can see the free energy is positive till $r_+ = 6$ then it becomes negative for large horizon in the case of negative cosmological constant. So it shows stable (positive) behavior till $r_+ = 6$ and unstable (negative) behavior for large horizon. On the other hand, for positive value of Λ, the free energy remains positive which shows stable behavior. Hence, we can conclude that $f(R)$ BH shows stable behavior for positive values of cosmological constant and exhibits unstable behavior for large horizon in the case of negative values of cosmological constant.

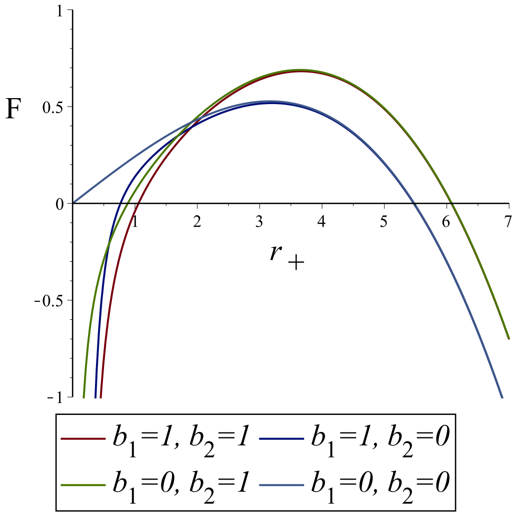

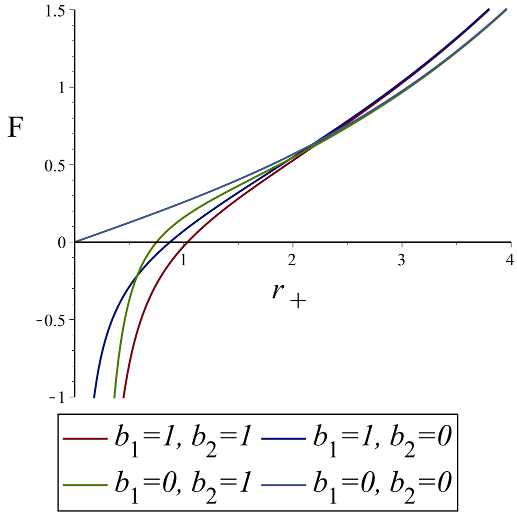

Figure 4.10: The plot of Helmhotz free energy for $f(R)$ BH for $\tilde{\beta} = 1.5$ and $\Lambda = -0.1$ (left panel), $\Lambda = 0.1$ (right panel)

Chapter 5

Accretion onto Some Well-Known Regular Black Holes

In this chapter, we discuss the accretion onto static spherically symmetric RBHs for specific choices of the EoS parameter. The underlying RBHs are FDD RBH, logistic distribution, non-linear electrodynamics, respectively, and KS asymptotically flat RBHs. We obtain the critical radius, critical speed, and squared sound speed during the accretion process near RBHs. We also study the behavior of radial velocity, energy density, and the rate of change of the mass for each of RBHs.

5.1 Charged Regular Black Hole Using Fermi-Dirac Distribution

The said RBH solution has the following metric functions [12]

$$X(r) = 1 - \frac{2M}{r}\left(\frac{\xi(\delta_2 r)}{\xi_\infty}\right)^{\delta_2} = Y(r), \tag{5.1.1}$$

where the FDD function is

$$\xi(\bar{x}) = \frac{1}{e^{\bar{x}}+1}. \tag{5.1.2}$$

By replacing $\bar{x} = \frac{q^2}{M\delta_2 r}$, we can obtain the distribution function as

$$\xi(\delta_2 r) = \frac{1}{e^{\frac{q^2}{M\delta_2 r}}+1}, \tag{5.1.3}$$

with normalization factor is $\xi_\infty = \frac{1}{2}$. Also the distribution function satisfies

$$\frac{\xi(r)}{\xi_\infty} \to 1, \tag{5.1.4}$$

where $r \to \infty$. Hence the metric functions turn out to be

$$X(r) = Y(r) = 1 - \frac{2M}{r}\left(\frac{2}{e^{\frac{q^2}{\delta_2 Mr}}+1}\right)^{\delta_2}, Z(r) = r^2. \tag{5.1.5}$$

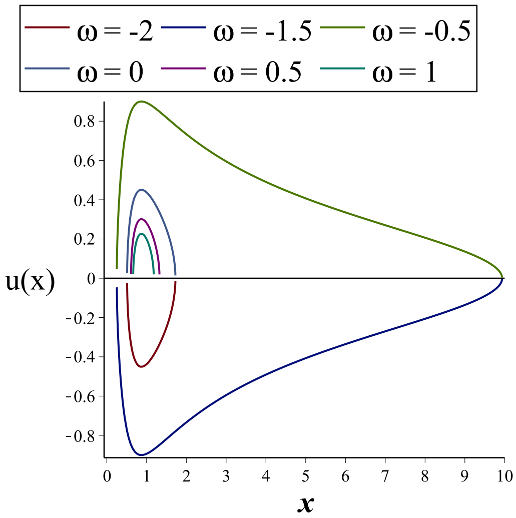

Figure 5.1: Velocity profile against $x = \frac{r}{M}$ for $\delta_2 = 1$, $q = 1.055M$, $M = 1$ and $A_4 = 0.45$ of charged FDD RBH.

If we set $\delta_2 \to 0$ and $\delta_2 \to \infty$, we obtain

$$X(r) = Y(r) = 1 - \frac{2M}{r} e^{\frac{-q^2}{Mr}}, \tag{5.1.6}$$

$$X(r) = Y(r) = 1 - \frac{2M}{r} e^{\frac{-q^2}{2Mr}}. \tag{5.1.7}$$

In both equations, the difference of factor 2 must be noted [12].

It is possible to integrate the conversation laws and obtain analytical expressions of the physical parameters. For simplicity, we will study the barotropic case where the fluid has an equation $p(r) = \omega \varepsilon(r)$. Using (2.6.5) and (2.6.11), we obtain

$$u(r) = \frac{\left(\left(2M \left(\frac{1}{2} e^{\frac{q^2}{\delta_2 Mr}} + \frac{1}{2} \right)^{-\delta_2} - r \right) (\omega + 1)^2 + A_4^2 r \right)^{1/2}}{(\omega + 1)\sqrt{r}}, \tag{5.1.8}$$

$$\varepsilon(r) = \frac{A_2(\omega + 1)}{r^{3/2} \sqrt{\left(2M \left(\frac{1}{2} e^{\frac{q^2}{\delta_2 Mr}} + \frac{1}{2} \right)^{-\delta_2} - r \right) (\omega + 1)^2 + A_4^2 r}}. \tag{5.1.9}$$

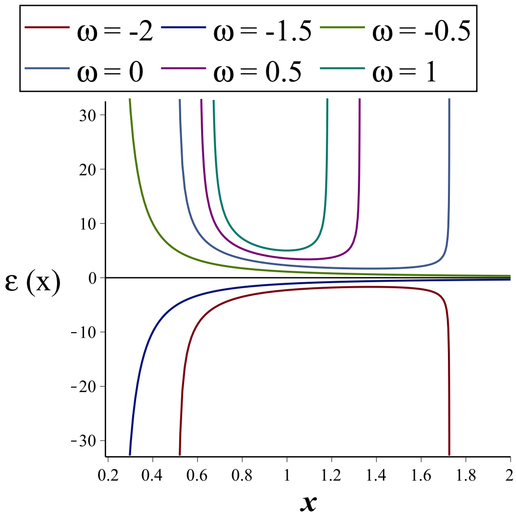

Figure 5.2: Energy density against $x = \frac{r}{M}$ for $\delta_2 = 1$, $q = 1.055M$, $M = 1$, $A_2 = 1$ and $A_4 = 0.45$ of charged FDD RBH.

The velocity profile for different values of ω is shown in Fig.**5.1**. Here $\omega = 1,\ 0,\ -1$ refer to stiff, dust, and cosmological constant, respectively, and $-1 < \omega < -1/3$ and $\omega < -1$ refer to quintessence and phantom energy. It can be seen that for $\omega = -1.5,\ -2$ the radial velocity of the fluid is negative and it is positive for $\omega = -0.5,\ 0,\ 0.5,\ 1$. If the flow is outward then $u < 0$ is not allowed and vice versa. In the case of $\omega = -1.5,\ -0.5$ the fluid is at rest at $x = 10$. Fig.**5.2** represents the behavior of energy density of fluids in the surrounding area of RBH. Obviously the WEC and DEC satisfied by dust, stiff, and quintessence fluids. When phantom fluid ($\omega = -1.5,\ -2$) moves towards RBH then energy density decreases and reverse will happen for dust, stiff and quintessence fluids ($\omega = -0.5,\ 0,\ 0.5,\ 1$). Asymptotically $\varepsilon \to 0$ at infinity for $\omega = -1.5,\ -0.5$, while it approaches to maximum at $x = 1.2,\ 1.3,\ 1.8$ and near BH.

Using this metric, Eqs.(2.6.19) and (5.1.9), the rate of change of mass of RBH due

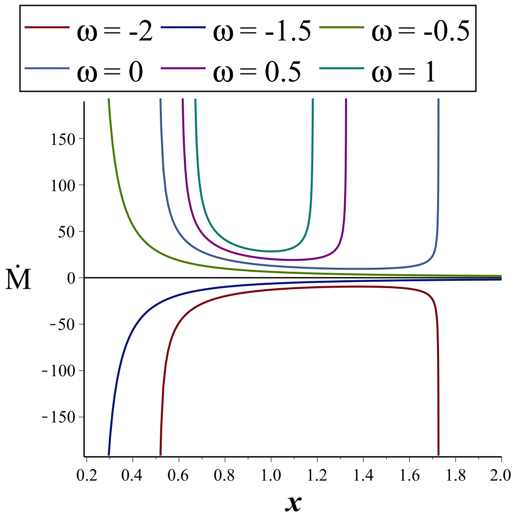

Figure 5.3: Rate of change of mass against $x = \frac{r}{M}$ for $\delta_2 = 1$, $q = 1.055M$, $M = 1$, $A_2 = 1$ and $A_4 = 0.45$ of charged FDD RBH.

to accretion becomes

$$\dot{M} = \frac{4\pi A_2^2 A_4(\omega+1)}{r^{3/2}\sqrt{\left(2M\left(\frac{1}{2}e^{\frac{q^2}{\delta_2 Mr}}+\frac{1}{2}\right)^{-\delta_2}-r\right)(\omega+1)^2+A_4^2 r}}. \tag{5.1.10}$$

Fig.**5.3** represents the change in RBH mass for different values of ω. The mass of the RBH will increase near it and at $x = 1.2,\ 1.3,\ 1.7$ for $\omega = 1,\ 0.5,\ 0$, respectively. On the other hand, mass of RBH decrease near it and at $x = 1.7$ for $\omega = -2$. Hence the mass of RBH increases due to accretion of quintessence, dust, and stiff matter, while it decreases due to accretion phantom like fluids.

The critical values, critical velocities and speed of sound are obtained for different values of the EoS parameter in Table **5.1**. Critical radius is shifting to left when $\omega \geq 0$ increases. Thus, the in-falling the fluid acquires supersonic speeds closer to RBH. Same critical radius is obtained for $\omega = -2,\ 0$ and $\omega = -1.5,\ -0.5$ with same critical velocities but in an opposite direction. We get negative speed of sound at $x = 7.5044$ and positive speed of sound for remaining critical radius. Also, the speed of sound

ω	r_c	$u(r_c)$	c_s^2
-2	1.37495	0.3138832070	.0000002580
-1.5	7.5044	0.2382908936	-.4999997476
-0.5	7.5044	-0.2382908936	-.4999997476
0	1.3749	-0.3138832070	.0000002580
0.5	1.092	-0.2476468259	0.503110174
1	0.999	-.1998921298	1.002986469

Table 5.1: Charged FDD RBH.

increases near the RBH. For this metric, we find that

$$u_c^2 = \frac{2^{\delta_2-1}\left(\left(Mr-q^2\right)e^{\frac{q^2}{\delta_2 Mr}}+Mr\right)}{r^2\left(e^{\frac{q^2}{\delta_2 Mr}}+1\right)^{\delta_2+1}}, \tag{5.1.11}$$

$$\mathbb{V}_c^2 = \frac{2^{\delta_2}\left(\left(Mr-q^2\right)e^{\frac{q^2}{\delta_2 Mr}}+Mr\right)}{2r^2\left(e^{\frac{q^2}{\delta_2 Mr}}+1\right)^{\delta_2+1}-2^{\delta_2}\left((3Mr+q^2)e^{\frac{q^2}{\delta_2 Mr}}+3Mr\right)}. \tag{5.1.12}$$

Also, the condition (2.6.18) yields

$$\frac{2^{\delta_2}\left(\left(Mr-q^2\right)e^{\frac{q^2}{\delta_2 Mr}}+Mr\right)}{r^4\left(e^{\frac{q^2}{\delta_2 Mr}}+1\right)^{\delta_2+1}} > 0. \tag{5.1.13}$$

5.2 Charged Regular Black Hole Using Logistic Distribution

The logistic distribution function is [12]

$$\xi(\bar{x}) = \frac{e^{-\bar{x}}}{(e^{-\bar{x}}+1)^2}, \tag{5.2.1}$$

in which replace $\bar{x} = \frac{2q^2}{M\delta_3 r}$ then we obtain the distribution function

$$\xi(\delta_3 r) = \frac{e^{\frac{-2q^2}{M\delta_3 r}}}{\left(e^{\frac{-2q^2}{M\delta_3 r}} + 1\right)^2}, \tag{5.2.2}$$

with normalization factor is $\xi_\infty = \frac{1}{4}$. Also the distribution function satisfies

$$\frac{\xi(r)}{\xi_\infty} \to 1, \tag{5.2.3}$$

where $r \to \infty$. The horizons can be obtained for $\delta_3 = 1$ where $q = 1.055M$. The metric function can be written as

$$X(r) = Y(r) = 1 - \frac{2M\left(4e^{-\sqrt{\frac{2q^2}{\delta_3 Mr}}}\right)^{\delta_3}}{r\left(e^{-\sqrt{\frac{2q^2}{\delta_3 Mr}}} + 1\right)^{2\delta_3}}, Z(r) = r^2. \tag{5.2.4}$$

If we set $\delta_3 \to 0$ then we obtain the SH-BH, and if we set $\delta_3 \to \infty$, we get

$$X(r) = Y(r) = 1 - \frac{2M}{r} e^{\frac{-q^2}{2Mr}}. \tag{5.2.5}$$

It is noteworthy that this metric function corresponds to an Ayon-Beato and Garcia BH [12].

The radial velocity and energy density for the metric (5.2.4) using Eqs. (2.6.5) and (2.6.10) are given by

$$u(r) = \frac{1}{(\omega+1)\sqrt{r}} \left(\left(r - \frac{2M\left(4e^{-\sqrt{\frac{2q^2}{\delta_3 Mr}}}\right)^{\delta_3}}{\left(e^{-\sqrt{\frac{2q^2}{\delta_3 Mr}}} + 1\right)^{2\delta_3}} \right) \left(\omega + 1\right)^2 - A_4^2 r \right)^{1/2}, \tag{5.2.6}$$

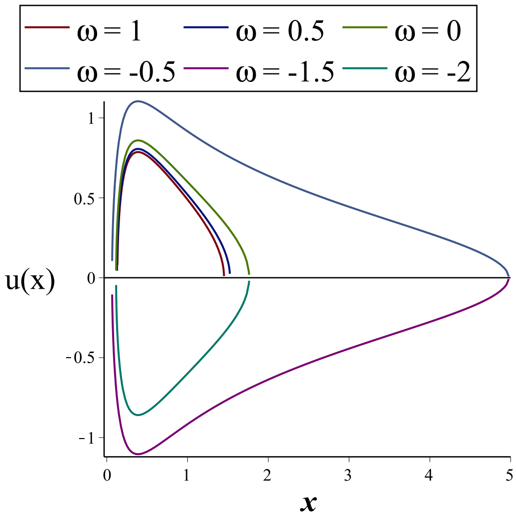

Figure 5.4: Velocity profile against $x = \frac{r}{M}$ for $\delta_3 = 1$, $q = 1.055M$, $M = 1$ and $A_4 = 0.4$ of charged RBH using logistic distribution.

$$\varepsilon(r) = -\frac{A_2(\omega+1)}{r^{3/2}\left(\left(-r+\frac{2M\left(4e^{-\sqrt{\frac{2q^2}{\delta_3 Mr}}}\right)^{\delta_3}}{\left(e^{-\sqrt{\frac{2q^2}{\delta_3 Mr}}}+1\right)^{2\delta_3}}\right)\left(\omega+1\right)^2+A_4^2 r\right)^{1/2}}. \tag{5.2.7}$$

The velocity profile for different values of ω is shown in Fig.**5.4**. It can be observed that for $\omega = -1.5, -2$ the radial velocity of the fluid is negative and it is positive for $\omega = -0.5, 0, 1$. If the flow is inward then $u > 0$ is not allowed and vice versa. In the case of $\omega = -2, 0$ the fluid is at rest at $x = 10$. Fig.**5.5** represents the behavior of energy density of fluids in the surrounding area of RBH. Obviously the WEC and DEC are satisfied by dust, stiff, and quintessence fluids. When phantom like fluid ($\omega = -1.5, -2$) moves towards BH then energy density decreases and reverse will happen for dust, stiff, and quintessence fluids ($\omega = -0.5, 0, 0.5, 1$).

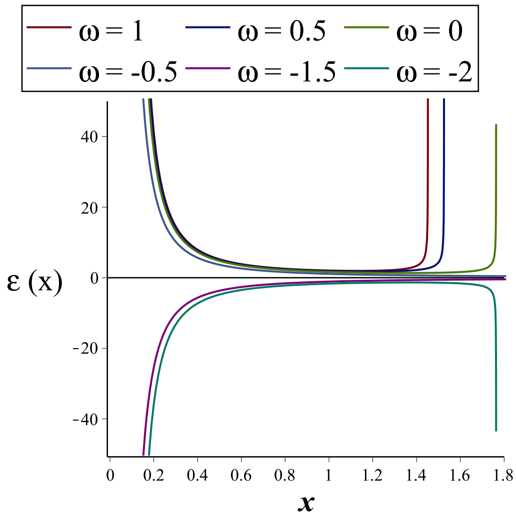

Figure 5.5: Energy density against $x = \frac{r}{M}$ for $\delta_3 = 1$, $q = 1.055M$, $M = 1$, $A_2 = 1$ and $A_4 = 0.4$ of charged RBH using logistic distribution.

The $\dot{M}$ of RBH for distinct EoS parameters is obtained by using (2.6.19)

$$\dot{M} = -\frac{4\pi A_2^2 A_4(\omega+1)}{r^{3/2}\left(\left(-r+\frac{2M\left(4e^{-\sqrt{\frac{2q^2}{\delta_3 Mr}}}\right)^{\delta_3}}{\left(e^{-\sqrt{\frac{2q^2}{\delta_3 Mr}}}+1\right)^{2\delta_3}}\right)\left(\omega+1\right)^2+A_4^2 r\right)^{1/2}}. \tag{5.2.8}$$

Fig.**5.6** represents the change in RBH mass against x. It is evident that the mass of RBH increases due to quintessence, dust, and stiff fluids and it decreases due to phantom fluids.

ω	r_c	$u(r_c)$	c_s^2
-2	1.36375	-0.3998729763	-0.1018620364
-1.5	3.777412	-0.3138895411	-0.5007414180
-0.5	3.77412	0.3138895411	-0.5007414180
0	1.36375	0.3998724197	-0.1018620364
0.5	1.1850	0.4018068205	0.116622918
1	1.12974	0.4014558621	0.231766770

Table 5.2: Charged RBH using logistics distribution.

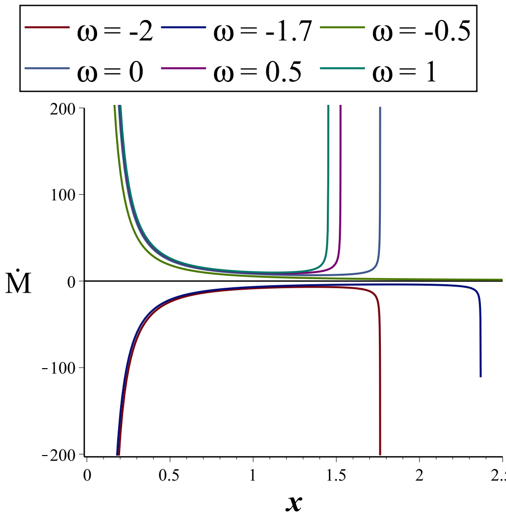

Figure 5.6: Rate of change of mass against $x = \frac{r}{M}$ for $\delta_3 = 1$, $q = 1.055M$, $M = 1$, $A_2 = 1$ and $A_4 = 0.4$ of charged RBH using logistic distribution.

The critical radius, critical velocity, and speed of sound are obtained for different values of EoS parameter in Table **5.2**. Critical radius is shifting to the right when $\omega \geq 0$ increases. Thus the in-falling fluid acquires supersonic speeds closer to RBH. For phantom like fluid, quintessence, dust, and stiff matter the critical radius and critical velocities are explained in Table **5.2**. Same critical radius is obtained for $\omega = -2,\ 0$ and $\omega = -1.5,\ -0.5$ with same critical velocities but differ in sign. We obtained negative speed of sound at $x = 1.36375,\ 3.777412$ and positive speed of sound at $x = 1.12974,\ 1.1850$. Near RBH speed of sound will increase. For this metric we find that

$$u_c^2 = \frac{2^{-2+2\delta_3}\sqrt{M}e^{\sqrt{\frac{2q^2\delta_3}{Mr}}}\left(\left(\sqrt{2}q\delta_3 + 2\sqrt{\delta_3 Mr}\right) + \left(-\sqrt{2}q\delta_3 + 2\sqrt{\delta_3 Mr}\right)e^{\sqrt{\frac{2q^2\delta_3}{Mr}}}\right)}{\sqrt{\delta_3}r^{3/2}\left(e^{\sqrt{\frac{2q^2\delta_3}{Mr}}}\right)}, \tag{5.2.9}$$

$$
\begin{aligned}
V_c^2 &= \left(2^{\delta_3} M e^{\sqrt{\frac{2q^2\delta_3}{Mr}}} \left(\left(\sqrt{2}q\delta_3 + 2\sqrt{\delta_3 M r}\right) + \left(-\sqrt{2}q\delta_3 + 2\sqrt{\delta_3 M r}\right) e^{\sqrt{\frac{2q^2\delta_3}{Mr}}}\right)\right) \\
&\left(4\sqrt{\delta_3 M} r^{3/2} \left(e^{\sqrt{\frac{2q^2\delta_3}{Mr}}}\right) - 2^{\delta_3} e^{-\sqrt{\frac{2\delta_3 q^2}{Mr}}} \left(\left(-\sqrt{2}Mq\delta_3 + 6\sqrt{\delta_3 r} M^{3/2}\right)\right.\right. \\
&\left.\left. e^{-\sqrt{\frac{2q^2}{\delta_3 M r}}} + \sqrt{2}Mq\delta_3 + 6\sqrt{\delta_3 r} M^{3/2}\right)\right)^{-1}. \qquad (5.2.10)
\end{aligned}
$$

Also, the condition (2.6.18) yields

$$
\frac{2^{-1+2\delta_3}\sqrt{M} e^{-\sqrt{\frac{2q^2\delta_3}{Mr}}} \left(\left(\sqrt{2}q\delta_3 + 2\sqrt{\delta_3 M r}\right) e^{-\sqrt{\frac{2q^2\delta_3}{Mr}}} + \left(-\sqrt{2}q\delta_3 + 2\sqrt{\delta_3 M r}\right)\right)}{\sqrt{\delta_3} r^{7/2} \left(e^{\sqrt{\frac{2q^2\delta_3}{Mr}}}\right)} > 0. \qquad (5.2.11)
$$

5.3 Charged Regular Black Hole from Nonlinear Electrodynamics

We use the line element

$$
X(r) = Y(r) = 1 - \frac{2M(r)}{r}, \qquad (5.3.1)
$$

here the function

$$
M(r) = M\left(1 - tanh\left(\frac{q^2}{2Mr}\right)\right). \qquad (5.3.2)
$$

Its associated electric field source is

$$
E = \frac{q}{r^2}\left(1 - tanh^2\left(\frac{q^2}{2Mr}\right)\right)\left(1 - \frac{q^2}{4Mr} tanh\left(\frac{q^2}{2Mr}\right)\right), \qquad (5.3.3)
$$

where q and M represent electric charge and mass, respectively [141]. The solution elaborate RBH and its global structure is like RN-BH. The asymptotic behavior of the solution is

$$
X(r) = 1 - \frac{2M}{r} + \frac{q^2}{r^2} + O\left(\frac{1}{r^4}\right). \qquad (5.3.4)
$$

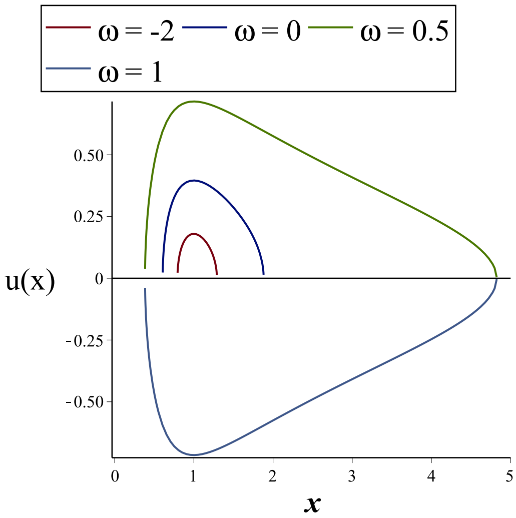

Figure 5.7: Velocity profile against $x = \frac{r}{M}$ for $q = 1.055M$, $M = 1$ and $A_4 = 0.7$ of charged RBH from nonlinear electrodynamics.

So we have metric function

$$X(r) = Y(r) = 1 - \frac{2M}{r}\left(M\left(1 - tanh(\frac{q^2}{2Mr})\right)\right), Z(r) = r^2. \tag{5.3.5}$$

The radial velocity and energy density for this metric are given by

$$u(r) = \frac{\sqrt{\left(-2Mtanh\left(\frac{q^2}{2Mr}\right) + 2M - r\right)(\omega+1)^2 + A_4^2 r}}{(\omega+1)\sqrt{r}}, \tag{5.3.6}$$

$$\varepsilon(r) = \frac{(\omega+1)A_2}{r^{3/2}\sqrt{\left(-2Mtanh(\frac{q^2}{2Mr} + 2M - r)\right)(\omega+1)^2 + A_4^2 r}}. \tag{5.3.7}$$

The absolute value of the velocity profile for different values of ω is shown in Fig.**5.7**. It can be observed that for $\omega = -2$ the radial velocity of the fluid is negative and it is positive for $\omega = 0.5,\ 0,\ 1$. If the flow is inward then $u > 0$ is not allowed and vice versa. In the case of $\omega = -2,\ 0$ the fluid is at rest at $x = 10$. Fig.**5.8** represents the energy density of fluids in the region of RBH. It is apparent that WEC and DEC is satisfied by phantom fluids. When phantom fluids move towards RBH the energy

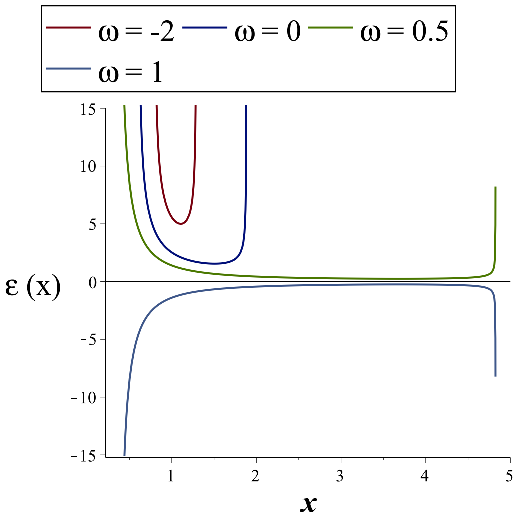

Figure 5.8: Energy density against $x=\frac{r}{M}$ for $q=1.055M$, $M=1$, $A_2=1$ and $A_4=0.7$ of charged RBH from nonlinear electrodynamics.

density increases; on the other hand it decreases for dust and stiff matter.

The rate of change of mass is given by

$$\dot{M}=-\frac{4\pi A_2^2A_4(\omega+1)}{r^{3/2}\sqrt{\left(-2Mtanh(\frac{q^2}{2Mr}+2M-r)\right)(\omega+1)^2+A_4^2r}}. \quad (5.3.8)$$

The rate of change of RBH mass against x is plotted in Fig.**5.9**. Due to accretion of dust and stiff matter the mass of RBH will increase for small values of x and vice versa for phantom fluids. It is also noted that the maximum rate of RBH mass increases due to $\omega = 1$ followed by $\omega=0.5,\ 0,\ -2$. The critical values, critical velocities

ω	r_c	$u(r_c)$	c_s^2
-2	3.685523529	-0.2993097288	-0.125
0	3.685523529	0.2993097288	-0.125
0.5	1.506050868	0.2844719573	0.312500584
1	1.106971797	0.1633564212	0.750003072

Table 5.3: Charged RBH from nonlinear electrodynamics.

and speed of sound are obtained for different values of EoS parameter in Table **5.3**.

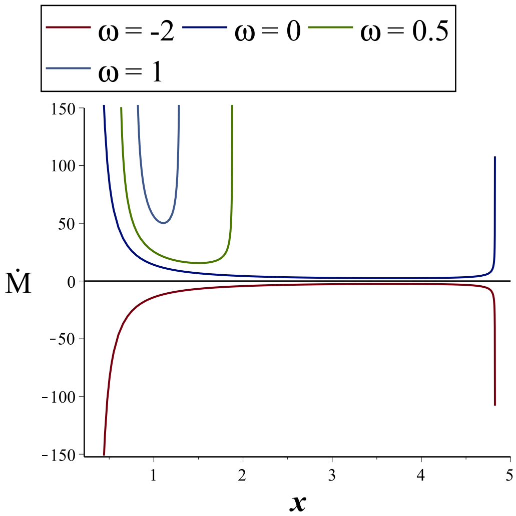

Figure 5.9: Rate of change of mass against $x = \frac{r}{M}$ for $q = 1.055M$, $M = 1$, $A_2 = 1$ and $A_4 = 0.7$ of charged RBH from nonlinear electrodynamics.

Critical radius is shifting to the right when $\omega \geq 0$ increases. Speed of sound is negative at $x = 3.685523529$ and near RBH the speed of sound will increase. For this RBH, we find that

$$u_c^2 = \frac{q^2\left(tanh^2\left(\frac{q^2}{2Mr}\right)-1\right)+2Mr\left(-tanh\left(\frac{q^2}{2Mr}\right)+1\right)}{4r^2}, \tag{5.3.9}$$

$$\mathbb{V}_c^2 = \frac{q^2\left(tanh^2\left(\frac{q^2}{2Mr}\right)-1\right)+2Mr\left(-tanh\left(\frac{q^2}{2Mr}\right)+1\right)}{4r^2+q^2\left(tanh^2\left(\frac{q^2}{2Mr}\right)-1\right)+6+Mr\left(tanh\left(\frac{q^2}{2Mr}\right)-1\right)}. \tag{5.3.10}$$

Also, the condition (2.6.18) yields

$$\frac{\left(tanh^2\left(\frac{q^2}{2Mr}\right)-1\right)q^2+2Mr\left(-tanh\left(\frac{q^2}{2Mr}\right)+1\right)}{2r^4} > 0. \tag{5.3.11}$$

5.4 Kehagias - Sftesos Asymptotically flat Regular Black Hole

KS studied the following RBH metric

$$X(r) = Y(r) = 1+\tilde{b}r^2-\sqrt{\tilde{b}^2r^4+4M\tilde{b}r}, Z(r) = r^2. \tag{5.4.1}$$

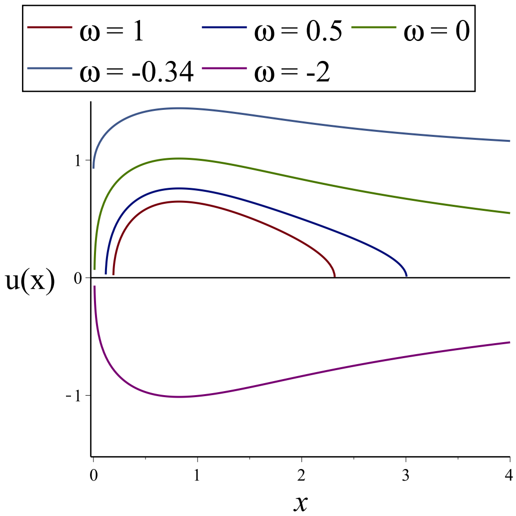

Figure 5.10: Velocity profile against $x = \frac{r}{M}$ for $M = 1$, $\tilde{b} = 0.9$ and $A_4 = 0.9$ of KS RBH.

In the frame work of Horava theory, where m is the mass, $\tilde{b}$ is the positive constant related to coupling constant of theory. The metric asymptotically behaves the usual SH-BH [142]

$$X(r) = Y(r) \approx 1 - \frac{2M}{r} + O\left(\frac{1}{r^4}\right), \tag{5.4.2}$$

for $r \gg (\frac{r}{\tilde{b}})^{1/3}$. The KS metric have two horizons at

$$r_{\pm} = M\left(1 \pm \sqrt{\left(1 - \frac{1}{2\tilde{b}M^2}\right)}\right), \tag{5.4.3}$$

with $2\tilde{b}M^2 \geq 1$ [142]. For $2\tilde{b}M^2 = 1$, we have an extreme BH and for $2\tilde{b}M^2 < 1$, we have naked singularity.

The radial velocity and energy density for this metric of different EoS parameters are given by

$$u(r) = \frac{\left(A_4^2 + \left(\sqrt{\tilde{b}^2 r^4 + 4M\tilde{b}r} - \tilde{b}r^2 - 1\right)(\omega + 1)^2\right)^{1/2}}{\omega + 1}, \tag{5.4.4}$$

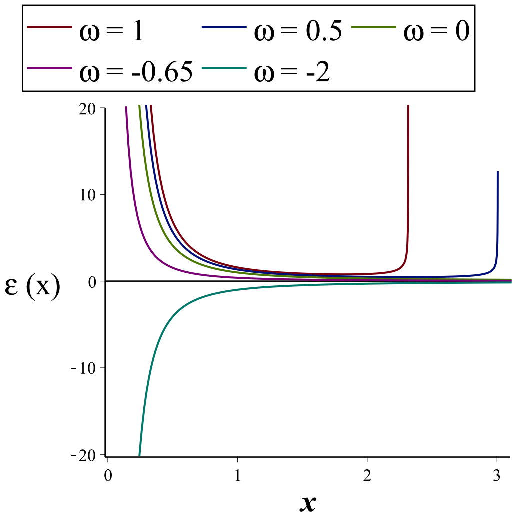

Figure 5.11: Energy density against $x = \frac{r}{M}$ for $M = 1, A_2 = 1, \tilde{b} = 0.9$ and $A_4 = 0.9$ of KS RBH.

$$\varepsilon(r) = \frac{A_2(\omega+1)}{r^2\left(A_4^2 + \left(\sqrt{\tilde{b}^2 r^4 + 4M\tilde{b}r} - \tilde{b}r^2 - 1\right)(\omega+1)^2\right)^{1/2}}. \tag{5.4.5}$$

The radial velocity for different values of ω is shown in Fig.**5.10**. The radial velocity is negative for phantom like fluid and positive for quintessence, dust, and stiff matter. The evolution of energy density of fluids in the surrounding area of RBH is plotted in Fig.**5.11**. The energy density for phantom fluids is negative, while the energy density for stiff, dust, and quintessence fluids is positive.

Using this metric and Eq.(2.6.19) we obtained rate of change of RBH mass is given by

$$\dot{M} = \frac{4\pi A_2^2 A_4(\omega+1)}{r^2\left(A_4^2 + \left(\sqrt{\tilde{b}^2 r^4 + 4M\tilde{b}r} - \tilde{b}r^2 - 1\right)(\omega+1)^2\right)^{1/2}}. \tag{5.4.6}$$

Fig.**5.12** represents the rate of change in RBH mass against x. We see that RBH mass will increase for $\omega = -0.35,\ 0,\ 0.5,\ 1$ and it will decrease for $\omega = -2$. The critical values, critical velocities and speed of sound for different values of ω is presented in the Table **5.4**. For quintessence matter we obtain very large critical radius. Similarly as before we obtain the same critical radius for dust and phantom like fluids and same

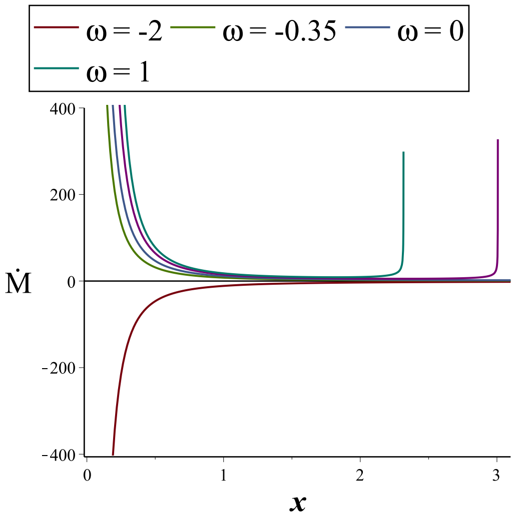

Figure 5.12: Rate of change of mass against $x = \frac{r}{M}$ for $M = 1$, $A_2 = 1$, $\tilde{b} = 0.9$ and $A_4 = 0.9$ of KS RBH.

ω	r_c	$u(r_c)$	c_s^2
-2	7.8946	-0.2505321935	0.0000008330
-0.34	30267.74	0.6327458490	-0.0513167023
0	7.8946	0.2505321736	0.0000008330
0.5	2.3185	0.3961993774	0.500013404
1	1.8183	0.3888079314	0.500013404

Table 5.4: KS RBH.

critical velocities but differ in sign. If we increase the EoS parameter then the critical radius is shifted near RBH. It is evident the critical velocity is negative for phantom like fluid and positive for quintessence, dust, and stiff matter. The speed of sound is negative at $x = 30267.74$ and positive for remaining critical radius. For this metric, we find that

$$u_c^2 = \frac{r}{4}\left(2\tilde{b}r - \frac{2\tilde{b}^2r^3 + 2M\tilde{b}}{\sqrt{r\left(\tilde{b}^2r^3 + 4M\tilde{b}\right)}}\right), \tag{5.4.7}$$

$$\mathbb{V}_c^2 = \frac{r^2\left(2\tilde{b}r - \frac{2\tilde{b}^2r^3+2M\tilde{b}}{\sqrt{r\left(\tilde{b}^2r^3+4M\tilde{b}\right)}}\right)}{r^2\left(2\tilde{b}r - \frac{2\tilde{b}^2r^3+2M\tilde{b}}{\sqrt{r\left(\tilde{b}^2r^3+4M\tilde{b}\right)}}\right) + 4r\left(1+\tilde{b}r^2 - \sqrt{r\left(\tilde{b}^2r^3+4M\tilde{b}\right)}\right)}. \tag{5.4.8}$$

The condition (2.6.18) yields

$$\frac{\left(2\tilde{b}r - \frac{2\tilde{b}^2r^3+2M\tilde{b}}{\sqrt{r\left(\tilde{b}^2r^3+4M\tilde{b}\right)}}\right)}{2r} > 0. \tag{5.4.9}$$

Chapter 6

Accreting Fluids onto Regular Black Holes Via Hamiltonian Approach

In this chapter, we study the steady state spherically symmetric accretion onto RBHs and develop the Hamiltonian dynamical system for the accretion problem. We discuss the motion of isothermal relativistic, ultra-relativistic, radiation and sub relativistic test fluids in the frame work of Hamiltonian dynamical system around RBHs. The thermodynamical properties of fluids have been studied for different choices of EoS parameter. Moreover, CPs and conserved quantities have been found for different fluids. The behavior of an accreting fluid has been discussed as subsonic and supersonic according to EoS and RBHs.

6.1 General Description

Here, we will derive the governing equations and analyze the flow of perfect fluid and accretion rate onto RBHs by utilizing the energy and particle conservation laws. In this way, we consider general spherical symmetric set-up and stationary line element is given in Eq.(2.1.2) in which $X(r) > 0$ is the function of r. The energy momentum tensor for perfect fluid is given by

$$T_{\mu\nu} = (p+\varepsilon)u_{\mu}u_{\nu} + pg_{\mu\nu}, \tag{6.1.1}$$

where p is the pressure, ε is the energy density and u^{μ} is the four-velocity which is given by

$$u^{\mu} = \frac{dx^{\mu}}{d\tau} = (u^{t}, u^{r}, 0, 0), \tag{6.1.2}$$

where τ is the proper time. Here, u^{θ} and u^{ϕ} become zero due to spherical symmetry restrictions. We define the current density or particle flux by $J^{\mu} = nu^{\mu}$. According to law of particle conservation, the divergence of particle flux is zero for this system, i.e.,

$$\nabla_{\mu}J^{\mu} = \nabla_{\mu}(nu^{\mu}) = 0, \tag{6.1.3}$$

where ∇_μ is covariant derivative. It is useful to mention here that all the flow variables $(p, \varepsilon, u^\mu, n)$ are spherically symmetric and we have a steady state according to definition of Michel [57, 58]. Using Eq.(2.1.2) and normalization condition $u^\mu u_\mu = -1$, we have

$$u_t = \pm\sqrt{u^2 + X(r)}, \tag{6.1.4}$$

where $u = dr/d\tau = u^r$, u^t can be negative or positive due to square root which represents the backward or forward in time conditions. However, $u < 0$ is required for accretion process, otherwise for any outward flows $u > 0$. The equation of continuity is

$$\nabla_\mu(nu^\mu) = \frac{1}{r^2}\partial_r(r^2 nu) = 0, \tag{6.1.5}$$

which leads to

$$r^2 nu = C_a, \tag{6.1.6}$$

where C_a is integration constant. The thermodynamics of perfect fluid is given by [143]

$$dp = n(dh - Tds), \quad d\varepsilon = hdn + nTds, \tag{6.1.7}$$

where $h = \frac{\varepsilon+p}{n}$ is the specific enthalpy, T is the temperature and s is the specific entropy.

Furthermore, the theorem of relativistic hydrodynamics (which is only applicable for smooth flows) states that the scalar quantities such as $hu_\mu\tilde{\eta}^\mu$ remain conserved along the trajectories of the fluid [143], i.e.,

$$u^\nu\partial_\mu(hu_\mu\tilde{\eta}^\mu) = 0, \tag{6.1.8}$$

where $\tilde{\eta}^\mu$ is a Killing vector of space-time. Considering $\tilde{\eta}^\mu = (1,0,0,0)$ of metric (2.1.2), we obtain

$$h\sqrt{u^2 + X(r)} = C_b, \tag{6.1.9}$$

where C_b is integration constant. It is also mention here that the specific entropy remains conserved along the fluid trajectories, i.e., $u^{\mu}\nabla_{\mu}s = 0$. Hence, the stress energy tensor $T_{\mu\nu}$ can be written as [144, 145]

$$T_{\mu\nu} = nhu_{\mu}u_{\nu} + (nh - \varepsilon)g_{\mu\nu},$$

and then projection of $T^{\mu\nu}$ onto u^{μ} turns out to be

$$u_{\nu}\nabla_{\mu}T^{\mu\nu} = u_{\nu}\nabla_{\mu}[nhu_{\mu}u_{\nu} + (nh - \varepsilon)g_{\mu\nu}] = -nTu^{\mu}\nabla_{\mu}s = 0. \tag{6.1.10}$$

Since fluid is stationary (independent of time) and moving along radial direction only in the present case, which leads to $\partial_r s = 0$ and hence s becomes constant. In this scenario, Eq.(6.1.7) reduces to

$$dp = ndh, \quad d\varepsilon = hdn. \tag{6.1.11}$$

Next, we will use Eqs.(6.1.6), (6.1.9) and (6.1.11) to analyze the flow. Since s becomes constant, and thus canonical form of EoS of simple fluid ($\varepsilon = \varepsilon(n,s)$) [144, 145] turns out to be barotropic form and is given by

$$\varepsilon = \tilde{F}(n). \tag{6.1.12}$$

In view of above relation Eq.(6.1.11) leads to

$$h = \frac{d\varepsilon}{dn} = \frac{d\tilde{F}(n)}{dn} = \tilde{F}'(n), \quad p' = n\tilde{F}'' \Longrightarrow p = n\tilde{F}' - \tilde{F}, \tag{6.1.13}$$

which provides the relationship between $\tilde{F}$ and $\tilde{G}$ ($p = \tilde{G}(n)$)as follows:

$$\tilde{G}(n) = n\tilde{F}'(n) - \tilde{F}(n). \tag{6.1.14}$$

Further, the sound speed can be defined as $a^2 = (\partial p/\partial \varepsilon)_s$, which reduces to $a^2 =$

$dp/d\varepsilon$ because s is constant. Using (6.1.11), we can find

$$\frac{dh}{h} = a^2 \frac{dn}{n}. \tag{6.1.15}$$

Using Eqs.(6.1.13) and (6.1.15), we obtain

$$a^2 = n(\ln \tilde{F}')'. \tag{6.1.16}$$

Since the motion is in radial direction, so the metric (2.1.2) reduces to

$$ds^2 = -(\sqrt{X(r)}dt)^2 + \left(\frac{dr}{\sqrt{X(r)}}\right)^2. \tag{6.1.17}$$

The ordinary three velocity of the fluid can be defined as $v \equiv \frac{dr/\sqrt{X(r)}}{\sqrt{X(r)}dt}$ and its expression can be obtained by using relations $u^t = dt/d\tau$, $u = u^r = dr/d\tau$, $u_t = -X(r)u^t$ and Eq.(6.1.4) as follows:

$$v^2 = \frac{u^2}{X(r)+u^2}, \tag{6.1.18}$$

which implies

$$u^2 = \frac{X(r)v^2}{1-v^2} \ \ and \ \ (u_t)^2 = \frac{X^2(r)}{1-v^2}. \tag{6.1.19}$$

Utilizing above relations in (6.1.6), we obtain

$$C_a^2 = \frac{r^4 n^2 X(r) v^2}{1-v^2}. \tag{6.1.20}$$

These results will be used in the following sections [144, 145].

6.2 Hamiltonian System

Here, we derive two integrals of motion (C_a, C_b) given in (6.1.6) and (6.1.9) by adopting Hamiltonian procedure. The idea of reformulating of the Michel flow problem as a Hamiltonian system for global flow is analyzed in detail by [129, 146, 147, 148].

The Hamiltonian H is a function of two variables (x,y) and its simplest form has one degree of freedom. Let H be the square of right hand side of Eq.(6.1.9):

$$H = h^2(X(r) + u^2). \tag{6.2.1}$$

Using Eq. (6.1.19) in above equation, we have

$$H(r,v) = \frac{X(r)h^2(r,v)}{1-v^2}, \tag{6.2.2}$$

and this is derived in [144, 145]. Here, we fixed dynamical variables to be (r,v). For the derivation of sonic points (CPs) are derived in following subsection.

6.2.1 Sonic Points

The dynamical system of Hamiltonian H given in (6.2.2) reads to be [144, 145]

$$\dot{v} = -H_{,\,r},\ \dot{r} = H_{,\,v}, \tag{6.2.3}$$

where dot represents the derivative with respect to $\bar{t}$ which is new "time" variable. The "time" variable $\bar{t}$ for the dynamical system is any variable on which Eq.(6.2.1) does not depend explicitly so that the dynamical system is autonomous. For finding CPs, we utilize Eq.(6.2.3) for which we require

$$\frac{d}{dr}H(r,v) = \frac{h^2}{1-v^2}\left(\frac{d}{dr}(X(r)) + 2X(r)\frac{d}{dr}(\ln h)\right), \tag{6.2.4}$$
$$\frac{d}{dv}H(r,v) = \frac{2X(r)h^2 v}{(1-v^2)^2}\left(1 + \frac{1-v^2}{v^2}\frac{d}{dv}(\ln h)\right). \tag{6.2.5}$$

Moreover, Eq.(6.1.15) can be expressed as

$$\frac{d}{dr}(\ln h) = a^2\frac{d}{dr}(\ln n), \tag{6.2.6}$$
$$\frac{d}{dv}(\ln h) = a^2\frac{d}{dv}(\ln n). \tag{6.2.7}$$

By keeping 'r' as a constant in Eq.(6.1.20), we have $\frac{nv}{\sqrt{1-v^2}}$ = constant, which under differentiation with respect to 'v' leads to

$$\frac{d}{dv}(\ln n) = -\frac{1}{v(1-v^2)} \Rightarrow \frac{d}{dv}(\ln h) = -\frac{a^2}{v(1-v^2)}. \tag{6.2.8}$$

Similarly,

$$\frac{d}{dr}(\ln n) = -\frac{r\frac{d}{dr}(\ln X(r))+4}{2r} \Rightarrow \frac{d}{dr}(\ln h) = -\frac{a^2\left(r\frac{d}{dr}(\ln X(r))\right)+4}{2r}. \tag{6.2.9}$$

Finally, by using Eqs.(6.2.3)-(6.2.9), we obtain

$$\dot{v} = -\frac{h^2}{r(1-v^2)}\left(r\big(\frac{d}{dr}X(r)\big)(1-a^2)-4X(r)a^2\right), \tag{6.2.10}$$

$$\dot{r} = -\frac{2X(r)h^2}{v(1-v^2)^2}\left(v^2-a^2\right). \tag{6.2.11}$$

By setting the above relations equal to zero, we can get CPs as follows

$$v_c^2 = a_c^2 \;\; and \;\; r_c(1-a_c^2)\frac{d}{dr_c}X(r_c) = 4X_ca_c^2. \tag{6.2.12}$$

Here $X_c \equiv X(r_c)$ and $\frac{d}{dr_c}X_c \equiv \frac{d}{dr}X(r)\mid_{r=r_c}$. The second relation of Eq.(6.2.12) represents the sound speed at the CP, i.e., a_c^2 in terms of r_c,

$$a_c^2 = \frac{r_c\frac{d}{dr_c}X_c}{4X_c+r_c\frac{d}{dr_c}X_c}. \tag{6.2.13}$$

In this scenario, the constant C_a^2 (6.1.20) can be written as

$$C_a^2 = r_c^4n_c^2v_c^2\frac{X_c}{1-v_c^2} = \frac{1}{4}r_c^5n_c^2\frac{d}{dr_c}X_c, \tag{6.2.14}$$

where we have used (6.2.12). Using C_a^2 in Eq.(6.1.20), we have

$$\left(\frac{n}{n_c}\right)^2 = \frac{r_c^5\left(\frac{d}{dr_c}X_c\right)(1-v^2)}{4r^4X(r)v^2}. \tag{6.2.15}$$

6.3 Regular Black Holes

In this section, we will discuss RBHs with fixed BH background, neglecting the self-gravity of the fluid.

6.3.1 Regular Black Hole using Dagum Distribution Function

Consider the line element (2.1.2) for generally spherically symmetric metric with

$$X(r) = 1 - \frac{2M}{r}\frac{\xi(r)}{\xi(\infty)}, \tag{6.3.1}$$

where the DDF [149] is

$$\xi(\bar{x}) = \frac{a_1 p_1 \bar{x}^{a_1 p_1 - 1}}{a_2^{a_1 p_1}\left(1+\left(\frac{\bar{x}}{a_2}\right)^{a_1}\right)^{p_1+1}}, \tag{6.3.2}$$

and a_1, a_2, p_1 are positive parameters. By assuming $a_2 = 1$ and $p_1 = 1/a_1$, we find

$$\xi(\bar{x}) = \frac{1}{\left(1+\bar{x}^{a_1}\right)^{\frac{a_1+1}{a_1}}}. \tag{6.3.3}$$

After replacing $\bar{x} \to \frac{q^2}{Mr}$ and simplifications leads to

$$X(r) = 1 - \frac{2M}{r}\left(\frac{1}{\left(1+r\left(\frac{q^2}{Mr}\right)^{a_1}\right)^{\frac{a_1+1}{a_1}}}\right)^{\delta_4}. \tag{6.3.4}$$

This RBH satisfies the WEC for $\delta_4 = \frac{3}{a_1+1}$ and hence we have

$$X(r) = 1 - \frac{2M}{r}\left(\frac{1}{1+r\left(\frac{q^2}{Mr}\right)^{a_1}}\right)^{3/a_1}. \tag{6.3.5}$$

Moreover, one can find the RBH metric by using DDF with a factor q/r^2, which behaves asymptotically as RN metric and its metric function is

$$X(r) = 1 - \frac{2M}{r}\left(\frac{1}{1+\eta_a\left(\frac{q^2}{Mr}\right)^{a_1}}\right)^{\frac{3}{a_1}} + \frac{q^2}{r^2}\left(\frac{1}{1+\eta_a\left(\frac{q^2}{Mr}\right)^{a_1}}\right)^{\frac{4}{a_1}}, \tag{6.3.6}$$

where $\eta_a > 0$ is a constant and $a_1 \geq 2$ is an integer. It should be noted that the associated solution satisfies the weak energy condition if we have $\eta_a \geq (2/3)^a$ as shown in [12]. The associated electric field expression is given by

$$E = \frac{q}{r^2}\left(\frac{3\eta_a(3+a_1)\left(\frac{q^2}{Mr}\right)^{a_1-1}}{2\left(1+\eta_a\left(\frac{q^2}{Mr}\right)^{a_1}\right)^{2+\frac{3}{a_1}}} + \frac{1-3\eta_a(3+a_1)\left(\frac{q^2}{Mr}\right)^{a_1}}{\left(1+\eta_a\left(\frac{q^2}{Mr}\right)^{a_1}\right)^{2(2+a_1)/a_1}}\right). \tag{6.3.7}$$

The metric with function (6.3.6) behave-like de Sitter BH metric as

$$X(r) \approx 1 - \frac{M^4}{\eta_a^{\frac{4}{a_1}} q^6}(2\eta_a^{\frac{1}{a_1}} - 1)r^2. \tag{6.3.8}$$

It can be noticed that the term proportional to r^2 cannot become zero because $\eta_a \geq (2/3)^{a_1}$. The metric function (6.3.6) remains regular, if we set $(1/2)^{a_1} \leq \eta_a < (2/3)^{a_1}$ but they have de Sitter center without satisfying the WEC. Therefore, if BH metric is regular and satisfies the WEC, then it has a de Sitter center. However, if the metric has a de Sitter behavior when approaching to the center, it does not necessarily satisfies the WEC. Furthermore, if we set $\eta_a < (1/2)^{a_1}$, BH metric is not regular. Finally, there is a known case which can be obtained as a particular case of Eq.(6.3.6) by choosing

$a_1 = 2$ and $\eta_a = \frac{M^2}{q^2}$, i.e,

$$X(r) = 1 - \frac{2M\left(\frac{r^2}{r^2+q^2}\right)^{3/2}}{r} + \frac{q^2}{r^2}\left(\frac{r^2}{r^2+q^2}\right)^2. \tag{6.3.9}$$

This case corresponds to RBH metric given in [9] and we will discuss the accretion onto this RBH in the following sections.

6.4 Isothermal Test Fluids

The fluid flowing at a constant temperature is known as isothermal fluids. In accretion process, sound speed of the fluid flow remains constant. Moreover, the speed of sound at sonic points is equal to the speed of sound of accretion flow at any radius [144]. Here, we follow [145] to find the general solution of isothermal EoS of the form $p = \omega\varepsilon$, which leads to $p = \omega\tilde{F}(n)$ and $\tilde{G}(n) = \omega\tilde{F}(n)$ given in Eqs.(6.1.12) and (6.1.14), respectively, where ω $(0 < \omega \leq 1)$ is the state parameter. The differential equation (6.1.14) becomes

$$n\tilde{F}'(n) - \tilde{F}(n) = \omega\tilde{F}(n), \tag{6.4.1}$$

using (6.1.12) and integrating above equation, we have

$$\varepsilon = \tilde{F} = \frac{\varepsilon_c}{n_c^{\omega+1}}n^{\omega+1}, \tag{6.4.2}$$

where $\frac{\varepsilon_c}{n_c^{\omega+1}}$ appears as integration constant and hence Eq.(6.1.13) becomes

$$h = \frac{(\omega+1)\varepsilon_c}{n_c}\left(\frac{n}{n_c}\right)^{\omega}. \tag{6.4.3}$$

Using Eq.(6.2.15), we have

$$h^2 \propto \left(\frac{1-v^2}{v^2 r^4 X(r)}\right)^{\omega}, \tag{6.4.4}$$

and

$$H(r,v) = \frac{X^{1-\omega}(r)}{\left(1-v^2\right)^{1-\omega} v^{2\omega} r^{4\omega}}, \tag{6.4.5}$$

where all constants get absorb in the redefinition of Hamiltonian H and the time $\bar{t}$. Next, we need to discuss the pressure physically. Using EoS $p = \omega\varepsilon$ and by substituting Eq.(6.2.15) in (6.4.2), we get

$$p \propto \left(\frac{1-v^2}{X(r)v^2r^4}\right)^{\frac{\omega+1}{2}}. \tag{6.4.6}$$

If this pressure approaches to the event horizon from the region where t is time like, then $X(r) \to 0$ and the speed $v \to 0$ or 1. In this situation, Hamiltonian remains constant on the solution curve. For $v \to 0$, the solution curve approaches to horizon and hence pressure diverges. For $v \to 1$, Eq. (6.4.6) remains finite in the surrounding of horizon [144, 145]. If $X(r) = 0$ has single root as $r \to r_h$ then using (6.4.6), one can observe the pressure diverges as

$$p \sim \left(r - r_h\right)^{-\frac{\omega+1}{2\omega}}. \tag{6.4.7}$$

If $X(r) = 0$ has double root then

$$p \sim \left(r - r_h\right)^{-\frac{\omega+1}{\omega}}. \tag{6.4.8}$$

The Hamiltonian (6.4.5) of the dynamical system is a constant along the solution curve. A global flow solution that extends to spatial infinity is

$$v \simeq v_1 r^{-\varsigma} + v_\infty \; as \; r \to \infty, \tag{6.4.9}$$

where $(v_1, |v_\infty| \leq 1, \varsigma > 0)$ are constants. Substituting Eq.(6.4.9) in Hamiltonian (6.4.5), we obtain

$$
\begin{aligned}
H &\simeq \frac{X^{1-\omega}(r)}{r^4\omega} \quad 0<|v_\infty|<1, &(6.4.10)\\
H &\simeq \frac{X^{1-\omega}(r)}{r^{(4-2\varsigma)\omega}} \quad |v_\infty|=0, &(6.4.11)\\
H &\simeq \frac{X^{1-\omega}(r)}{r^{(4\omega+\omega\varsigma-\varsigma)}} \quad |v_\infty|=1. &(6.4.12)
\end{aligned}
$$

Now the behavior of the fluid is analyzed by considering different choices of state parameter ω such as $\omega=1/4$ (sub-relativistic fluid), $\omega=1/3$ (radiation fluid), $\omega=1/2$ (ultra-relativistic fluid) and $\omega=1$ (ultra-stiff fluid), and these are discussed in following subsections.

6.4.1 Solution for Ultra-Stiff Fluid $(\omega=1)$

We assume the fluids with EoS $p=\varepsilon$ and these are ultra-stiff fluids. For instance, the usual EoS for the ultra-stiff fluids is $p=\omega\varepsilon$, i.e., the value of state parameter is defined as $\omega=1$. The Hamiltonian (6.4.5) reduces to

$$H=\frac{1}{v^2r^4}. \tag{6.4.13}$$

In this case, the metric function $X(r)$ does not involve and it is discussed in detail in [129, 144, 145].

6.4.2 Solution for Ultra-Relativistic Fluid $(\omega=1/2)$

Here, we consider the fluids with EoS $p=\varepsilon/2$ and these fluids are ultra-relativistic. The Hamiltonian takes the simple form

$$H=\frac{\sqrt{X(r)}}{r^2|v|\sqrt{1-v^2}}. \tag{6.4.14}$$

One can observe that the point $(r, v^2) = (r_h, 1)$ is not a CP of the dynamical system. Eq.(6.4.14) can be solved for some given value of $H = H_c$ and find v^2 as follows

$$v^2 = \frac{1 \pm \sqrt{1 - 4f(r)}}{2} \tag{6.4.15}$$

where $f(r) \equiv \frac{X(r)}{H_c r^4}$. We plot the above velocity of fluid (v) versus r for aforementioned two RBHs such as KS RBH and DDF RBH by inserting the corresponding values of $X(r)$ as shown in the left and right panels of Fig.**6.1**, respectively. The trajectories in Fig.**6.1** corresponds to values of $H_0 = \{H_c, H_c \pm 0.04, H_c \pm 0.09\}$ where $H = H_c = 0.170615$ (for KS RBH) and $H = H_c = 0.170615$ (for DDF RBH). However the values of (r_h, r_c, v_c) are approximately equal to (1.66, 2.1575, 0.707107) and (1.32, 1.75626, 0.707107) for KS RBH and DDF RBH, respectively. For $H = H_c = 0.170615$ (KS RBH) and $H = H_c = 0.232518$ (DDF RBH), the solution curves pass through the CPs $(r_c, -v_c)$ and (r_c, v_c). It is observed that the heteroclinic orbit exists in the range $-v_c < v < v_c$ and also passes through two CPs $(r_c, -v_c)$ and (r_c, v_c). It can also be seen that the fluid flow is closer to DDF RBH instead of KS RBH. It is mentioned here that the fluid experiences the particle emission or fluid flow-out when $v > 0$, while fluid accretes for $v < 0$. Moreover, Fig.**6.1** describes the following four types of fluid.

- We observe the supersonic/subsonic flows out of the fluid in the ranges $v_c < v < 1$ and $0 < v < v_c$, while subsonic/supersonic accretion appear in the ranges $-v_c < v < 0$ and $-1 < v < -v_c$, respectively.
- We have purely supersonic outflow for $v > v_c$ and purely supersonic accretion for $v < -v_c$.
- We have subsonic flow-out followed by subsonic accretion for $v_c > v > -v_c$.
- We have supersonic out flow followed by subsonic motion, (upper plot) and subsonic accretion followed by supersonic accretion (lower plot).

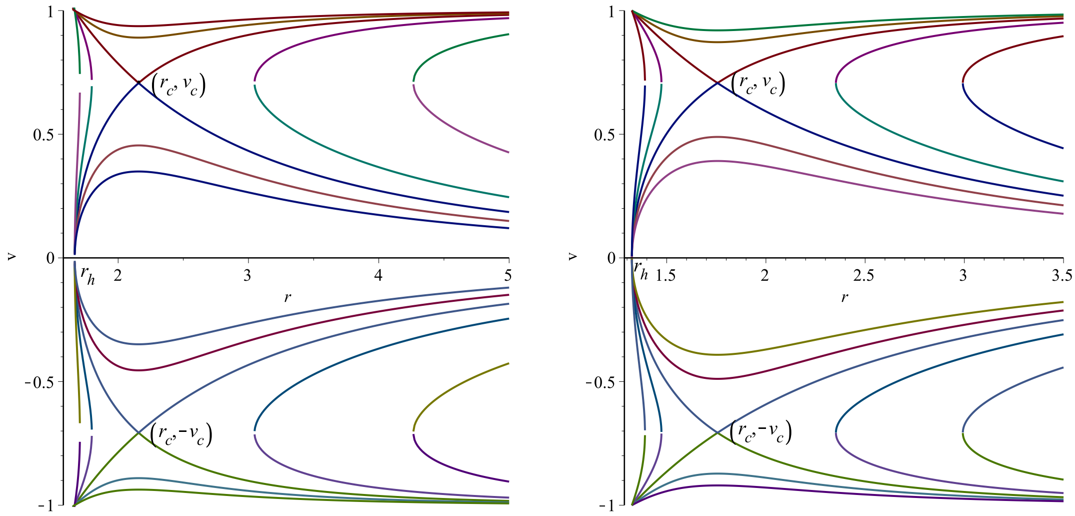

Figure 6.1: Case $\omega = 1/2$. Left Panel: Plot of (6.4.15) for KS BH with $M = 1$, $\tilde{b} = 0.9$. Right Panel: Plot of (6.4.15) for DDF RBH with $M = 1$, $q = 0.6$.

According to above discussion, we can say that the fluid outflow starts at horizon because of its high pressure, which leads to divergence (can be seen from Eq.(6.4.7)) and the fluid under the effects of its own pressure flows back to spatial infinity [145]. From Fig.**6.1**, we observe that the supersonic accretion is followed by subsonic accretion and vanishes inside the horizon which does not give support to the claim that "the flow must be supersonic at the horizon" [150]. Thus, the flow of the fluid is neither transonic nor supersonic near the horizon [151, 152]. These new solutions correspond to fine tunning and instability problems in dynamical systems. The issue of stability is related to the nature of saddle points (CPs (r_c, v_c) and $(r_c, -v_c)$) of the Hamiltonian function. Further analysis of stability could be done by using Lyapunov's theorem or linearization of dynamical system [153, 154, 155] and their variations [156]. Another stability issue is the outflow of the fluid which starts in the surrounding of horizon under the effect of pressure divergent. This outflow is unstable because it follow a subsonic path passing through the saddle point (r_c, v_c) and becomes supersonic with speed approaches the speed of the light. The point $(r = r_h, v = 0)$ can be observed as attractor as well as repeller where solution curves converge and diverge, respectively,

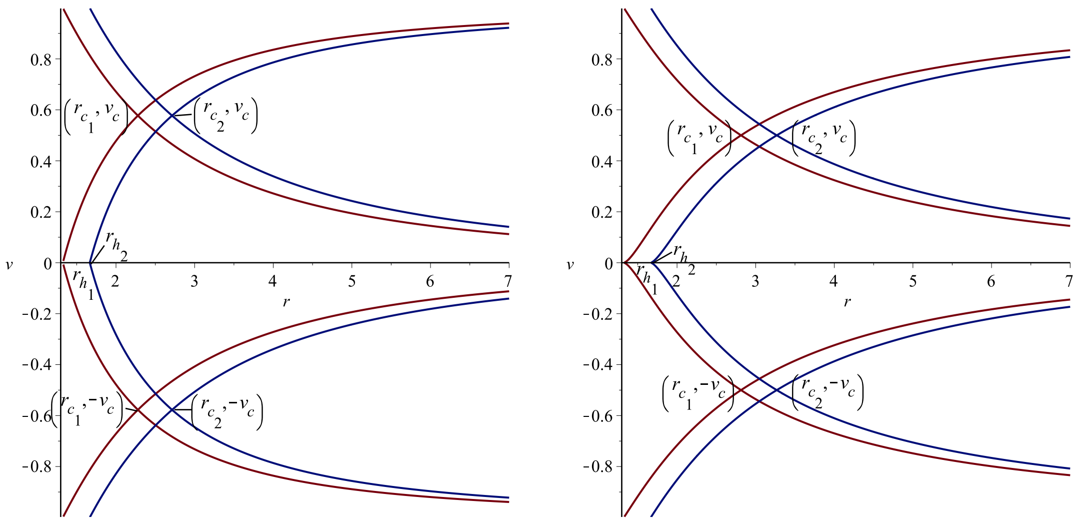

Figure 6.2: Left panel: Case $\omega = 1/3$. Red plot of (6.4.16) for DDF RBH with $q = 0.6$ and $M = 1$. The parameters are $r_h \simeq 1.33$, $r_{c_1} = 2.2787$ and $v_c = \frac{1}{\sqrt{3}} \simeq 0.57736$. The solution curve passes through the saddle CPs (r_{c_1}, v_c) and $(r_{c_1}, -v_c)$ for which $H = H_c \simeq 0.261266$. Blue plot of (6.4.16) for KS RBH with $\tilde{b} = 0.9$ and $M = 1$. The parameters are $r_h \simeq 1.68$, $r_{c_2} = 2.71329$ and $v_c = \frac{1}{\sqrt{3}} \simeq 0.57736$. The solution curve passes through the saddle CPs (r_{c_2}, v_c) and $(r_{c_2}, -v_c)$ for which $H = H_c \simeq 0.22373$. Right panel: Case $\omega \leq 1/4$. Red plot of (6.4.17) for DDF RBH with $q = 0.6$ and $M = 1$. The parameters are $r_h \simeq 1.367$, $r_{c_1} = 2.81368$ and $v_c = 0.5$. The solution curve passes through the saddle CPs (r_{c_1}, v_c) and $(r_{c_1}, -v_c)$ for which $H = H_c \simeq 0.29985$. Blue plot of (6.4.17) for KS RBH with $\tilde{b} = 0.9$ and $M = 1$. The parameters are $r_h \simeq 1.717$, $r_{c_2} = 3.2682$ and $v_c = 0.5$. The solution curve passes through the saddle CPs (r_{c_2}, v_c) and $(r_{c_2}, -v_c)$ for which $H = H_c \simeq 0.273276$.

from the cosmological point of view [145, 156].

6.4.3 Solutions for $(\omega = 1/3)$ and $(\omega = 1/4)$: Separatrix Heteroclinic Flows

The EoS with $\omega = 1/3$ and $\omega = 1/4$ describes the fluid such as photon gas and Sub-relativistic fluids (those fluids whose energy density exceeds their isotropic pressure), respectively. The Hamiltonian (6.4.5) for above mentioned fluids takes the following form

$$H = \frac{X^{2/3}(r)}{r^{4/3}|v|^{2/3}(1-v^2)^{2/3}}, \qquad \text{for} \quad \omega = 1/3 \tag{6.4.16}$$

$$H = \frac{X^{3/4}(r)}{r|v|^{1/2}(1-v^2)^{3/4}}. \qquad \text{for} \quad \omega = 1/4 \tag{6.4.17}$$

It is clear from (6.4.16) and (6.4.17) that $(r, v^2) = (r_h, 1)$ are not CPs of dynamical system. Fig.**6.2** represents the contour plots of (6.4.16) and (6.4.17) in (r, v) for $\omega = 1/3$ (left panel) and $\omega = 1/4$ (right panel). We compare the fluid flow for DDF RBH (red plot) and KS RBH (blue plot) in left panel ($\omega = 1/3$) and right panel ($\omega = 1/4$). For the case $\omega = 1/3$, there are two saddle points $(r_{c_1}, -v_{c_1})$ and (r_{c_1}, v_{c_1}) for DDF RBH and two saddle points $(r_{c_2}, -v_{c_2})$ and (r_{c_2}, v_{c_2}) for KS RBH. It is observed that the subsonic flow proceeds from upper branch in lower plot, passes through CPs $(r_{c_1}, -v_{c_1})$ (DDF RBH) and $(r_{c_2}, -v_{c_2})$ (KS RBH), then crosses the horizon r_{h_1} (DDF RBH) and r_{h_2} (KS RBH). On the other hand, supersonic flows proceeds from the lower branch in lower plot again passes through the CPs $(r_{c_1}, -v_{c_1})$ and $(r_{c_2}, -v_{c_2})$; as the fluid approaches the horizon, then v vanishes. The supersonic accretion proceeds from the upper branch of upper plot and passes through CPs (r_{c_1}, v_{c_1}) (DDF RBH) and (r_{c_2}, v_{c_2}) (KS RBH) and so on. For subsonic accretion, fluid proceeds from the lower branch of upper plot and passes through CPs and crosses the horizons. A similar behavior of fluid could be observed for the case $\omega = 1/4$ in the right panel of Fig.**6.2**.

The left panel of Fig.**6.3** represents the comparison of (6.4.16) ($\omega = 1/3$) and (6.4.17) ($\omega = 1/4$) for KS RBH. It can be seen that if the value of ω increases, then the saddle points shifted towards the KS RBH. Also, the right Panel of Figure **6.3** represents the comparison of (6.4.16) ($\omega = 1/3$) and (6.4.17) ($\omega = 1/4$) for DDF RBH. Similar behavior of CPs is observed for DDF RBH.

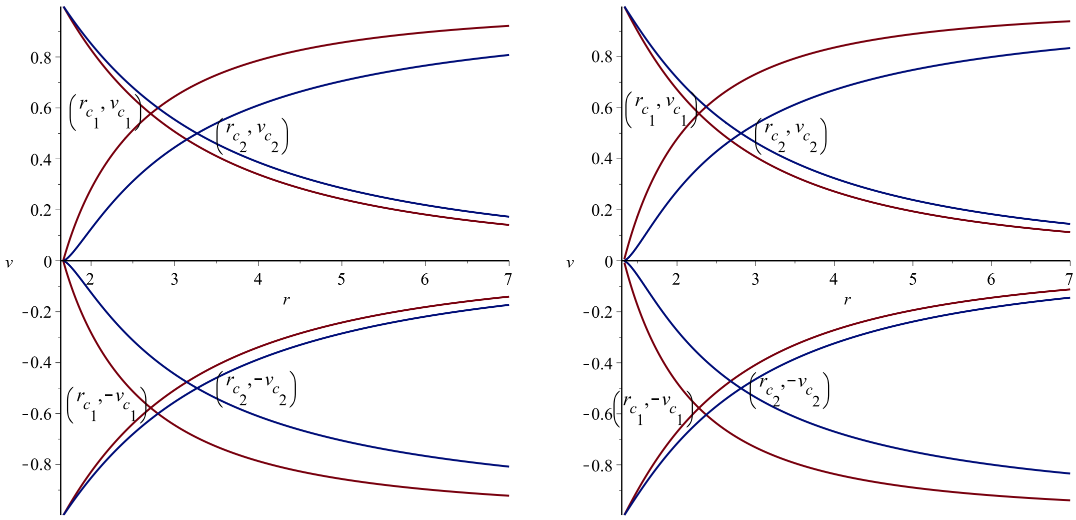

Figure 6.3: Case $\omega \leq 1/3$. Left panel: Red plot of (6.4.16) for KS RBH with $\tilde{b} = 0.9$ and $M = 1$ ($\omega = 1/3$). The parameters are $r_h \simeq 1.717$, $r_{c_1} = 2.71329$ and $v_{c_1} = \frac{1}{\sqrt{3}} \simeq 0.57736$. Blue plot of (6.4.17) for KS RBH $\tilde{b} = 0.9$ and $M = 1$ ($\omega = 1/4$). The parameters are $r_h \simeq 1.717$, $r_{c_2} = 3.2682$ and $v_{c_2} = 0.5$. Right panel: Red plot of (6.4.16) for DDF RBH with $q = 0.6$ and $M = 1$ ($\omega = 1/3$). The parameters are $r_h \simeq 1.33$, $r_{c_1} = 2.2787$ and $v_{c_1} = \frac{1}{\sqrt{3}} \simeq 0.57736$. Blue plot of (6.4.17) for KS RBH $\tilde{b} = 0.9$ and $M = 1$ ($\omega = 1/4$). The parameters are $r_h \simeq 1.33$, $r_{c_2} = 2.2787$ and $v_{c_2} = 0.5$.

6.5 Polytropic Test Fluids

The polytropic EoS is

$$p = \tilde{G}(n) = Kn^{\alpha_1}, \tag{6.5.1}$$

where K and α_1 are constants. One can apply the constraint $\alpha_1 > 1$ for ordinary matter. From Eqs.(6.1.14) and (6.5.1), one can easily construct the expression of specific enthalpy:

$$h = m + \frac{K\alpha_1 n^{\alpha_1 - 1}}{\alpha_1 - 1}, \tag{6.5.2}$$

where m is the baryonic mass. Using above equation and the three-dimensional speed of sound (6.1.16), we have

$$a^2 = \frac{(\alpha_1 - 1)U}{m(\alpha_1 - 1) + U}, \tag{6.5.3}$$

where $(U \equiv K\alpha_1 n^{\alpha_1 - 1})$. Eqs.(6.5.2) and (6.5.3) leads to

$$h = m\frac{\alpha_1 - 1}{\alpha_1 - 1 - a^2}. \tag{6.5.4}$$

Furthermore, using (6.2.2) and (6.5.2), we have

$$h = m\left(1 + Q\left(\frac{1 - v^2}{r^4 X(r) v^2}\right)^{(\alpha_1 - 1)/2}\right), \tag{6.5.5}$$

where

$$Q \equiv \frac{K\alpha_1 n_c^{\alpha_1 - 1}}{m(\alpha_1 - 1)}\left(\frac{r_c^5 X(r_c)_{,r_c}}{4}\right)^{(\frac{\alpha_1 - 1}{2})} = constant. \tag{6.5.6}$$

Inserting (6.5.5) into (6.2.2), the Hamiltonian system takes the following form

$$H = \frac{X(r)}{1 - v^2}\left(1 + Q\left(\frac{1 - v^2}{r^4 X(r) v^2}\right)^{(\frac{\alpha_1 - 1}{2})}\right)^2, \tag{6.5.7}$$

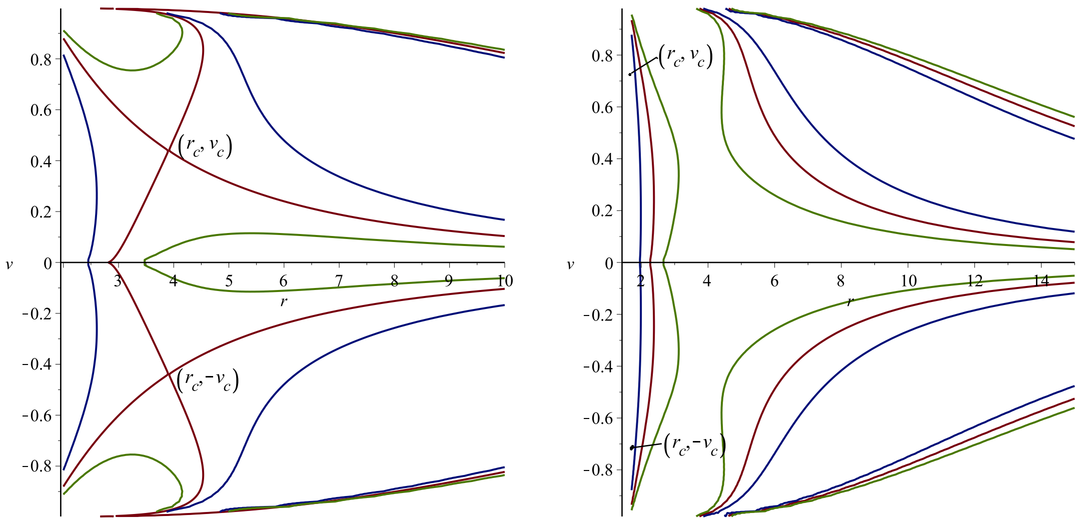

Figure 6.4: Left Panel: Contour plot of (6.5.7) for KS RBH with $\tilde{b} = 0.9$, $M = 1$, $\alpha_1 = 0.5$, $Q = -1/8$ and $n_c = 0.19$. The parameters are $r_h \simeq 1.666666667$, $r_c \simeq 3.928297284$ and $v_c \simeq 0.4377733181$. The Solution curve passing the the CP (r_c, v_c) for $H = H_c \simeq 0.3173998409$. Right Panel: Contour plot of (6.5.7) for DDF BH with $q = 0.5$, $M = 1$, $\alpha_1 = 0.5$, $Q = -1/8$ and $n_c = 0.19$. The parameters are $r_h \simeq 1.614278177$, $r_c \simeq 1.988815258$ and $v_c \simeq 0.7359530796$. The Solution curve avoiding the CP (r_c, v_c) for $H = H_c \simeq 0.2143193585$.

where m^2 has been absorbed into a redefinition of $(\bar{t}, H)$. It is observed that $\frac{dX(r)}{dr} > 0$ for all r which implies that $Q > 0$ with $\alpha_1 > 1$. Hence, the square term in Eq.(6.5.7) is positive, while the coefficient $\frac{X(r)}{1-v^2}$ diverges as r approaches to infinity $(0 \leq 1 - v^2 < 1)$. Thus the Hamiltonian also diverges. Using the technique of authors [144, 145], we finally come to the following system

$$(\alpha_1 - 1 - v_c^2)\left(\frac{1 - v_c^2}{r_c^4 X(r_c) v_c^2}\right)^{(\alpha_1 - 1)/2} = \frac{n_c}{2Q}\left(r_c^5 X(r_c)_{r_c}\right)^{\frac{1}{2}} v_c^2, \tag{6.5.8}$$

$$v_c^2 = \frac{r_c X(r_c)_{r_c}}{r_c X(r_c)_{r_c} + 4X(r_c)}. \tag{6.5.9}$$

By plugging Eq.(6.5.9) in (6.5.8), we find r_c and then corresponding v_c from (6.5.9). It is observed from Eq.(6.5.8) that $\alpha_1 < 1$, $v_c^2 > \alpha_1 - 1$ as mentioned in [144]. The left panel of Fig.**6.4** represents the contour plot of (6.5.7) for KS RBH with $\tilde{b} = 0.9$, $M = 1$, $\alpha_1 = 0.5095$, $Q = -1/8$ and $n_c = 0.19$. We find the new behavior of the

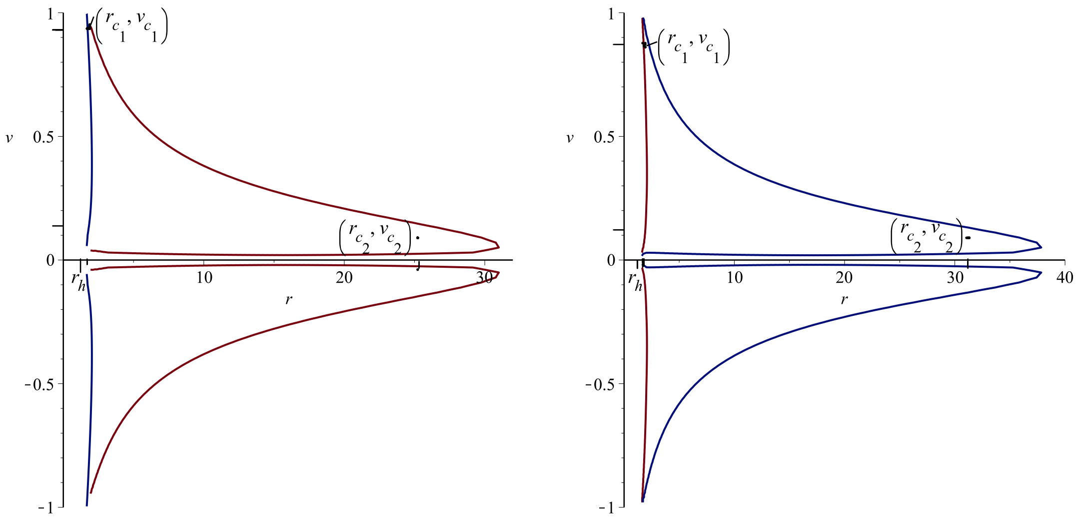

Figure 6.5: Left Panel: Contour plot of (6.5.7) for KS RBH with $\tilde{b} = 0.9$, $M = 1$, $\alpha_1 = 1.9$, $Q = 1/8$ and $n_c = 0.001$. The parameters are $r_h \simeq 1.666666667$, $r_{c_1} \simeq 1.719016508$, $v_{c_1} \simeq 0.9439334159$, $r_{c_2} \simeq 25.49303509$ and $v_{c_2} \simeq 0.1443387155$. Red plot is the solution curve passing through $(r_{c_2}, v_{c_2})$and $(r_{c_2}, -v_{c_2})$ with $H = H_{c_2} = 0.9452241039$. Blue plot is the solution curve passing through $(r_{c_1}, v_{c_1})$and $(r_{c_1}, -v_{c_1})$ with $H = H_{c_2} = .2028972112$. Right Panel: Contour plot of (6.5.7) for DDF RBH with $q = 0.5$, $M = 1$, $\alpha_1 = 1.8$, $Q = 1/8$ and $n_c = 0.001$.The parameters are $r_h \simeq 1.614278177$, $r_{c_1} \simeq 1.724674282$, $v_{c_1} \simeq 0.8893889966$, $r_{c_2} \simeq 31.59490067$ and $v_{c_2} \simeq 0.1283035425$. Blue plot is the solution curve passing through $(r_{c_2}, v_{c_2})$and $(r_{c_2}, -v_{c_2})$ with $H = H_{c_2} = 0.9576657920$. Red plot is the solution curve passing through $(r_{c_1}, v_{c_1})$and $(r_{c_1}, -v_{c_1})$ with $H = H_{c_2} = 0.2585395967$.

fluid by finding the exact CP $r_c \simeq 3.928297284$, $v_c \simeq 0.4377733181$ for which $H = H_c \simeq 0.3173998409$. It can be observed that the accretion starts from subsonic flow for $r \to \infty$ then follow supersonic passing through the saddle point and ends into the horizon. However, the supersonic flow out observed in the vicinity of horizon passing through the saddle point and ends subsonically for $r \to \infty$. The right panel of Fig.**6.4** represents the contour plot of (6.5.7) for DDF RBH with $q = 0.5$, $M = 1$, $\alpha_1 = 0.5$, $Q = -1/8$ and $n_c = 0.19$. We find the CP at $r_c \simeq 1.988815258$, $v_c \simeq 0.7359530796$ for which $H = H_c \simeq 0.2143193585$. We notice that the accretion starts from subsonic flow for $r \to \infty$ then follow supersonic avoiding the saddle point and ends into the horizon. However, the supersonic flow out observed in the vicinity of horizon avoiding the saddle point and ends subsonically for $r \to \infty$. These features agrees with GR BHs [144, 145].

In Fig.**6.5**, we assume $\alpha_1 = 1.9, Q = 1/8, n_c = 0.001$ in left panel for KS RBH and $\alpha_1 = 1.8, Q = 1/8, n_c = 0.001$ in right panel for DDF RBH which lead to four CPs for each RBH, but none of them is saddle point. There are three types of flow: (1) non heteroclinic flow because the solution curves avoiding the CPs and accretion starting from leftmost point until the horizon, (2) followed by non relativistic outflow and (3) subsonic non-global. There are two other fluids flow: (1) partly subsonic accretion and flow-out with source-sink at rightmost point of both graphs and (2) partly supersonic accretion and flow-out with source-sink at rightmost point of both graphs. Other solutions could also be found at $\alpha_1 = 1.8$ for KS RBH and at $\alpha_1 = 5.5/3$ for DDF RBH. Since the fluid is considered as a test matter in geometry of BH, we observe no homoclinic flow i.e. flow following closed path [144, 145].

Chapter 7

Tidal Forces in Kiselev Black Hole

In this chapter, we examine the tidal forces occurring in a Kiselev black hole surrounded by radiation and dust fluids. It is noted that the radial and angular components of the tidal force change the sign between event and Cauchy horizons. We solve the geodesic deviation equation for radially free-falling bodies toward Kiselev black holes. We explain the geodesic deviation vector graphically and point out the location of the event and Cauchy horizons for specific values of the radiation and dust parameters.

7.1 Kiselev Black Holes and its Two Special Cases

The line element of static charged BH surrounded by energy-matter is given in Eq.(2.1.2) with

$$X(r) = 1 - \frac{2M}{r} + \frac{q^2}{r^2} - \frac{\sigma}{r^{3\omega+1}}, \tag{7.1.1}$$

where M and q are the mass and electric charge, σ and ω are normalization parameter and state parameter of matter around BH, respectively [85]. We assume $\omega = 1/3$ which becomes Kiselev BH surrounded by radiation and $\omega = 0$, for Kiselev BH surrounded by dust. For Kiselev BH surrounded by radiation, the radial coordinated of horizons are obtained by taking $X(r) = 0$, i.e.

$$r_{\pm} = M + \sqrt{M^2 - q^2 + \sigma_r}, \tag{7.1.2}$$

where σ_r is parameter of radiation. We will assume only the cases in which $M^2 - q^2 + \sigma_r \geq 0$ because naked singularities ($M^2 - q^2 + \sigma_r < 0$) do not occur in nature if the cosmic conjecture is true. Eq.(7.1.2) give the location of event as well as Cauchy horizon of BH, respectively.

Similarly, for Kiselev BH surrounded by dust ($\omega = 0$), the radial coordinated of horizons are

$$r_{\pm} = \frac{2M + \sigma_d \pm \sqrt{(2M + \sigma_d)^2 - 4q^2}}{2}, \tag{7.1.3}$$

where σ_d is parameter of dust. We choose the case in which $(2M+\sigma_d)^2 \geq 4q^2$ because naked singularities ($(2M+\sigma_d)^2 < 4q^2$) do not occur in nature if the cosmic conjecture is true [157]. Eq.(7.1.3) give the location of event as well as Cauchy horizon of the BH, respectively [85].

7.1.1 Radial Geodesics

Radial geodesic motion for line element (2.1.2) in spherically symmetric spacetimes is obtained by considering $ds = d\tau$ in Eq.(2.1.2), which is [157]

$$X(r)\dot{t}^2 - X(r)^{-1}\dot{r}^2 = 1, \tag{7.1.4}$$

where a dot represents the derivative with respect to proper time τ. Because of the assumption of radial motion, we have $\dot{\theta} = \dot{\phi} = 0$. $E = X(r)\dot{t}$ is well known conserved energy. By putting this in Eq.(7.1.4), we have

$$\frac{\dot{r}^2}{2} = \frac{E^2 - X(r)}{2}. \tag{7.1.5}$$

For the radial infall of a test particle from rest at position b, we get $E = \sqrt{X(r=b)}$ from Eq.(7.1.5) [90]. Newtonian radial acceleration is defined by [158]

$$A^R = \ddot{r}, \tag{7.1.6}$$

Using Eqs.(7.1.5) and (7.1.6), we obtain

$$A^R = -\frac{X'(r)}{2}, \tag{7.1.7}$$

where prime represents the derivative with respect to r (radial coordinate). For Kiselev BH surrounded by radiation and dust, we obtain

$$A^R_r = -\frac{M}{r^2} + \frac{q^2}{r^3} - \frac{\sigma_r}{r^3}, \quad A^R_d = -\frac{M}{r^2} + \frac{q^2}{r^3} - \frac{\sigma_d}{r^2}. \tag{7.1.8}$$

The terms $\frac{q^2}{r^3} - \frac{\sigma_r}{r^3}$ and $\frac{q^2}{r^3} - \frac{\sigma_d}{r^2}$ in Eq.(7.1.8) represents the purely relativistic effect. Eq.(7.1.8) explain the ”exertion” of Kiselev space-time surrounded by radiation and dust on a neutral free falling of massive test body. Interestingly, in a free fall test particle from rest at $r = b$ (for $q, \sigma_r, \sigma_d \neq 0$) would bounce back at radius R^{stop}. The radius R^{stop} for Kiselev space-time surrounded by radiation (R_r^{stop}) and dust (R_d^{stop}) could be found as

$$R_r^{stop} = \frac{b(q^2 - \sigma_r)}{2Mb - q^2 + \sigma_r}, \tag{7.1.9}$$

$$R_d^{stop} = \frac{b\, q^2}{(2Mb + b\sigma_d - q^2)}, \tag{7.1.10}$$

where b is the initial position starting from rest of test particle. R^{stop} located inside the Cauchy (internal) horizon. One can find in the limit $b \to \infty$, $R_r^{stop} \to (q^2 - \sigma_r)/2M$ for radiation and $R_d^{stop} \to q^2/(2M - \sigma_d)$ for dust. The particle in Kiselev BH surrounded by radiation and dust would emerge in different asymptotically flat region in maximal analytic extension. Thus, the particle is physically unstable in maximal analytic extension beyond the internal (Cauchy) horizons of Kiselev space-time surrounded by radiation and dust.

7.2 Tidal forces in Kiselev Space-Time on a Neutral Body in Radial Free Fall

The equation for the space-like components of the geodesic deviation vector ζ^α that describes the distance between two infinitesimally close particles in free fall is given by [74, 75]

$$\frac{D^2\zeta^\alpha}{D\tau^2} - R^\alpha_{\beta\gamma\delta} v^\beta v^\gamma \zeta^\delta = 0, \tag{7.2.1}$$

where v^{γ} is the unit vector tangent to the geodesic. We use the tetrad basis for radial free fall reference frames [77]

$$\begin{aligned}
\hat{e}^{\alpha}_{\hat{0}} &= \left(\frac{E}{X(r)}, -\sqrt{E^2 - X(r)}, 0, 0\right), && (7.2.2)\\
\hat{e}^{\alpha}_{\hat{1}} &= \left(\frac{-\sqrt{E^2 - X(r)}}{X(r)}, E, 0, 0\right), && (7.2.3)\\
\hat{e}^{\alpha}_{\hat{2}} &= r^{-1}(0,0,1,0), && (7.2.4)\\
\hat{e}^{\alpha}_{\hat{3}} &= (r\sin(\theta))^{-1}(0,0,0,1), && (7.2.5)
\end{aligned}$$

where $(x^0, x^1, x^2, x^3) = (t, r, \theta, \phi)$. These unit vectors satisfy the following orthonomality condition:

$$\hat{e}^{\mu}_{\hat{\alpha}} \hat{e}_{\hat{\gamma}\mu} = \zeta_{\hat{\alpha}\hat{\gamma}}, \tag{7.2.6}$$

where $\zeta_{\hat{\alpha}\hat{\gamma}}$ is the Minkowski metric [74]. We have $\hat{e}^{\alpha}_{\hat{0}} = v^{\alpha}$. The geodesic deviation vector, also called Jacobi vector, can be written as

$$\zeta^{\alpha} = \hat{e}^{\alpha}_{\hat{\gamma}} \zeta^{\hat{\gamma}}. \tag{7.2.7}$$

Here we note that $\zeta^{\hat{0}} = 0$ [74] and $\hat{e}^{\alpha}_{\hat{\gamma}}$ are all parallelly transported vectors along the geodesic.

The non-zero independent components of the Riemann tensor in spherically symmetric space-times are

$$\begin{aligned}
R^{1}_{010} &= \frac{X(r)X''(r)}{2}, R^{1}_{212} = -\frac{rX'(r)}{2}, R^{1}_{313} = -\frac{rX'(r)}{2}\sin^2\theta\\
R^{2}_{020} &= \frac{X(r)X'(r)}{2r}, R^{2}_{323} = (1 - X(r))\sin^2\theta, R^{3}_{030} = \frac{X(r)X'(r)}{2r}.
\end{aligned}$$

Using above equations in Eq.(7.2.1), we find the following equations for radial free fall tidal forces [76]:

$$
\begin{aligned}
\ddot{\zeta}^{\hat{1}} &= -\frac{X''}{2}\zeta^{\hat{1}}, && (7.2.8)\\
\ddot{\zeta}^{\hat{i}} &= -\frac{X'}{2r}\zeta^{\hat{i}}, && (7.2.9)
\end{aligned}
$$

where $i = 2,3$. For aforementioned cases of Kiselev BH, Eqs.(7.2.8) and (7.2.9) provided that the tidal forces depend on the mass and electric charge of a BH as well as radiation and dust fluid. Tidal forces are identical to Newtonian tidal forces with the force $-\frac{X'}{2}$ in radial direction which can be observed in Eqs.(7.2.8) and (7.2.9). Further, we will explore Eqs.(7.2.8) and (7.2.9) for Kiselev space-time in detail.

7.2.1 Radial Tidal Forces

Radial tidal forces vanishes at $r = R_0^{rtf}$ (for radiation) and $r = R_1^{rtf}$ (for dust) by using Eqs.(7.2.8) and (7.2.9),

$$
\begin{aligned}
R_0^{rtf} &= \frac{3(q^2-\sigma_r)}{2M}, && (7.2.10)\\
R_1^{rtf} &= \frac{3q^2}{2M+\sigma_d}. && (7.2.11)
\end{aligned}
$$

The maximum value of radial tidal force is at R_{0max}^{rtf} for radiation and R_{1max}^{rtf} for dust such that

$$
\begin{aligned}
R_{0max}^{rtf} &= \frac{2(q^2-\sigma_r)}{M}, && (7.2.12)\\
R_{1max}^{rtf} &= \frac{2q^2}{M+\sigma_d}. && (7.2.13)
\end{aligned}
$$

The maximum radial stretching for above equations are

$$
\begin{aligned}
\ddot{\zeta}^{1}|_{max} &= \frac{M^4}{16(q^2-\sigma_r)^4}, && (7.2.14)\\
\ddot{\zeta}^{1}|_{max} &= \frac{(M+\sigma_d)^4}{16q^6}. && (7.2.15)
\end{aligned}
$$

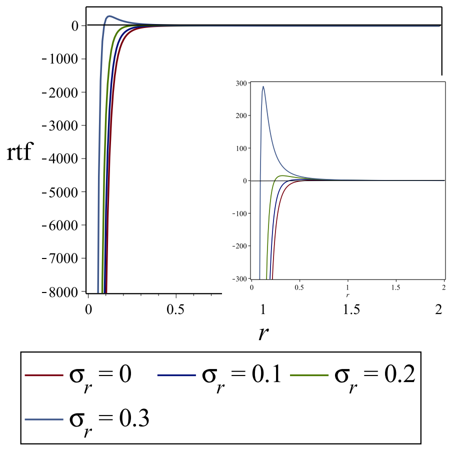

Figure 7.1: Radial tidal force for Kiselev BH surrounded by radiation for chosen values radiation parameter, also $q = 0.6$, $M = 1$ and $b = 100$.

The radial tidal force using Eqs.(7.2.10) and (7.2.11) for Kiselev BH surrounded by radiation and dust for their different choices are shown in Figs.**7.1** and **7.2**. The local maximum of radial tidal force for radiation is greater than for dust near the singularity.

7.2.2 Angular Tidal Forces

The angular tidal forces vanish at

$$R_0^{atf} = \frac{q^2 - \sigma_r}{M}, \tag{7.2.16}$$

$$R_1^{atf} = \frac{2q^2}{(2M + \sigma_d)}, \tag{7.2.17}$$

by using Eqs.(7.1.1) and (7.2.9) for Kiselev spacetime surrounded by radiation and dust, respectively. Also one can find the following conditions from Eqs.(7.1.2), (7.1.3), (7.2.16) and (7.2.17)

$$r_- \leq R_0^{atf} \leq r_+, \tag{7.2.18}$$

$$r_- \leq R_1^{atf} \leq r_+. \tag{7.2.19}$$

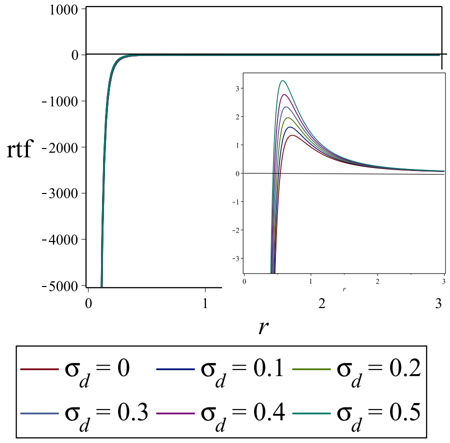

Figure 7.2: Radial tidal force for Kiselev BH surrounded by dust for chosen values dust parameter, also $q = 0.6$, $M = 1$ and $b = 100$.

On the basis of these relations, it is pointed out here that the angular tidal forces becomes zero at some points between the event horizon and Cauchy horizon. The angular tidal force for different choices of σ_r and σ_d for Kiselev BH surrounded by radiation and dust is given in Figs.**7.3** and **7.4**. The local minimum of radial tidal force for radiation is greater as compared to the dust near the singularity. Indeed, the maximum value of angular tidal force for Kiselev BH surrounded by radiation and dust parameter is infinite near the singularity.

7.3 Solutions of the Geodesic Equations for Kiselev Black Hole

We solve the geodesic deviation Eqs.(7.2.8) and (7.2.9) and find the geodesic deviation vectors as functions of r for radially free-falling geodesics. Eqs.(7.2.8) and (7.2.9) along with $\frac{dr}{d\tau} = -\sqrt{E^2 - X(r)}$ lead to the following differential equations

$$(E^2 - X(r))\zeta^{\hat{1}\prime\prime} - \frac{X'(r)}{2}\zeta^{\hat{1}\prime} + \frac{X''(r)}{2}\zeta^{\hat{1}} = 0, \quad (7.3.1)$$

$$(E^2 - X(r))\zeta^{\hat{i}\prime\prime} - \frac{X'(r)}{2}\zeta^{\hat{i}\prime} + \frac{X'(r)}{2r}\zeta^{\hat{i}} = 0. \quad (7.3.2)$$

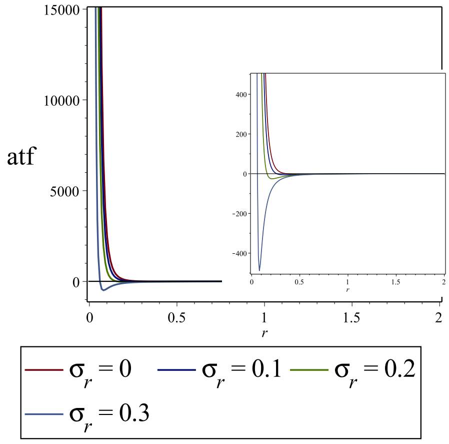

Figure 7.3: Angular tidal force for Kiselev BH surrounded by radiation for chosen values radiation parameter, also $q = 0.6$, $M = 1$ and $b = 100$.

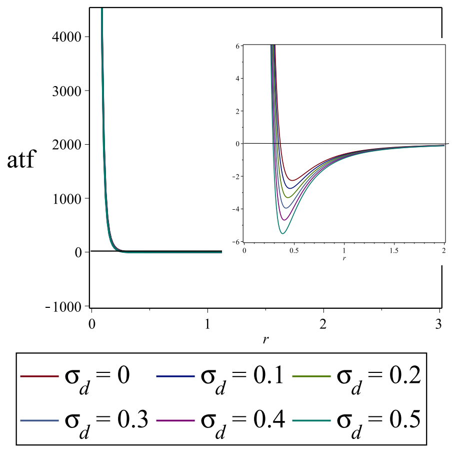

Figure 7.4: Angular tidal force for Kiselev BH surrounded by dust for chosen values dust parameter, also $q = 0.6$ and $b = 100$.

The general solution of radial component using Eqs.(7.2.8) and (7.2.9) is given by

$$\zeta^{\hat{1}}(r) = \sqrt{E^2 - X(r)}\left(C_1 + C_2\int\frac{dr}{(E^2 - X(r))^{3/2}}\right), \qquad (7.3.3)$$

and similarly the angular component

$$\zeta^{\hat{i}}(r) = r\left(C_3 + C_4\int\frac{dr}{r^2(E^2 - X(r))^{1/2}}\right), \qquad (7.3.4)$$

where C_1, C_2, C_3 and C_4 are integration constants [77]. Since we are considering two cases of Kiselev space-time i.e. surrounded by radiation and dust. We consider the geodesic corresponding to a body released from rest at $r = b$. Then the solution to the geodesic deviation equations about the geodesic for the case of radiation is given by

$$\begin{aligned}
\zeta^{\hat{1}}(r) &= \frac{b^3}{Mb - q^2 + \sigma_r}\dot{\zeta}^{\hat{1}}(b)\sqrt{-\frac{2M}{b} + \frac{q^2}{b^2} - \frac{\sigma_r}{b^2} + \frac{2M}{r} - \frac{q^2}{r^2} + \frac{\sigma_r}{r^2}} + \zeta^{\hat{1}}(b) \\
&\times \left[\left(\frac{3Mb^2\sqrt{2Mrb(b-r) - (q^2 - \sigma_r)(b^2 - r^2)}(Mb - q^2 + \sigma_r)}{(2Mb - q^2 + \sigma_r)^{5/2}br}\right)\right. \\
&\times \arctan\left(\frac{(-2Mb + q^2 - \sigma_r)r + Mb^2}{\sqrt{2Mrb(b-r) - (q^2 - \sigma_r)(b^2 - r^2)}\sqrt{2Mb - q^2 + \sigma_r}}\right) \\
&+ \frac{1}{(2Mb - q^2 + \sigma_r)^2(Mb - q^2 + \sigma_r)br}\big(M^2(6Mr - 3q^2 + 3\sigma_r)b^4 \\
&- 2M^3r^2b^3 + 10M^2rb_1^3(q^2 - \sigma_r) - 4Mb^3(q^2 - \sigma_r)^2 + \big(5M^2r^2 \\
&+ 5r(q^2 - \sigma_r)M - 2(q^2 - \sigma_r)^2\big)(q^2 - \sigma_r)b^2 - 4Mr^2(q^2 - \sigma_r)^2 b \\
&\left.+ r^2(q^2 - \sigma_r)^3\big)\right]. \qquad (7.3.5)
\end{aligned}$$

The angular component turns out to be

$$\zeta^{\hat{i}}(r) = \left(\frac{\zeta^{\hat{i}}(b)}{b} + \frac{2b}{\sqrt{q^2 - \sigma_r}}\dot{\zeta}^{\hat{i}}(b)tan^{-1}\sqrt{\frac{(q^2 - \sigma_r)(b - r)}{2Mbr - (q^2 - \sigma_r)(b + r)}}\right)r. \qquad (7.3.6)$$

Similarly, the solution to the geodesic deviation equations about the geodesic for the case of dust is given by

$$
\begin{aligned}
\zeta^{\hat{1}}(r) &= \frac{2b^3}{2Mb-2q^2+b\sigma_d}\dot{\zeta}^{\hat{1}}(b)\sqrt{-\frac{2M}{b}+\frac{q^2}{b^2}-\frac{\sigma_d}{b}+\frac{2M}{r}-\frac{q^2}{r^2}+\frac{\sigma_d}{r}}+\zeta^{\hat{1}}(b)\\
&\times \left[\left(\frac{3b\sqrt{(b-r)\left((2M+\sigma_d)br-q^2b-q^2r\right)}\left(\left(M+\frac{\sigma_d}{2}\right)b-q^2\right)}{\left(M+\frac{\sigma_d}{2}\right)^{-1}\left(2(Mb+\sigma_d)-q^2\right)^{5/2}r}\right)\right.\\
&\times tan^{-1}\left(\frac{\left(M+\frac{\sigma_d}{2}\right)(b^2-2br)+rq^2}{\sqrt{(b-r)\left(((2M+\sigma_d)r-q^2)b-q^2r\right)\left(((2M+\sigma_d)b-q^2\right)}}\right)\\
&+ \frac{1}{\left(2(Mb+\sigma_d)-q^2\right)^2br\left(\left(M+\frac{\sigma_d}{2}\right)b-q^2\right)}\left(3\left(M+\frac{\sigma_d}{2}\right)^2b^4\right.\\
&\times \left(2(Mb+\sigma_d)-q^2\right)+4q^4b^3\left(M+\frac{\sigma_d}{2}\right)-10q^2rb^3\left(M+\frac{\sigma_d}{2}\right)^2\\
&- 2r^2b^3\left(M+\frac{\sigma_d}{2}\right)^3-2q^4+5rq^2b^2\left(M+\frac{\sigma_d}{2}\right)+5r^2q^2b^2\left(M+\frac{\sigma_d}{2}\right)^2\\
&- \left.\left.4r^2q^4b\left(M+\frac{\sigma_d}{2}\right)+q^6r^2\right)\right]. \qquad (7.3.7)
\end{aligned}
$$

For Kiselev BH dust case, angular component becomes

$$
\zeta^{\hat{i}}(r)=\left(\frac{\zeta^{\hat{i}}(b)}{b}+\frac{2b^2}{q}\dot{\zeta}^{\hat{i}}(b)tan^{-1}\sqrt{\frac{q^2(b-r)}{2Mbr-bq^2-br\sigma_d-q^2r}}\right)r. \qquad (7.3.8)
$$

Here, $\zeta^{\hat{1}}(b)$ and $\zeta^{\hat{i}}(b)$ are the radial and angular components of the initial geodesic deviation vector at $r=b$ and $\dot{\zeta}^{\hat{1}}(b)$ and $\dot{\zeta}^{\hat{i}}(b)$ are the corresponding derivatives with respect to the proper time τ. Figs.**7.5**-**7.10** represent the radial and angular components of the geodesic deviation vector of a body in-falling from rest at $r=b$ towards BH for different choices of the radiation and dust parameters. We choose the initial condition (IC1) $\zeta^{\hat{1}}(b)>0$, $\dot{\zeta}^{\hat{1}}(b)=0$ and $\zeta^{\hat{i}}(b)>0$, $\dot{\zeta}^{\hat{i}}(b)=0$. It represents the releasing a body at rest consisting of dust with no internal motion. On the other hand, we choose the initial condition (IC2) $\zeta^{\hat{1}}(b)=0$, $\dot{\zeta}^{\hat{1}}(b)>0$ and $\zeta^{\hat{i}}(b)=0$, $\dot{\zeta}^{\hat{i}}(b)>0$. It corresponds to letting such a body explode from a point at $r=b$. The behavior of the geodesic deviation vector is almost identical for different values of radiation and dust parameter until r becomes of the same order as the horizon radius.

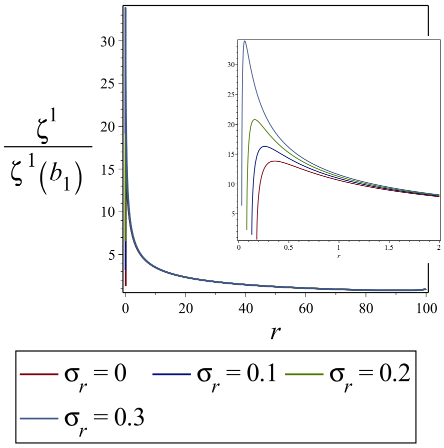

Figure 7.5: Radial components of geodesic deviation for Kiselev BH surrounded by radiation with **IC**1 for different values radiation parameter with $M = 1$, $q = 0.6$ and $b = 100$.

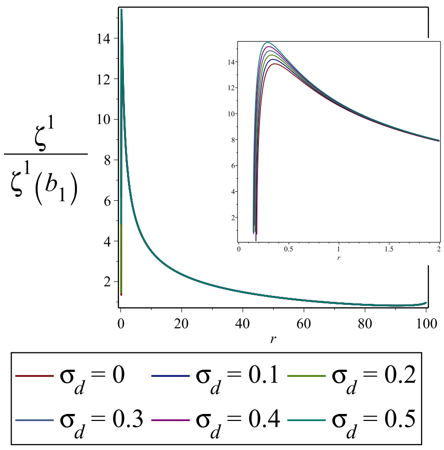

Figure 7.6: Radial components of geodesic deviation for Kiselev BH surrounded by dust with **IC**1 for different values dust parameter with $M = 1$, $q = 0.6$ and $b_1 = 100$.

In Fig.**7.5**, the radial tidal force for Kiselev BH surrounded by radiation depends upon the radiation parameter with **IC**1 i.e. it attains the highest maximum value at $\sigma_r = 0.3$ while as the radiation parameter decrease the maximum value of radial tidal force also decreases. Also the maximum value is shifting towards BH as the radiation parameter increases. For $\sigma_r > 0.3$, it becomes unphysical. Fig.**7.6** represents the radial tidal force for Kiselev BH surrounded by dust for different choices of dust parameter with **IC**1. It is clear from figure the maximum value of radial tidal force is increasing as the value of dust parameter increases as well as it shifting towards BH. It is concluded that the maxima of radial tidal force depends upon radiation and dust parameter; they increase for large values of σ_r and σ_d. Figs.**7.7** and **7.8** represent the radial tidal force for Kiselev BH surrounded by radiation and dust parameter for its different choices with **IC**2. In Fig.**7.7**, maxima of radial tidal force is increasing for higher values of radiation parameter and attains the maximum value at $\sigma_r = 0.3$, and also it is shifted towards BH as the radiation parameter increases. But in Fig.**7.8**, the maximum value of radial tidal force is same for all chosen values of dust parameter. However, the radial tidal force is shifting towards BH as the dust parameter increases.

The angular tidal force for Kiselev BH surrounded by radiation and dust parameter with **IC**1 is similar as explained in [77], as it does not depend upon radiation and dust parameter. However, the angular tidal force with **IC**2 are discussed in Figs.**7.9** and **7.10** for Kiselev BH surrounded by radiation and dust, respectively. It can be seen in Fig.**7.9** that the angular tidal force is increasing from $r = 100$ and attains maximum value at $r = 50$, then it starts to decrease, reflecting the compressing nature of angular component. At some point near BH, angular tidal force start increasing as shown in Fig.**7.9**. Also, it is shifting towards the singularity as radiation parameter increases. In Fig.**7.10**, the angular tidal force have the maximum value for $\sigma_d = 0$, while it decreases for large values of dust parameter.

Tables **7.1** - **7.4** represent the location of event horizon and Cauchy horizon for chosen values of radiation and the dust parameter. Here, we find the location of event and Cauchy horizons of radial tidal forces (Figs.**7.1** and **7.2**), angular tidal forces (Figs.**7.3**

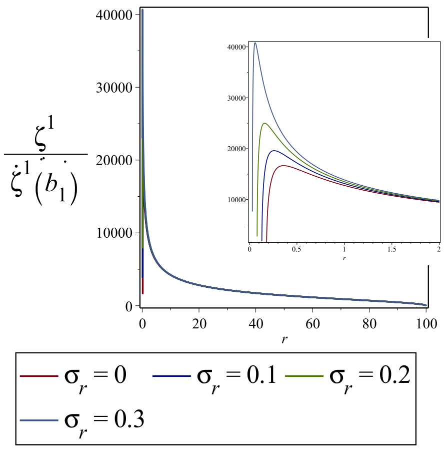

Figure 7.7: Radial components of geodesic deviation for Kiselev BH surrounded by radiation with **IC**2 for different values radiation parameter with $M = 1$, $q = 0.6$ and $b = 100$.

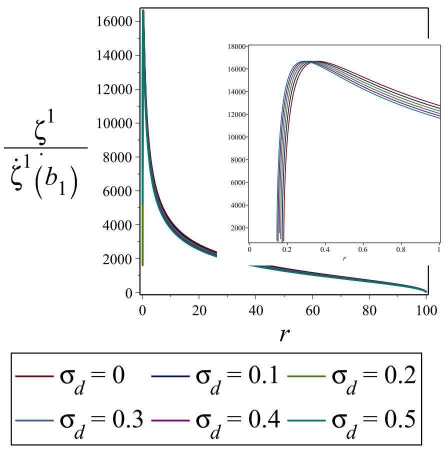

Figure 7.8: Radial components of geodesic deviation for Kiselev BH surrounded by dust with **IC**2 for different values dust parameter with $M = 1$, $q = 0.6$ and $b = 100$.

σ_d	r_+	rtf	atf	Figure 7.6	Figure 7.8	Figure 7.10
0	1.8	0.2400	-0.1371	8.2543	9935.44	19160.04
0.1	1.9116	0.2197	-.1233	8.0509	9455.87	19221.57
0.2	2.0219	0.2015	-.1115	7.8615	9020.038	19271.458
0.3	2.1310	0.1852	-.1013	7.6845	8622.22	19312.18
0.4	2.2392	0.1707	-0.0925	7.5186	8257.65	19345.57
0.5	2.3465	0.1578	-0.0848	7.3627	7922.33	19373.02

Table 7.1: Location of event horizon for chosen values of dust parameter.

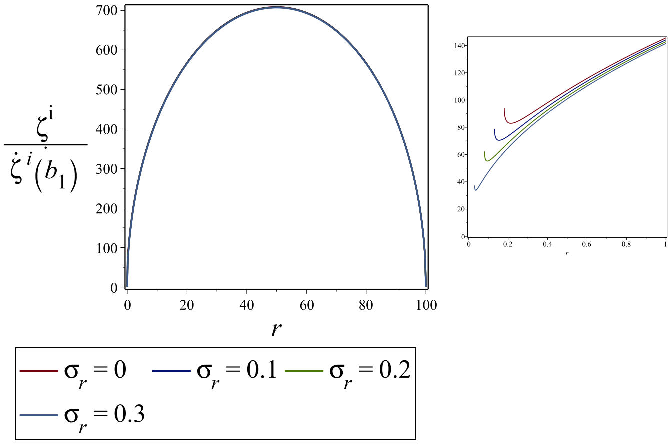

Figure 7.9: Angular components of geodesic deviation for Kiselev BH surrounded by radiation with IC2 for different values radiation parameter with $M = 1$, $q = 0.6$ and $b = 100$.

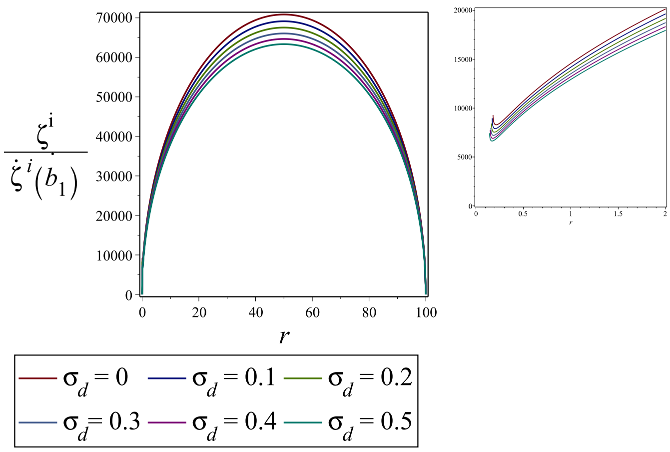

Figure 7.10: Angular components of geodesic deviation for Kiselev BH surrounded by dust with IC2 for different values dust parameter with $M = 1$, $q = 0.6$ and $b = 100$.

σ_d	r_-	rtf	atf	Figure 7.6	Figure 7.8	Figure 7.10
0	0.2	-425.00	100.00	8.2542	9935.44	8343.08
0.1	0.1883	-544.31	129.03	8.0508	9455.87	7966.709
0.2	0.1780	-684.94	163.34	7.8615	9020.03	7625.47
0.3	0.1689	-849.08	203.51	7.6845	8622.22	7314.24
0.4	0.1607	-1039.06	250.10	7.5186	8257.65	7028.92
0.5	0.1534	-1257.28	303.70	7.3627	7922.33	6766.19

Table 7.2: Location of Cauchy horizon for chosen values of dust parameter.

σ_r	r_+	rtf	atf	Figure 7.6	Figure 7.8	Figure 7.10
0	1.8	0.24	-.1371	8.2542	9935.44	191.60
0.1	1.8602	0.2455	-.1336	8.2522	9925.43	193.59
0.2	1.9165	0.2485	-.1302	8.2501	9915.44	195.40
0.3	1.9695	0.2498	-.1269	8.2480	9905.47	197.05

Table 7.3: Location of event horizon for chosen values of radiation parameter.

σ_r	r_-	rtf	atf	Figure 7.6	Figure 7.8	Figure 7.10
0	0.2	-425.00	100.00	8.2542	9935.44	83.4308
0.1	.1397	-1311.44	315.06	8.2521	9925.43	71.5674
0.2	0.08348	-6443.99	1575.13	8.2500	9915.44	57.0569
0.3	0.0304	-138248.39	34292.71	8.2479	9905.47	36.0236

Table 7.4: Location of Cauchy horizon for chosen values of radiation parameter.

and **7.4**), the radial tidal force with **IC**1 (Figs.**7.5** and **7.6**) and **IC**2 (Figs.**7.7** and **7.8**), respectively and angular tidal force with **IC**2 (Fig.**7.9** and **7.10**) for chosen values of radiation and dust parameter, respectively. It is noted that the radial tidal force (in Figs.**7.1** and **7.2**) and angular tidal force (in Figs.**7.3** and **7.4**) change their sign between event and Cauchy horizons. Event horizon is increasing (away from singularity) and Cauchy horizon is decreasing (shifting towards singularity) as the radiation and the dust parameter increase.

Chapter 8

Conclusions and Open Problems

In this thesis, we have made versatile study of well-known BHs/RBHs by using various phenomena's such as thermal fluctuations, accretion and tidal forces. The summary and brief discussion of results are presented below.

Chapter **TWO** deals with the study of the new exact regular spherically symmetric solution of the non-minimal Einstein-Yang- Mill theory with magnetic charge of Wu-Yang gauge field and the cosmological constant. We have only considered the positive non-minimal parameter $\mathfrak{q}$, as zero and negative values lead to space-time curvature singularities. After calculating the mass, entropy and temperature, we have discussed the effect of thermal fluctuation on non-minimal RBH. We have also utilized the logarithmic correction of the entropy and discussed the behavior of pressure and specific heat. We assumed that a BH is a thermodynamic system in equilibrium at Hawking temperature, and systematically analyzed its small statistical fluctuations around equilibrium. These fluctuations give rise to a non-trivial multiplicative factor in front of the expression for the density of states, whose logarithm gives the corrected entropy formula. We have observed that the pressure reduces due to the logarithmic correction when decreasing the value of the cosmological constant.

We have also investigated the ratio of the specific heat at constant pressure and volume (γ); we observe that due to logarithmic correction the value of γ increases. We have also noticed that the values of γ are higher and more stable for negative values of the cosmological constant while it becomes unstable upon positive values of the cosmological constant for a large horizon. We have observed that the first law of thermodynamics is satisfied for non-minimal RBH even in the presence of thermal fluctuations. It is mentioned here that the logarithmic correction term increases the chance of the first law of thermodynamics to be satisfied. We have also investigated the phase transition for the non-minimal RBH and found its CPs. We have observed that the range of horizon radius for local stability of BH increases for negative cosmological constant as compared to positive and zero cosmological constant, respectively.

We have noticed that if we increase the value of the cosmological constant, the phase transition shifted towards BH and vice versa. We have also discussed the free energy in grand canonical (Gibbs free energy) and canonical (Helmholtz free energy) ensembles. We have noticed that the free energy reduces in the presence of a logarithmic correction. It is concluded that the non-minimal RBH becomes more stable globally as well as locally if we increase the value of the cosmological constant and vice versa. We have also noticed that the thermodynamics of the non-minimal RBH gets modified because of the general uncertainty principle [159, 160]. Such correction terms are non-trivial, which is evident from our results and they may lead to interesting consequences like the existence of BH remnants.

In chapter **THREE**, we have considered RN-AdS BH with GM and $f(R)$ BH, and discussed the thermodynamics in the presence of higher order corrections of entropy. We have utilized the results of corrected entropy by setting first order term is logarithmic and second order term is inversely proportional to original entropy. In these scenarios, we have studied the behavior of pressure and specific heat for both BHs.

- It is observed that the pressure reduces for second order correction term for both BHs but the pressure of RN-AdS BH with GM also decreases by considering higher values of cosmological constant while there is no change in pressure with respect to cosmological constant in $f(R)$ BH.

- We have also discussed the ratio of specific heat (γ) at constant pressure and volume for both BHs. We have observed that the value of γ increases due to the effect of higher order correction terms for both BHs. The value of γ for RN-AdS BH with GM exhibits more stable behavior for lower values of cosmological constant while $f(R)$ BH shows similar behavior for both (negative and positive) cases of Λ.

- We have also discussed the ratio of specific heat (γ) at constant pressure and volume for both BHs. We have observed that the value of γ increases due to the effect of higher order correction terms for both BHs. The value of γ for RN-AdS BH with GM exhibits more stable behavior for lower values of cosmological constant while $f(R)$ BH shows similar behavior for both (negative and positive) cases of Λ.

- We have also studied the phase transition due to the effect of higher order correction terms for both BHs and obtained its critical points. We have noticed that the range of local stability and the CPs of phase transition increases due to the effect of second order correction term and the higher values of cosmological constant for both BHs.

- We have investigated the free energy in canonical (Helmhotz free energy) and and grand canonical (Gibb's free energy) ensembles. We have observed that the free energy reduces due to higher order correction terms. The Helmhotz free energy shows stable behavior for both BHs in case of positive cosmological constant while it shows unstable behavior for larger horizon for negative cosmological constant.

- Similarly, we noticed that Gibb's free energy exhibits stable behavior for both BHs for positive cosmological constant while it shows conditionally stable behavior for RN-AdS BH with GM and unstable behavior for $f(R)$ BH for negative cosmological constant.

- Hence, it is concluded that both BHs exhibit more stability (locally as well as globally) for growing values of cosmological constant and higher order correction terms, and vice versa which is agree with [44].

- Hence, we have shown that presence of the first and second order corrections of the entropy yield to unstable/stable phase transition, and led to stability of black hole at the allowed region of the event horizon.

In chapter **FOUR**, we have investigated the accretion onto various RBHs such as RBH using the FDD, RBH using the logistic distribution, RBH using nonlinear electrodynamics, and KS asymptotically flat RBH. These RBHs lead to SH and RN BHs asymptotically (most of them satisfy the WEC). We obtained the CPs, critical velocities, and the behavior of the speed of sound for the chosen RBHs. Moreover, we have analyzed the behavior of the radial velocity, the energy density, and the rate of change of mass for RBHs for various EoS parameters. For calculating these quantities, we have assumed the barotropic EoS and found the relationship between the conservation law and the barotropic EoS. We have found that the radial velocity (u) of the fluid is positive for stiff, dust, and quintessence matter and it is negative for phantom-like fluids. If the flow is inward then $u < 0$ is not allowed and $u > 0$ is not allowed for outward flow. Also, we have seen that the energy density remains positive for quintessence, dust, and stiff matter, while it becomes negative for a phantom-like fluid near RBHs.

In addition, the rate of change of mass of BH is a dynamical quantity, so the analysis of the nature of its mass in the presence of various dark energy models may become very interesting in the present scenario. Also, the sensitivity (increasing or decreasing) of BHs mass depends upon the nature of the fluids which accrete onto it. Therefore, we have considered the various possibilities of accreting fluids, such as dust and stiff matter, quintessence, and phantom. We have found that the rate of change of the mass of all RBHs increases for dust and stiff matter, and quintessence-like fluids, since these fluids do not have enough repulsive force. However, the mass of all RBHs decreases in the presence of a phantom-like fluid (and the corresponding energy density and radial velocity become negative) because it has a strong negative pressure. This result shows the consistency with several works [51, 64]. Also, this result favors the phenomenon that the universe undergoes the big rip singularity, where all the gravitationally bounded objects are dispersed due to the phantom DE.

In chapter **FIVE**, we have studied the steady state spherically symmetric accretion onto RBHs. We have developed the Hamiltonian dynamical system, we tackle the accretion problem. The pressure, baryon number density and other densities diverge on horizon, while the three-velocity has remained bounded by -1 and 1, and hence it does not diverge on the horizon. We have studied the motion of isothermal relativistic, ultra-relativistic, radiation and sub-relativistic test fluids in the frame work of Hamiltonian dynamical system around RBHs. The thermodynamical properties of fluids have been studied for different choices of EoS parameter. Moreover, CPs and conserved quantities have been found for different fluids. The behavior of an accreting fluid has been discussed as subsonic and supersonic according to EoS and RBHs. We have compared the fluid flow for two different RBHs and observed that the fluid flow and CPs are closer to DDF RBH instead of KS RBH (Fig.**6.1**). If CP is the saddle point, then the solution curve divides the (r, v) plane into the regions where fluid flow is physical for higher values of the Hamiltonian and unphysical in lower values of the Hamiltonian.

It has been observed that the supersonic accretion followed by subsonic accretion ends inside the horizon and it does not give support to the claim that the flow must be supersonic at the horizon [150]. Hence the flow of the fluid is neither transonic nor supersonic near the horizon [151, 152]. These new solutions correspond to fine tunning and instability problems in dynamical systems. Furthermore, we have observed from Fig.**6.3** that if the value of EoS parameter (ω) increases, then the CPs shifted towards both RBHs. Hence, it is concluded that the three-velocity depends on CPs and EoS parameter on phase space. It is interesting to mention here that the results obtained in Fig.**6.1** agree with [144, 145]. We have also observed from the right panel of Fig.**6.4** that accretion starts from the subsonic case and ends at the supersonic case into the horizon, but avoiding the saddle points for the DDF RBH. Hence no saddle point occurs in the solution of the DDF RBH. Furthermore, the subsonic flow appears to be almost non-relativistic. These features agrees with GR BHs [144, 145]. On the other hand, in the left panel of Fig.**6.4**, it has been seen that accretion starts from the subsonic case and ends in the supersonic case into the horizon but passing through the saddle points for KS RBH. Hence, the saddle point occurs in the solution of KS RBH. These features are different from [144, 145].

In chapter **SIX**, we have investigated the tidal forces of the Kiselev BHs by assuming its two special cases, i.e. Kiselev BHs surrounded by radiation and dust. We have observed that the radial tidal forces can change behavior from stretching to compressing for specific choices of the radiation and the dust parameters and the angular tidal forces can only be zero between the event and Cauchy horizons of BH. It is also mentioned here that the radial and angular tidal forces possesses the ability to change sign between the event and Cauchy horizons. The event horizon is increasing (away from the singularity) and the Cauchy horizon is decreasing (shifting towards singularity) as the radiation and the dust parameters increase.

Furthermore, the geodesic deviation equations can be solved analytically about a radially free-falling geodesic for a Kiselev BH. The behavior of the geodesic deviation vector for such a geodesic under the influence of the tidal forces has been examined. We choose the initial condition IC1, which represents releasing a body at rest consisting of dust with no internal motion and IC2 corresponds to letting such a body explode from a point at $r = b$. It is pointed out here that the radial tidal forces for a Kiselev BH surrounded by radiation attains the maximum value at $\sigma_r = 0.3$, as shown in Fig.**37**, and it becomes unphysical for $\sigma_r > 0.3$. Moreover, the maxima of the radial tidal forces for a Kiselev BH surrounded by dust is increasing as well as shifting towards BH as the dust parameter increases. These results are the agreement with [77]. Hence it is concluded that the radial component of the geodesic deviation vector becomes zero, while the angular component remains finite for certain initial conditions.

It would be worthwhile to examine the effects of thermal fluctuations onto rotating BHs and extend this analysis to explore Joule-Thomson expansion. One can also explore the work in chapter **FIVE** and **SIX** for non-static fluids without assuming any EoS which may give interesting results. It would be also interesting to examine the tidal forces in non-commutative, regular or super massive BHs and solve the geodesic equation for radially free-falling bodies towards these BHs. This is left for future considerations.

Bibliography

[1] Thorne, K.S. (1994). Black holes and time warps: Einstein's outrageous legacy, *Commonwealth Fund Book Program, New York, NY: W.W. Norton and London: Picador, c1994*.

[2] Falanga, M., Belloni, T., Casella, P., Gilfanov, M., Jonker, P. and King, A. (2014), The Physics of Accretion Onto Black Holes, *Space Sciences Series of ISSI, Springer*, volume 49.

[3] Elizalde, E. and Hildebrandt, S.R. (2002). Family of regular interiors for nonrotating black holes with $T_{00} = T_{11}$, *Phys. Rev. D* 65, 124024.

[4] Zaslavskii, O.B. (2010). Regular black holes and energy conditions, *Phys. Lett. B* 688, 278-280.

[5] Hawking, S.W. and Ellis, G.F. (1973). The Large Scale Structure of SpaceTime, *Cambridge Univ. Press, Cambridge*.

[6] Senovilla, J.M.M. (1998). Singularity Theorems and Their Consequences, *Gen. Relat. Gravity* 30, 701-848.

[7] Bardeen, J.M. (1968). Non-singular general-relativistic gravitational collapse, *The 5th International Conference on Gravitation and the Theory of Relativity*, USSR, Tbilisi, Georgia, p. 174.

[8] Borde, A. (1997). Regular black holes and topology change, *Phys. Rev. D* 55, 7615.

[9] Ayon-Beato, E. and Garcia, A. (1998). Regular Black Hole in General Relativity Coupled to Nonlinear Electrodynamics, *Phys. Rev. Lett.* 80, 5056-5059.

[10] Hayward, S.A. (2006). Formation and Evaporation of Nonsingular Black Holes, *Phys. Rev. Lett.* 96, 031103.

[11] Berej, W. et al. (2006). Regular black holes in quadratic gravity, *Gen. Relat. Gravity* 38(5), 885-906.

[12] Balart, L. and Vagenas, E.C. (2014). Regular black holes with a nonlinear electrodynamics source, *Phys. Rev. D* 90, 124045.

[13] Kehagias, A. and Sfetsos, K. (2009). The black hole and FRW geometries of non-relativistic gravity, *Phys. Lett. B* 678, 123-126.

[14] Horndeski, G.W. (1978). Static spherically symmetric solutions to a system of generalized Einstein-Maxwell field equations, *Phys. Rev. D* 17, 391-395.

[15] Muller-Hoissen, F. and Sippel, R. (1988). Modification of Einstein-Yang-Mills theory from dimensional reduction of the Gauss-Bonnet action, *Class. Quantum Gravity* 5, 1473-1488.

[16] Balakin, A.B., Sushkov, S.V. and Zayats, A.E. (2007). Nonminimal Wu-Yang wormhole, *Phys. Rev. D* 75, 084042.

[17] Balakin, A.B., Lemos, J.P.S. and Zayats, A.E. (2010). Nonminimal coupling for the gravitational and electromagnetic fields: Traversable electric wormholes, *Phys. Rev. D* 81, 084015.

[18] Balakin, A.B., Bochkarev, V.V. and Lemos, J.P.S. (2008). Nonminimal coupling for the gravitational and electromagnetic fields: Black hole solutions and solitons, *Phys. Rev. D* 77, 084013.

[19] Balakin, A.B. and Zayats, A.E. (2015). Nonminimal black holes with regular electric field, *Int. J. Mod. Phys. D* 24, 1542009.

[20] Balakin, A.B. and Zayats, A.E. (2007). Non-minimal Wu-Yang monopole, *Phys. Lett. B* 644, 294-298.

[21] Wu, T.T. and Yang, C.N. (1969). Some Solutions of the Classical Isotopic Gauge. Field Equations, *in Properties of Matter under Unusual Conditions, in Honor of Edward Tellers 60th Birthday*, ed. by H. Mark, S. Fernbach (Interscience, New York), p. 349.

[22] Shnir, Y. (2005). Magnetic Monopoles, *Springer, Berlin*.

[23] Balakin, A.B., Lemos, J.P.S. and Zayats, A.E. (2016). Regular nonminimal magnetic black holes in spacetimes with a cosmological constant, *Phys. Rev. D* 93, 024008.

[24] Balakin, A.B., Lemos, J.P.S. and Zayats, A.E. (2016). Magnetic black holes and monopoles in a nonminimal Einstein-Yang-Mills theory with a cosmological constant: Exact solutions, *Phys. Rev. D* 93, 084004.

[25] Bekenstein, J.D. (1973). Black Holes and Entropy, *Phys. Rev. D* 7, 2333-2346.

[26] Bardeen, J.M., Carter, B. and Hawking, S.W. (1973). The four laws of black hole mechanics, *Commun. Math. Phys.* 31, 161-170.

[27] Hawking, S.W. (1975). Particle Creation by Black Holes, *Commun. Math. Phys.* 43, 199-220.

[28] Dethridge, J. C. and Guttmann, A. J. (2008). Prudent Self-Avoiding Walks, *Entropy* 10, 309-318.

[29] Grimm, U. and Heuer, M. (2008). On the Entropy and Letter Frequencies of Powerfree Words, *Entropy* 10, 590-612.

[30] Dewar, R. L., Hole, M. J., McGann, M., Mills, R., Hudson, S. R. (2008). Relaxed Plasma Equilibria and Entropy-Related Plasma Self-Organization Principles, *Entropy* 10, 621-634.

[31] Broadbridge, P. (2008). Entropy Diagnostics for Fourth Order Partial Differential Equations in Conservation Form, *Entropy* 10, 365-379.

[32] Singh, M. and Vishnoi, N.K., (2014). Entropy, optimization and counting. In *Proceedings of the forty-sixth annual ACM symposium on Theory of computing* 50-59.

[33] Hawking, S.W. (1974). Black hole explosions?, *Nature* 248, 30-31.

[34] Bekenstein, J. D. (1972). Nonexistence of Baryon Number for Black Holes, *Phys. Rev. D* 5, 1239-1246; Bekenstein, J. D. (1972). Nonexistence of Baryon Number for Black Holes. II, *Phys. Rev. D* 5, 2403-2412.

[35] More, S. S. (2005). Higher Order Corrections to Black Hole Entropy, *Clas. Quantum Grav.* 22, 4129-4139.

[36] Rama, S. K. (1999). Holographic Principle in the Closed Universe : a Resolution with Negative Pressure Matter, *Phys. Lett. B* 457, 268-274.

[37] Ashtekar, A. (1991). Lectures on non-perturbative canonical gravity, *in Advanced Series in Astrophysics and Cosmology*, World Scientific, Singapore.

[38] Pourhassan, B. and Fazal, M. (2015). Thermal Fluctuations in a Charged AdS Black Hole, *Euro. phys. Lett.* 111, 40006.

[39] Govindarajan et al. (2001). Logarithmic correction to the Bekenstein-Hawking entropy of the BTZ black hole, *Class. Quantum Gravity* 18, 2877-2885.

[40] Carlip, S. (2000). Logarithmic Corrections to Black Hole Entropy from the Cardy Formula, *Class. Quantum Gravity* 17, 4175-4186.

[41] Mann, R.B. and Solodukhin, S.N. (1998). Universality of Quantum Entropy for Extreme Black Holes, *Nucl. Phys. B* 523, 293-3.7.

[42] Medved, A.J.M. and Kunstatter, G. (1999). Quantum corrections to the thermodynamics of charged 2D black holes, *Phys. Rev. D* 60, 104029.

[43] Jing, J. and Yan, M.L. (2001). Statistical entropy of a stationary dilaton black hole from the Cardy formula, *Phys. Rev. D* 63, 024003.

[44] Birmingham, D. and Sen, S. (2001). Exact black hole entropy bound in conformal field theory, *Phys. Rev. D* 63, 047501.

[45] Pourhassan, B., Upadhyay, S. and Farahani, H. (2017). Thermodynamics of higher dimensional black holes with higher order thermal fluctuations, *Gen. Relat. Gravity* 49, 144.

[46] Pourhassan et al. (2016). Effects of thermal fluctuations on the thermodynamics of modified Hayward black hole, *Eur. Phys. J. C* 76, 145.

[47] Perlmutter, S. et al. (1999). Measurements of Omega and Lambda from 42 High-Redshift Supernovae, [Supernova Cosmology Project Collaboration], *Astrophys. J.* 517, 565-586.

[48] Spergel, D.N. et al. (2007). Three-year Wilkinson microwave anisotropy probe (WMAP) observations: polarization analysis, [WMAP Collaboration], *Astrophys. J. Suppl.* 170, 335-376.

[49] Eisenstein, D.J. et al. (2005). Detection of the baryon acoustic peak in the large-scale correlation function of SDSS luminous red galaxies, [SDSS Collaboration], *Astrophys. J.* 633, 560-574.

[50] Riess, A.G. et al. (1998). Observational evidence from supernovae for an accelerating universe and a cosmological constant, [Supernova Search Team Collaboration], *Astron. J.* 116, 10091.38.

[51] Bahamonde, S. and Jamil, M. (2015). Accretion processes for general spherically symmetric compact objects, *Eur. Phys. J. C* 75, 508.

[52] Bondi, H. (1952). On Spherically Symmetrical Accretion, *Mon. Not. R. Astron. Soc.* 112, 195-204.

[53] Michel, F.C. (1972). Accretion of matter by condensed objects, *Astrophys. Space Sci.* 15, 153-160.

[54] Moncrief, V. (1980). Stability of stationary, spherical accretion onto a Schwarzschild black hole, *Astrophys. J.* 235, 1038-1046.

[55] Babichev, E. et al. (2004). Black Hole Mass Decreasing due to Phantom Energy Accretion, *Phys. Rev. Lett.* 93, 021102.

[56] Guzman, F.S. and Lora-Clavijo, F.D. (2011). Exploring the effects of pressure on the radial accretion of dark matter by a Schwarzschild supermassive black hole, *MNRAS* 415, 225-234.

[57] Karkowski, J. and Malec, E. (2013). Bondi accretion onto cosmological black holes, *Phys. Rev. D* 87, 044007.

[58] Mach, P. and Malec, E. (2013). Stability of relativistic Bondi accretion in Schwarzschild(anti)de Sitter spacetimes, *Phys. Rev. D* 88, 084055.

[59] Lora-Clavijo, F.D., Gracia-Linares, M. and Guzman, F.S. (2014). Horizon growth of supermassive black hole seeds fed with collisional dark matter, *MNRAS* 443, 2242-2251.

[60] Ananda, D.B., Bhattacharya, S. and Das, T.K. (2015). Acoustic geometry through perturbation of mass accretion rate - radial flow in static spacetimes, *Gen. Relat. Gravit.* 47, 96.

[61] Pun, C.S.J. et al., (2008). Thin accretion disks in $f(R)$ modified gravity models *Phys. Rev. D* 78, 024043.

[62] Chakraborty, S. (2015). Equilibrium configuration of perfect fluid orbiting around black holes in some classes of alternative gravity theories, *Class. Quant. Grav.* 32, 075007.

[63] Gonzalez, J.A. and Guzman, F.S. (2009). Accretion of phantom scalar field into a black hole, *Phys. Rev. D* 79, 121501.

[64] Debnath, U. (2015). Accretion and evaporation of modified Hayward black hole, *Eur. Phys. J. C* 75, 129.

[65] Azreg-Anou, M. (2017). Cyclic and heteroclinic flows near general static spherically symmetric black holes: semi-cyclic flowsaddendum and corrigendum, *Eur. Phys. J. C* 77, 36.

[66] Kim, S.W. and Kang, Y. (2012). Dark Energy and Dark Matter Accretion onto a Black Hole in Expanding Uinverse, *Int. J. Mod. Phys. Conf. Ser.* 12, 320-329.

[67] Jimenez Madrid, J.A and Gonzalez-Diaz, P.F. (2008). Evolution of a Kerr-Newman black hole in a dark energy universe, *Gravit. Cosmol.* 14, 213-225.

[68] Sharif, M. and Abbas, G. (2011). Phantom accretion onto the Schwarzschild de-Sitter black hole, *Chin. Phys. Lett.* 28, 090402.

[69] Sharif, M. and Abbas, G. (2012). Phantom Energy Accretion by a Stringy Charged Black Hole, *Chin. Phys. Lett.* 29, 010401.

[70] Perez,D. et al. (2013). Accretion disks around black holes in modified strong gravity, *Astronomy and Astrophysics.* 551, A4.

[71] Ahmed, A.K. et al. (2016). Astrophysical flows near $f(T)$ gravity black holes, *Eur. Phys. J. C* 76, 269.

[72] Ahmed, A.K. et al. (2016). Cyclic and heteroclinic flows near general static spherically symmetric black holes, *Eur. Phys. J. C* 76, 280.

[73] Azreg-Anou, M. (2017). Cyclic and heteroclinic flows near general static spherically symmetric black holes: semi-cyclic flows - addendum and corrigendum, *Eur. Phys. J. C* 77, 36.

[74] dInverno, R. (1992). Introducing Einsteins Relativity, *Clarendon Press, Oxford.*

[75] Hobson, M.P., Efstathiou, G. and Lasenby, A.N. (2006). General Relativity an Introduction for Physicists, *Cambridge University Press, Cambridge.*

[76] Hartle, J.B. (2002). Gravity: An Introduction to Einsteins General Relativity, *J.B. Addison-Wesley, San Francisco*.

[77] Crispino, L.C.B. et al. (2016). Tidal forces in ReissnerNordström spacetimes, *Eur. Phys. J. C* 76, 168.

[78] Abdel-Megied, M. and Gad, R.M. (2005). On the singularities of ReissnerNordström spacetime, *Chaos Solitons Fract.* 23, 313-320.

[79] Chandrasekhar, S. (1983). The Mathematical Theory of Black Holes, *Clarendon Press, Oxford*.

[80] Misner, C., Thorne, K. and Wheeler, J. (1973). Gravitation, *Freeman, San Francisco*.

[81] Adler, R., Bazin, M. and Schiffer, M. (1975). Introduction to General Relativity, *McGraw-Hill, New York, 2nd edn*.

[82] Bekenstein, J.D. (1975). Black holes with scalar charge, *Ann. Phys.* 91, 75.

[83] Ayon-Beato, E. and Garcia, A. (1999). Non-Singular Charged Black Hole Solution for Non-Linear Source, *Gen. Relat. Grav.* 31, 629.

[84] Garfinkle, D., Horowitz, G.T. and Strominger, A. (1991). Charged black holes in string theory, *Phys. Rev. D* 43, 3140.

[85] Kiselev, V.V. (2003). Quintessence and black holes, *Class. Quant. Grav.* 20, 1187.

[86] Jiao, L. and Yang, R. (2017). Accretion onto a moving Reissner-Nordström black hole, *Eur. Phys. J. C* 77, 356.

[87] Younas A. et al., (2015). Strong gravitational lensing by Kiselev black hole, *Phys. Rev. D* 92, 084042.

[88] Majeed, B., Jamil, M. and Pradhan, P. (2015). Thermodynamic Relations for Kiselev and Dilaton Black Hole, *Adv. High Energy Phys.* 2015, 124910.

[89] Frolov, V.P. and Novikov, I.D. (1997). Black Hole Physics: Basic Concepts and New Developments, *Kluwer Acad. Publ.*.

[90] Wald, R.M. (1984). General Relativity, *The University of Chicago Press, Chicago*.

[91] Penrose, R. (1969). Gravitational collapse: The role of general relativity, *Riv. Nuovo Cim.* 1, 252276.

[92] Vercnocke, B. (2010). Hidden Structures of Black Holes, Ph.D. Thesis, *K.U.Leuven, Belgium*.

[93] Hamilton, A. J. S., General Relativity, Black Holes, and Cosmology, (http://jila.colorado.edu/ajsh/astr5770-14/grbook.pdf).

[94] Bronnikov, K. A. and Rubin, S. G. (2012). Blackholes Cosomology and Extra Dimensions, *World Scientific*.

[95] Borde, A. (1994). Open and closed universes, initial singularities, and inflation, *Phys. Rev. D* 50, 3692-3702.

[96] Javed, W. (2013). Hawking Radiation from Some Particular Black Holes, Ph.D. Thesis, *University of Punjab, Lahore, Pakistan.*

[97] Bronnikov, K.A. (2001). Regular magnetic black holes and monopoles from nonlinear electrodynamics, *Phys. Rev. D* 63, 044005.

[98] Dymnikova, I. (1998). Spherically Symmetric Space-Time with Two Cosmological Constants, *Gen. Rel. Grav.* 30, 17751793.

[99] Sakharov, A.D. (1966). The Initial Stage of an Expanding Universe and the Appearance of a Nonuniform Distribution of Matter, *Sov. Phys. JETP* 22, 241-249.

[100] Gliner, E.B. (1966). Algebraic Properties of the Energy-momentum Tensor and Vacuum-like States $o+$ Matter, *Sov. Phys. JETP* 22, 378-382.

[101] Matyjasek, J. (2007). Vacuum polarization of massive spinor and vector fields in the spacetime of a nonlinear black hole, *Phys. Rev. D* 76, 084003.

[102] Mann, R. B. (2015). Black Holes: Thermodynamics, Information, and Firewalls, *Springer Briefs in Physics*.

[103] Kerner, R.J. (2008). Black Hole Thermodynamics and the Tunnelling Method for Particle Emission, Ph.D. Thesis, *University of Waterloo*.

[104] Majhi, B.R. (2011). Quantum Tunneling in Black Holes, Ph.D. Thesis, *University of Calcutta*.

[105] $https://en.wikipedia.org/wiki/Thermal_fluctuationscite_note-1$.

[106] Pourhassan, B., Upadhyay, S. and Farahani, H. (2017). Thermodynamics of higher dimensional black holes with higher order thermal fluctuations, *Gen. Relativ. Gravit.* 49, 144.

[107] Dolan, B.P. (2011). Pressure and volume in the first law of black hole thermodynamics, *Class. Quantum Gravity* 28, 235017.

[108] Hawking, S. and Page, D. N. (1983). Thermodynamics of black holes in anti-de Sitter space, *Commun. Math. Phys.* 87, 577-588.

[109] Gibbons, G. W., Hawking, S. W. and Perry, M. J. (1978). Path Integrals and the Indefiniteness of the Gravitational Action, *Nucl. Phys. B* 138, 141-150.

[110] Hartle, J. B. and Hawking, S. W. (1976). Path-integral derivation of black-hole radiance, *Phys. Rev. D* 13, 2188-2203.

[111] Sobreiro, R. F. and Otoya, V. J. V. (2007). Effective gravity from a quantum gauge theory in Euclidean spacetime, *Class. Quant. Grav.* 24, 4937-4953.

[112] Bonora, L. and Bytsenko, A. A. (2011). Partition Functions for Quantum Gravity, Black Holes, Elliptic Genera and Lie Algebra Homologies, *Nucl. Phys. B* 852, 508-537.

[113] Gibbons, G. W. and Hawking, S. W. (1977). Action integrals and partition functions in quantum gravity, *Phys. Rev. D.* 15, 2752-2756.

[114] Iyer, V. and Wald, R. M. (1995). Comparison of the Noether charge and Euclidean methods for computing the entropy of stationary black holes, *Phys. Rev. D.* 52, 4430-4439.

[115] Perlmutter, S. et al., (1999). Measurements of Ω and Λ from 42 High-Redshift Supernovae *Astrophys. J.* 517, 565.

[116] Spergel, D.N. et al. (2007). Three-year Wilkinson Microwave Anisotropy Probe (WMAP) observations: implications for cosmology, *The Astrophysical Journal Supplement Series* 170(2), 377.

[117] Eisenstein, D.J. et al. (2005). Detection of the Baryon acoustic peak in the large-scale correlation function of SDSS luminous red galaxies, *Astrophys. J* 633, 560.

[118] Johri, V.B. (2004). Phantom cosmologies, *Phys. Rev. D* 70, 041303.

[119] Lobo, F. S. N. (2005). Phantom energy traversable wormholes, *Phys. Rev. D* 71, 084011.

[120] Nojiri, S. and Odintsov, S. (2011). Unified cosmic history in modified gravity: From F(R) theory to Lorentz non-invariant models, *Phys. Rep.* 505, 59-144.

[121] Armendariz-Picon, C., Mukhanov, V.F., Steinhardt, P.J. (2000). Dynamical Solution to the Problem of a Small Cosmological Constant and Late-Time Cosmic Acceleration, *Phys. Rev. Lett.* 85, 4438-4441.

[122] Gasperini, M. et al., (2002). Quintessence as a runaway dilaton, *Phys. Rev. D* 65, 023508.

[123] Gumjudpai, B. and Ward, J. (2009). Generalized DBI quintessence, *Phys. Rev. D* 80, 023528.

[124] Martin, J. and Yamaguchi, M. (2008). DBI-essence, *Phys. Rev. D* 77, 123508.

[125] Wei, H., Cai, R.G. and Zeng, D.F. (2005). Hessence: A New View of Quintom Dark Energy, *Class. Quantum Gravity* 22, 3189-3202.

[126] Sen, A. (2002). Tachyon Matter, *JHEP* 0207, 065.

[127] Kamenshchik, A.Y., Moschella, U. and Pasquier, V. (2001). An alternative to quintessence, *Phys. Lett. B* 511, 265-268.

[128] Copeland, E.J., Sami, M. and Tsujikawa, S. (2006). Dynamics of dark energy, *Int. J. Mod. Phys. D* 15, 1753-1935.

[129] Chaverra, E. and Sarbach, O. (2015). Radial accretion flows on static spherically symmetric black holes, *Class. Quant. Grav.* 32, 15006.

[130] Sadeghi, J., Jafarzade, K. and Pourhassan, B. (2012). Thermodynamical quantities of Horava-Lifshitz black hole, *Int. J. Theor. Phys.* 51, 3891-3902.

[131] Ahmed, A., Camci, U. and Jamil, M. (2016). Accretion on ReissnerNordström (anti)-de Sitter black hole with global monopole, *Class. Quant. Grav.* 33, 215012.

[132] Barriola, M. and Vilenkin, A. (1989). Gravitational field of a global monopole, *Phys. Rev. Lett.* 63, 341-343.

[133] Bronnikov, K. A., Meierovich, B. E. and Podolyak, E. R. (2002). Global Monopole in General Relativity, *J. Exp. and Theor. Phys.* 95, 392-403.

[134] Yu, H. (2002). Decay of massive scalar hair in the background of a black hole with a global monopole, *Phys. Rev. D* 65, 087502.

[135] Starobinsky, A. A. (1980). A New Type of Isotropic Cosmological Models Without Singularity, *Phys. Lett. B* 91, 99102.

[136] Ohta, N., Percacci, R. and Vacca, G. P. (2015). Flow equation for $f(R)$ gravity and some of its exact solutions, *Phys. Rev. D* 92, 061501.

[137] Soroushfar, S., Saffari, R., Kunz, J. and Lammerzahl, C. (2015). Analytical solutions of the geodesic equation in the spacetime of a black hole in $f(R)$ gravity, *Phys. Rev. D* 92, 044010.

[138] Farooq, M. U., Jamil, M., Momeni, D. and Myrzakulov, R. (2013). Reconstruction of $f(T)$ and $f(R)$ gravity according to (m,n)-type holographic dark energy, *Can. J. Phys.* 91, 703-708.

[139] Majeed, B. and Jamil, M. (2017). Dynamics and center of mass energy of colliding particles around black hole in $f(R)$ gravity, *Int. J. Mod. Phys. D* 26, 1741017.

[140] Saffari, R. and Rahvar, S. (2008). $f(R)$ gravity: From the Pioneer anomaly to cosmic acceleration, *Phys. Rev. D* 77, 104028.

[141] Sharif, M. and Jawad, A. (2010). Energy Contents of a Class of Regular Black Hole Solutions in Teleparallel Gravity, *Mod. Phys. Lett. A* 25, 3241-3250.

[142] Culetu, H. (2015). On the source of the Kehagias-Sfetsos black hole, *Astrophys. Space Sci.* 2, 360.

[143] Rezzolla, L. and Zanotti, O. (2013). Relativistic Hydrodynamics, *Oxford University Press, Oxford.*

[144] Ahmed et al. (2016). Astrophysical flows near $f(T)$ gravity black holes, *Eur. Phys. J. C* 76, 269.

[145] Ahmed et al. (2016). Cyclic and heteroclinic flows near general static spherically symmetric black holes, *Eur. Phys. J. C* 76, 280.

[146] Chaverra, E. and Sarbach, O. (2011). Polytropic spherical accretion flows on Schwarzschild black holes, *AIP Conf. Proc.* 1473, 54-58.

[147] Chaverra, E., Morales, M.D. and Sarbach, O. (2015). Quasinormal acoustic oscillations in the Michel flow, *Phys. Rev. D* 91, 104012.

[148] Chaverra, E., Mach, P. and Sarbach, O. (2016). Michel accretion of a polytropic fluid with adiabatic index $\gamma > 5/3$: global flows versus homoclinic orbits, *Class. Quant. Grav.* 33, 105016.

[149] Dagun, C. (1977). A new model of personal income distribution: Specification and estimation, *Economie Appliquée* 30, 413-437.

[150] Chakrabarti, S.K. (2011). Fundemental Concepts in Transonic Flow Paradigm of Black Hole *Astrophys. J.*, 20, 1723-1731.

[151] Novikov, I. and Thorne, K.S. (1973). in Black Holes, ed. by DeWitt, C. and DeWitt B. *Gordon and Breach, New York,* p. 343.

[152] Chakrabarti, S.K. (1990). Theory of Transonic Astrophysical Flows, *World Scientific, Singapore*.

[153] Nagle, R.K., Saff, E.B. and Snider, A.D. (2012). Fundamentals of differential equations and boundary value problems, 6th edn. *Pearson, International Edition, UK*.

[154] Polking, J., Boggess, A. and Arnold, D. (2006). Diffrential Equations with Boundary Value Problems, 2nd edn. *Prentice Hall, Upper Saddle River*.

[155] Bugl, P. (1995). Differential Equations: Matrices and Models, *Prentice Hall, Englewood Cliffs*.

[156] Azreg-Anou, M. (2013). Phase-space analysis of the cosmological 3-fluid problem: families of attractors and repellers, *Class. Quantum Grav.* 30, 205001.

[157] Penrose, R. (1979). Singularities and time asymmetry, in General Relativity, An Einstein Centenary Survey, ed. by Hawking, S.W. and Israel, W. *Cambridge University Press, Cambridge*.

[158] Martel, K. and Poisson, E. (2002). One-parameter family of time-symmetric initial data for the radial infall of a particle into a Schwarzschild black hole, *Phys. Rev. D* 66, 084001.

[159] Faizal, M. and Khalil, M. (2015). GUP-corrected thermodynamics for all black objects and the existence of remnants, *Int. J. Mod. Phys. A* 30, 1550144.

[160] Ali, A.F. (2012). No Existence of Black Holes at LHC Due to Minimal Length in Quantum Gravity, *JHEP* 1209, 067.

Appendix

List of Publications

The contents of this thesis are based on the following research papers published or submitted in journals of International repute. These papers are also attached herewith.

1. Jawad, A. and **Shahzad, M. U.** (2016). Accretion onto some well-known regular black holes, *Eur. Phys. J. C* 76, 123. **(IF 5.331)**

2. Jawad, A. and **Shahzad, M. U.** (2017). Effects of thermal fluctuations on non-minimal regular magnetic black hole, *Eur. Phys. J. C* 77, 349. **(IF 5.331)**

3. **Shahzad, M. U.** and Jawad, A. (2017). Tidal forces in Kiselev black hole, *Eur. Phys. J. C* 77, 372. **(IF 5.331)**

4. Jawad, A. and **Shahzad, M. U.** (2017). Accreting fluids onto regular black holes via Hamiltonian approach, *Eur. Phys. J. C* 77, 515. **(IF 5.331)**

5. **Shahzad, M. U.** and Jawad, A. Thermodynamics of Higher Order Corrected Entropy on some well known Black holes (submitted for publication).

Also, the following papers related to this thesis have been published, accepted or submitted for publication.

1. Jawad, A., Ali, F., **Shahzad, M. U.** and Abbas, G. (2016). Dynamics of particles around time conformal Schwarzschild black hole, *Eur. Phys. J. C* 76, 586. **(IF 5.331)**

2. Jawad, A. and **Shahzad, M. U.** (2017). Particle dynamics around time conformal regular black holes via Noether symmetries, *Int. J. Mod. Phys. D* 26, 1750059. **(IF 2.476)**

3. Jawad, A., Ali, F. and **Shahzad, M. U.** Particle Dynamics near Time Conformal Slowly Rotating Kerr Black Hole (submitted for publication).